INFORMATION TO USERS

This manuscript has been reproduced from the microfilm master. UMI films the text directly from the original or copy submitted. Thus, some thesis and dissertation copies are in typewriter face, while others may be from any type of computer printer.

The quality of this reproduction is dependent upon the quality of the copy submitted. Broken or indistinct print, colored or poor quality illustrations and photographs, print bleedthrough, substandard margins, and improper alignment can adversely affect reproduction.

In the unlikely event that the author did not send UMI a complete manuscript and there are missing pages, these will be noted. Also, if unauthorized copyright material had to be removed, a note will indicate the deletion.

Oversize materials (e.g., maps, drawings, charts) are reproduced by sectioning the original, beginning at the upper left-hand corner and continuing from left to right in equal sections with small overlaps. Each original is also photographed in one exposure and is included in reduced form at the back of the book.

Photographs included in the original manuscript have been reproduced xerographically in this copy. Higher quality 6" x 9" black and white photographic prints are available for any photographs or illustrations appearing in this copy for an additional charge. Contact UMI directly to order.

UMI

A Bell & Howell Information Company
300 North Zeeb Road, Ann Arbor MI 48106-1346 USA
313/761-4700 800/521-0600

TOWARDS VOLTAGE-GATED ION CHANNELS, MOLECULAR DIODES

by

Xin Zhou
B.Sc. Fudan University, 1983

A Dissertation Submitted in Partial Fulfillment of the
Requirements for the Degree of

DOCTOR OF PHILOSOPHY

in the Department of Chemistry

We accept this thesis as conforming
to the required standard

Dr. T.M. Fyles, Supervisor (Department of Chemistry)

Dr. G.A. Poulton, Departmental Member (Department of Chemistry)

Dr. C. Bohne, Departmental Member (Department of Chemistry)

Dr. J. Ausio, Outside Member (Department of Biochemistry and Microbiology)

Dr. J.C. Sherman, External Examiner (University of British Columbia)

Supervisor: Dr. Thomas M. Fyles

ABSTRACT

The goals of this project were to synthesize voltage-gated ion channels based upon previously studied pore-formers and to further explore the mechanism of ion transport with this type of pore-former.

The syntheses of bis-macrocyclic bola-amphiphiles started with two different macrocycles prepared via a two-step cyclization from maleic anhydride by reaction with 1,8-octanediol alone or with triethyleneglycol. The macrocycles were then modified to a set of mono-adducts and bis-adducts by Michael addition of thiols (3-mercaptopropanol, 2-mercaptoacetic acid, or 3-mercaptopropionic acid). The mercaptopropanol adduct was converted to a mesylate and coupled with a carboxylate derivative to form a bis-macrocycle. Repetitious gel permeation chromatography gave a bis-macrocycle bearing only one head group, a carboxylate. The second head group was added via Michael addition to give a bis-macrocyclic bola-amphiphile which could have either the same head groups or different head groups. Two symmetrical transporters were synthesized via another route: two macrocycles reacted with 2-mercaptoethyl sulfide to generate a bis-macrocycle, and the same head group was then simultaneously added to both ends to give a symmetrical bola-amphiphile. Transporters with different combinations of head groups were synthesized to compare head group effects on cation transport properties, while different macrocycles were used in the backbone of transporter candidates to give two series of compounds for comparison of

their behaviors.

The second phase of this project investigated the transport properties of candidates using pH-stat titration. The pH-stat titration of bilayer vesicles allowed determination of dynamic transport properties: transport rate, apparent kinetic order and cation selectivity. Combined with information from planar bilayer experiments (done by D. Loock), it was found that an asymmetrical bis-macrocyclic bola-amphiphile with an acetate and a succinate head group behaves as voltage-gated ion channel in planar bilayers. An ion transport mechanism of the present system was proposed which involves the formation of active aggregates (probably dimers or oligomers).

Examiners:

Dr. T.M. Fyles, Supervisor (Department of Chemistry)

Dr. G.A. Poulton, Departmental Member (Department of Chemistry)

Dr. C. Bohne, Departmental Member (Department of Chemistry)

Dr. J. Austin, Outside Member (Department of Biochemistry and Microbiology)

Dr. J.C. Sherman, External Examiner (University of British Columbia)

TABLE OF CONTENTS

LIST OF TABLES

LIST OF FIGURES

LIST OF SCHEMES

LIST OF ABBREVIATIONS

DMSO	dimethylsulfoxide
DMF	N,N-dimethylformamide
THF	tetrahydrofuran
FCCP	carbonyl cyanide 4-(trifluoromethoxy)phenylhydrazone
TLC	thin layer chromatography
HPLC	high pressure liquid chromatography
GPC	gel permeation chromatography
NMR	nuclear magnetic resonance
s	singlet
tri	triplet
m	multiplet
br	broad
COSY	Correlation Spectroscopy
HETCOR	HETeronuclear shift CORrelation spectroscopy
LSIMS	liquid secondary ionic mass spectrum
mNBA	meta-nitrobenzyl alcohol

GLOSSARY OF BIOCHEMICAL TERMINOLOGY

Unilamellar vesicles: Vesicles which are bounded by a single lamella consisting of two layers of lipid molecules (a single bilayer). This is in contrast to multilamellar vesicles which are isolated by many bilayers.

FCCP: Carbonyl cyanide 4-(trifluoromethoxy)phenylhydrazone, a proton carrier which facilitates the release of protons from vesicles.

Electroneutral proton-cation antiport: This process is proton / cation counter transport in which the cation concentration gradient drives cation fluxes inward across the vesicle bilayer via some transporters and the pH gradient drives proton fluxes outward from the vesicle. The process remains electroneutral throughout.

Voltage-gated ion channels: Ion channels are opened above some value of applied voltage and are closed at potentials below the threshold or at potentials opposite in sign.

ACKNOWLEDGMENTS

I would like to express my thanks to the supervisor, Dr. Tom Fyles for his help, guidance and patience throughout this project. Thanks to Daniela Loock for allowing me use some of her experimental data in this thesis, and for the great collaboration and many helpful discussions. Many thanks to Wilma van Straaten-Nijenhuis, Pedro Montoya-Pelaez, Binqi Zeng, Lynn Cameron, Allana Pryhitaka, and David Lycon, for their help and thoughtful discussions, and thanks to Dave Robertson for his endeavors to make pH-stat titration have more fun. I would like to acknowledge the assistance of the technical staff in Department of Chemistry, in particular Mrs. Christine Greenwood and Dr. David McGillivary. Thanks for the financial assistance from Department of Chemistry and University of Victoria. And finally, I am grateful to my wife for her support throughout this long course.

CHAPTER 1 INTRODUCTION

1.1 Natural ion channels

1.1.1 Ion channel proteins

The flow of ions and molecules between a cell and its environment is precisely regulated by specific transport systems. These system will regulate cell volume and maintain the intracellular pH and ionic composition to provide a favorable environment for enzyme activity, will extract and concentrate metabolic fuels and building blocks from the environment and extrude toxic substances, and will generate ionic gradients which are essential for the excitability of nerve and muscle[1]. All known naturally occurring transport systems are channels[1]. These conduits, such as the Na^+-K^+ pump, play an important role in intercellular communication and transfer of metabolites.

1.1.2 Antibiotics, simple natural ion channels

Channel proteins are very complicated[2, 3]. A typical channel protein has a molecular weight of *ca.* 250,000 Da, and its conformation often changes either in different solvents or by itself. Thus the complete three-dimensional structures of these multi-subunit membrane proteins are unlikely to be easily obtained. A less difficult approach which has been successful in elucidating some features of the structure and function of transport proteins is to study small molecule transport antibiotics produced by microorganisms. Because these antibiotics, mainly channel forming peptides, have molecular weights of only 1000 ~ 2000 Da, thus greatly simplify obtaining and manipulating

materials. During the past decade, advances in the analysis of the biophysical properties of channel forming peptides have permitted unprecedented insight into structure and function at a molecular level, which in many cases can be related to structure and function in full-size proteins. Three of the best examples are gramicidin, alamethicin, and amphotericin B, of which the first two are generally considered as models of ion channel proteins. All three display characteristic ion channel behaviors to different degrees: ion selectivity, voltage dependence, subconductance states and blocking, and modulation properties in lipid membranes[4, 5].

Gramicidin is a linear peptide produced by *Bacillus brevis*, which consists of 15 alternating L- and D-amino acid residues[6]. In organic solvents, such as methanol, gramicidin exists as a mixture of dimeric forms in equilibrium with monomers[7]. The most abundant species is an antiparallel, left-handed β double helical dimer[8]. However, a series of experiments indicated that gramicidin forms a head-to-head single-helix dimer channel to span a lipid bilayer membrane (both N-termini are at the bilayer mid plane)[5].

The channel is about 4 Å diameter and is lined by polar peptide carbonyl groups[5]. The hydrophobic side-chains are on the periphery of the channel in contact with hydrocarbon chains of the lipid membrane. The hydrophilic carbonyl groups form an aqueous pore and transiently coordinate to the cation as it passes down the axis of the channel[1]. Gramicidin channels conduct monovalent cations and have an alkali metal cation selectivity in the order Cs^+

> Rb^+ > K^+ > Na^+ > Li^+ [9]. The channel can be blocked by divalent cations, such as Ca^{2+} or Ba^{2+} [10]. Side-chain modifications to produce related peptides can change the conductance properties of gramicidin-based channels due to conformational changes or to electrostatic effects[5].

(HCO)HN-L-Val-Gly-L-Ala-D-Leu-
L-Ala-D-Val-L-Val-D-Val-L-Trp-D-Leu-
L-Trp-D-Leu-L-Trp-D-Leu-L-Trp-
$CO(NHCH_2CH_2OH)$

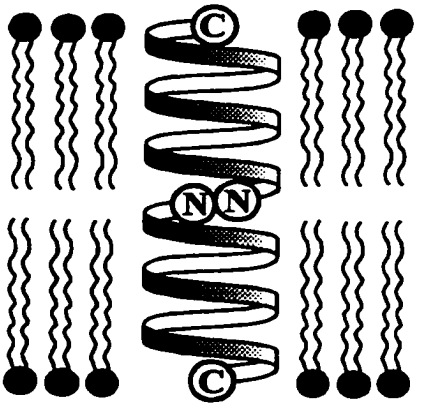

Figure 1.1: Gramicidin A

Amphotericin B is the prototype of membrane ion channels thought to be formed from barrel-like aggregates of amphipathic structures[11]. It is one of a large group (>200) of non-peptide, polyene macrolide antibiotics produced by *Streptomyces sp.* Amphotericin B contains a rigid non-polar heptaene unit and a more flexible polyol region fused together in a macrolactone ring. A mycosamine group and a carboxyl group at one end of the molecule generate a zwitterion in neutral aqueous solutions. The overall length of the molecule is nearly 25 Å which is about half the thickness of a phospholipid bilayer. Based on the result of the conductance across bilayer vs. amphotericin B concentration which shows a high power dependence[12,13], the classic, so called

"barrel-stave model" has been suggested to represent the active amphotericin B channel structure as shown in Figure 1.2. The non-polar hydrophobic polyene would interact with the alkyl chains of the phospholipids to stabilize the aggregate in bilayers, while the polar polyol segments in an aggregate of amphotericin B might self-associate within the membrane to form a hydrated pore. The zwitterionic head groups of the aggregate would be expected to align favorably with the phospholipid head groups. It is proposed that the number of "staves" would be 8 ~ 12 amphotericin molecules, and that the conducting pore has an internal radius of about 4 Å. Other experiments, such as planar bilayer studies, and spectral studies of the amphotericin B complex with steroids, suggest the channels come in several distinct forms[11]. The actual structures of the different channels are still unknown and await further exploration.

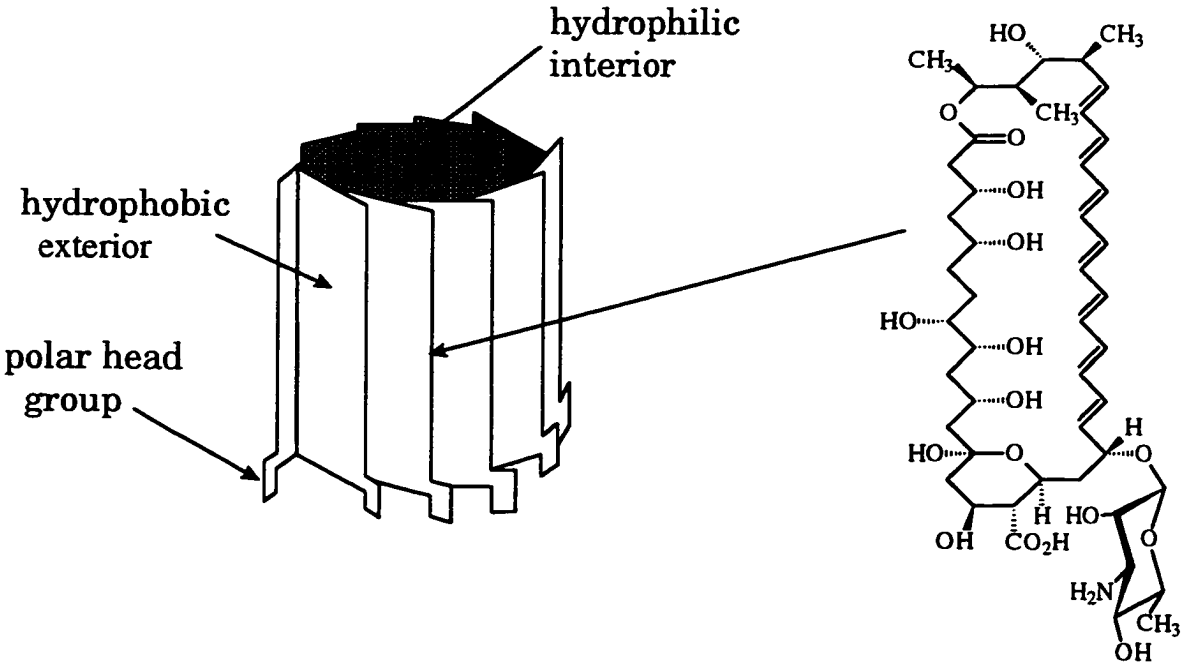

Figure 1.2: Amphotericin B

Alamethicin, which is generated by the fungus *Trichoderma viride*, is a transport antibiotic that has been studied extensively. It is composed of 19 amino acids and 1 amino alcohol: Ac-Aib-Pro-Aib-Ala-Aib-Ala-Gln-Aib-Val-Aib-Gly-Leu-Aib-Pro-Val-Aib-Aib-Glx-Gln-Pheol (Aib refers to α-aminoisobutyric acid or α-methylalanine). The crystal structure of alamethicin shows that it exists in α-helices in contrast to the gramicidin β-helices[5]. Alamethicin is monomeric in most common organic solvents, but in aqueous solutions aggregates have been found to occur. In lipid bilayer membranes, alamethicin aggregates to form a helical bundle, also called a "barrel-stave" model, with a central lumen through which ions can flow[5]. Unlike gramicidin, alamethicin does not show saturation of either current or voltage at high ionic concentration[14]. This suggests that the alamethicin channel aggregates can expand in size in response to transmembrane conditions.

Although alamethicin seems have no selectivity for cations, the most significant feature is its voltage dependence. When it is added to planar bilayers, alamethicin induces a macroscopic current which is strongly voltage dependent as shown in Figure 1.3[15]. Currently there are several different models to try to explain the mechanism of alamethicin channel formation, but the details of the structure of the alamethicin channel are less well characterized when compared to gramicidin. Since α-helices are commonly found in proteins, it is believed that alamethicin may in fact more closely mimic protein ion channels than gramicidin does[4, 5].

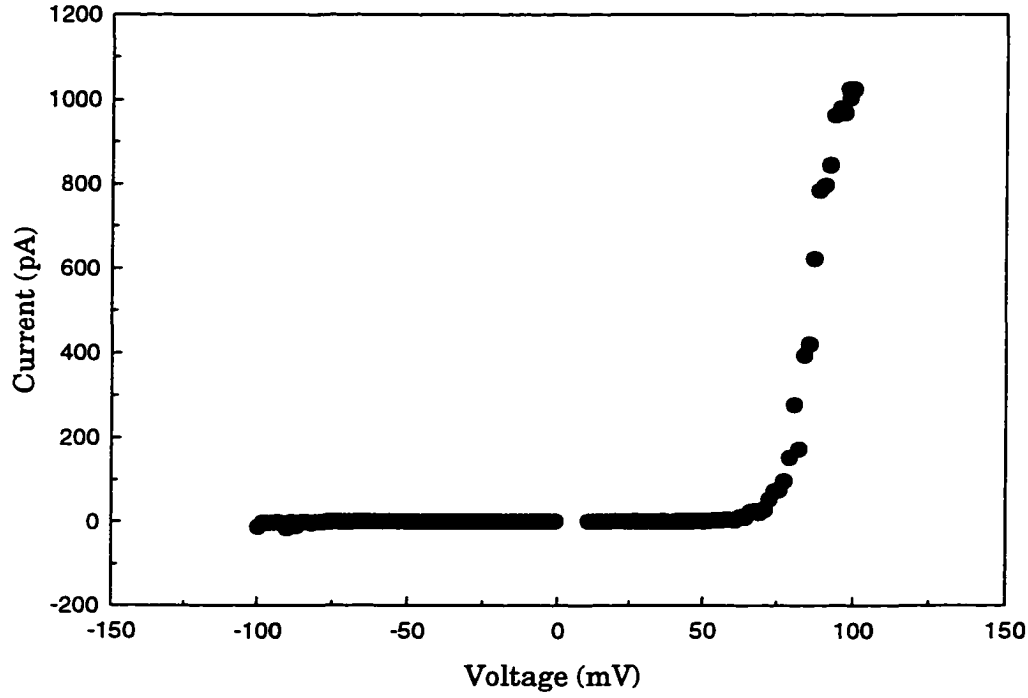

Figure 1.3: Current-voltage (I-V) curve for alamethicin in diphytanoylphosphatidyl choline (DiPhyPC) membrane[15]

1.2 Overview of synthetic ion channels

Although structural information is emerging from molecular biology[2, 3], most of the molecular detail about natural ion channels comes from low molecular weight compounds such as gramicidin, amphotericin, or alamethicin as discussed above[4, 5, 16]. These structural details provide a range of molecular mechanisms for the different natural ion transporters, as shown in Figure 1.4. At one extreme, a carrier mechanism can be envisioned in which a carrier-cation complex is formed which crosses the bilayer by diffusion. For example,

the ionophore antibiotic valinomycin is a typical carrier. At the other extreme, ion channels could be formed by a complete membrane-spanning transporter, such as gramicidin. The channel provides a solvation pathway for ions as they pass through the lipid barrier. Ion channels formed by aggregate pores, like amphotericin and alamethicin, would provide a loosely structured environment containing some water at the core of the aggregate to facilitate stabilization of ions in transit. Lastly, membrane disrupting agents, such as melittin (a peptide from bee venom) or simple detergents, could cause defect structures within bilayers. These might be deep aqueous fjords within the bilayer and represent an extremely primitive type of ion "channel" capable of transport.

In order to elucidate the mechanism of ion transport, and to understand how to achieve ion selectivity and channel gating, several research groups have devoted their efforts to the synthesis of simple artificial ion channels[17]. In comparison with natural ion channels, chemists hope that these devised model systems will provide insight into the functions of transmembrane proteins.

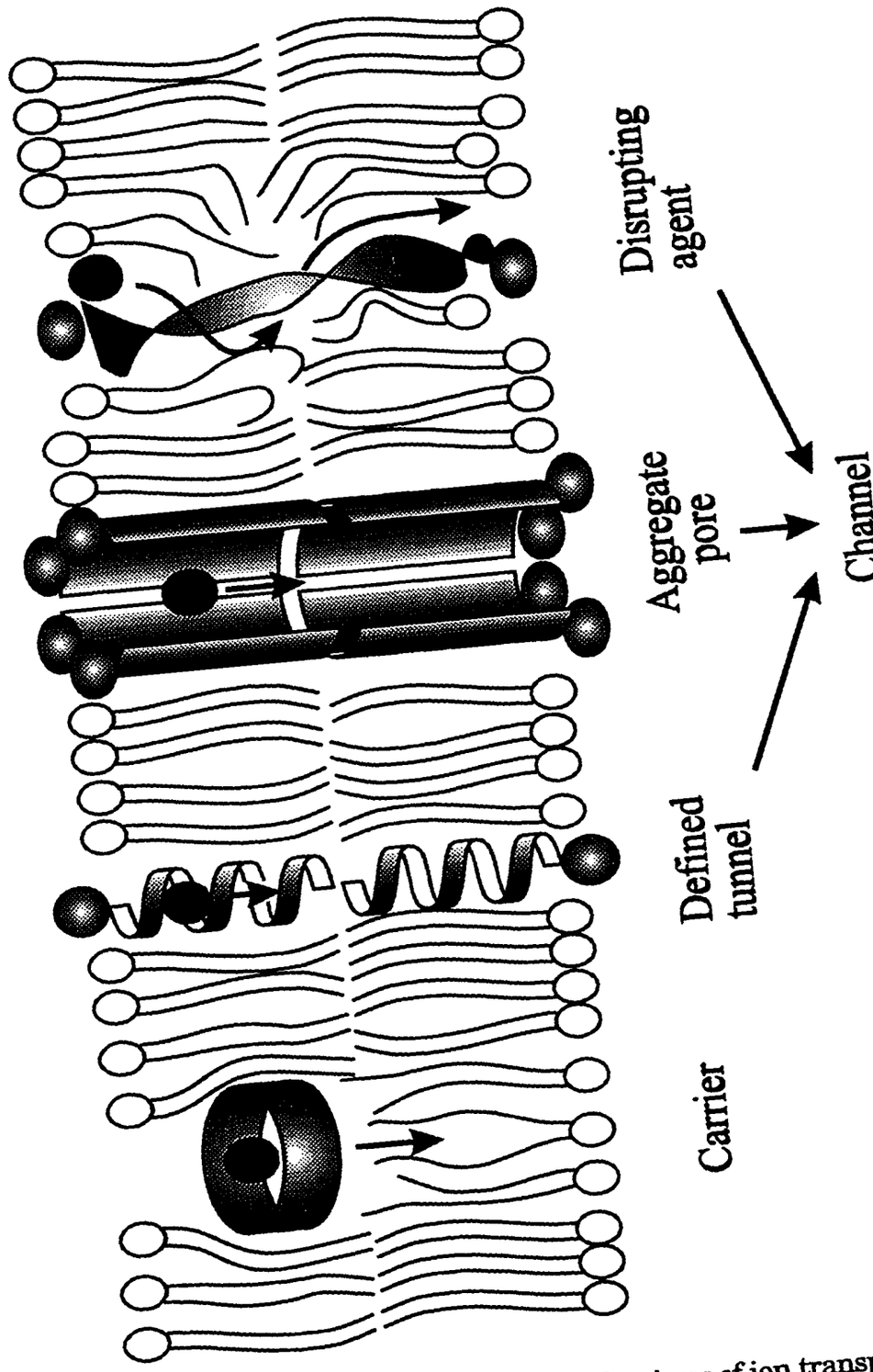

Figure 1.4: Schematic description of mechanisms of ion transporters

To study ion channel proteins, one approach is to synthesize simplified peptides and compare their activity with natural channels. Two examples are noted here. Mutter, Montal and coworkers[18] designed template-assembled synthetic proteins (TASPs) to adopt globular, four-helix bundle structures which form ion channels in lipid bilayers. Their studies suggested the protein molecules aggregated to form heterogeneous conductive oligomers. DeGrado and co-workers synthesized a 21 residue peptide, H_2N-(Leu-Ser-Ser-Leu-Leu-Ser-Leu)$_3$-$CONH_2$, to resemble the acetylcholine receptor which is one of the most studied ion channel proteins[19]. They found the peptide formed single channels in planar bilayers with well defined ion permeability and lifetime. Perhaps due to the complexity of the synthesis and structure modification, there has been no further development from those explorations.

The earliest pioneering work with non-peptide models was designed by Tabushi and coworkers[20]. They used β-cyclodextrin as the backbone of the target which is shown in Figure 1.5. Its fourteen secondary hydroxyl groups provide the polarity to contact the aqueous surface, and the four hydrophobic chains attached to the primary hydroxyl groups stabilize the amphiphile in bilayers. It was described as a "half channel". The channel transported copper and cobalt, and the transport rate was much faster than a specific carrier, diaza-18-crown-6.

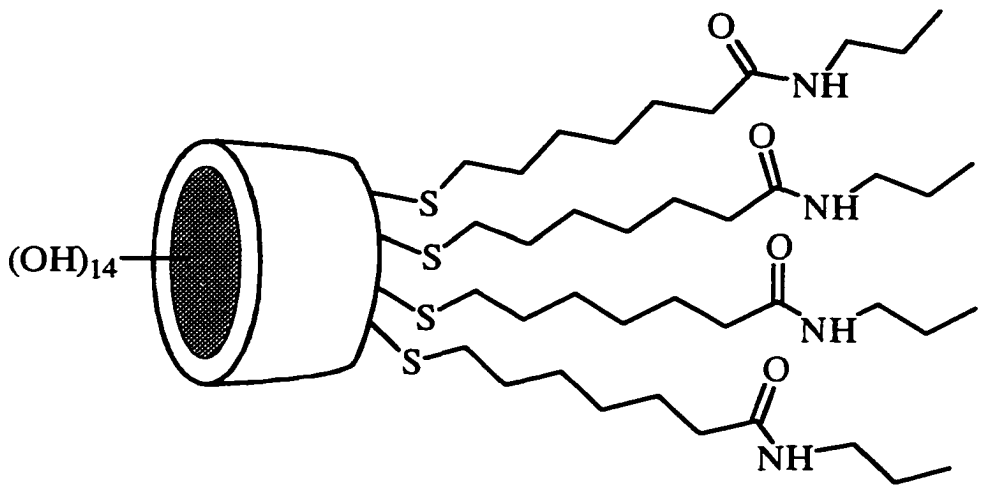

Figure 1.5: Tabushi's β-cyclodextrin ion channel

In order to mimic gramicidin, a unimolecular structure with tunnel-like geometry must be designed to span a bilayer. One example is the so called "chundle[21]", (later changed to "bouquet" molecules) reported by Lehn and coworkers[22]. An 18-crown-6 or a cyclodextrin derivative was used as a rigid collar to which poly(ethylene oxide) chains or polyalkyl chains, and carboxylate head groups were attached (Figure 1.6). Vesicles containing LiCl were prepared from egg PC (phosphatidyl choline) and DPPC (dipalmitoyl phosphatidyl choline). Opposing gradients of Li^+ (inside) and Na^+ (outside of vesicles) were created and the transport of Li^+ and Na^+ down their concentration gradients was monitored directly by ^7Li and ^{23}Na NMR. It was found these "bouquet" molecules caused a one-for-one exchange of Na^+ for Li^+ via a channel mechanism. However, the transport rates for the "bouquet" molecules were relatively slow, their rate constants were $5 \sim 23 \times 10^{-5}$ s^{-1} for the concentrations between 5 to 140 μM.

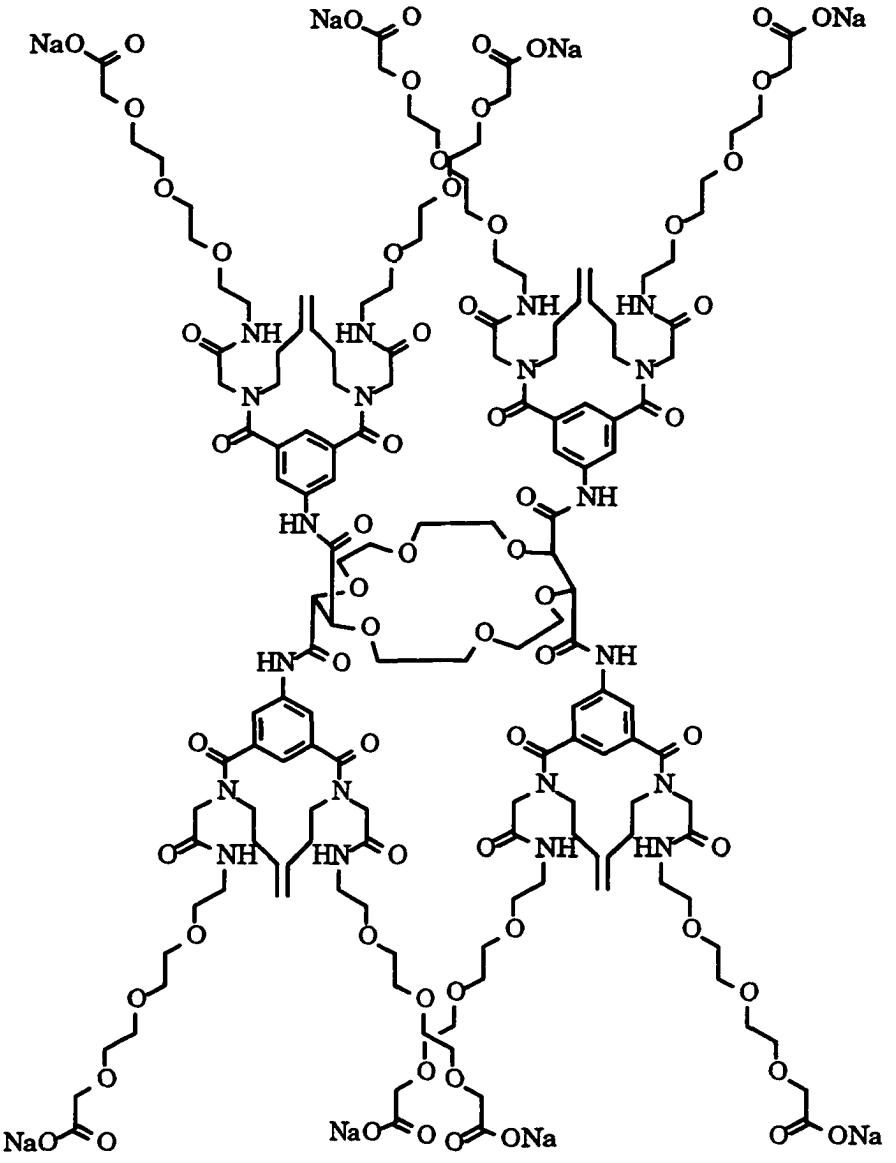

Figure 1.6: One of Lehn's "bouquet" molecules

Another rigid tunnel-like model was reported by Voyer and Robitaille[23]. They synthesized a 21 amino acid peptide composed of fifteen L-leucines and six 21-crown-7-L-phenylalanines. The peptide backbone formed an α-helical chain, so by placing the crown ethers on every fourth residue, the crown ethers would all be located on the same side of the helix to form a channel for ions. A pH-

stat titration method indicated that the peptide spanned bilayer vesicles to form a channel, although there was no monovalent cation selectivity.

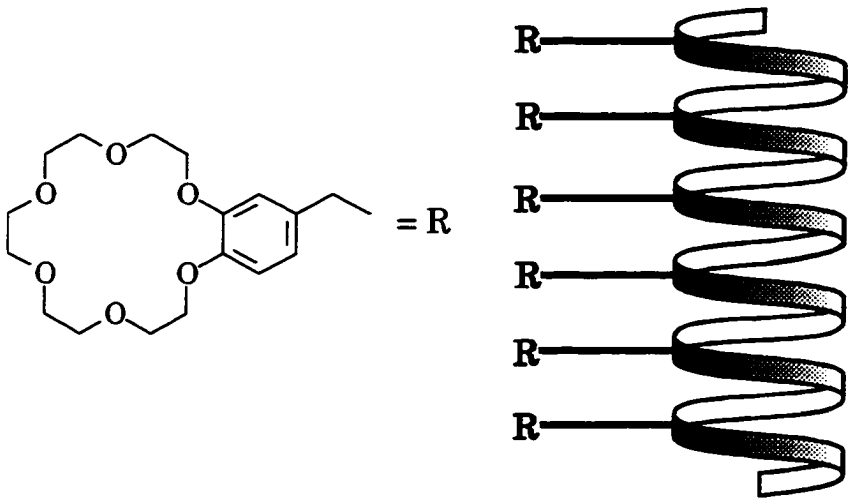

Figure 1.7: Voyer's ion channel model

Structurally sophisticated aggregate channels were synthesized by Ghadiri's group[24]. The system is a eight amino acid cyclic polypeptide, cyclo[(Trp-D-Leu)$_3$Gln-D-Leu-] (Figure 1.8). The amino acid side chains were placed roughly along the equator of the cycle and directed away from the center. When the peptide is incorporated into bilayer membranes, a channel is formed through hydrophobic side chain - lipid interactions and hydrogen bonding between cyclic peptides similar to β-sheet formation. The system is active in both vesicle and planar bilayers, and shows typical single channel conductance behavior. The pore formed by stacking the cyclic peptide is 0.5 nm in diameter, and it does not have a significant alkali metal ion selectivity.

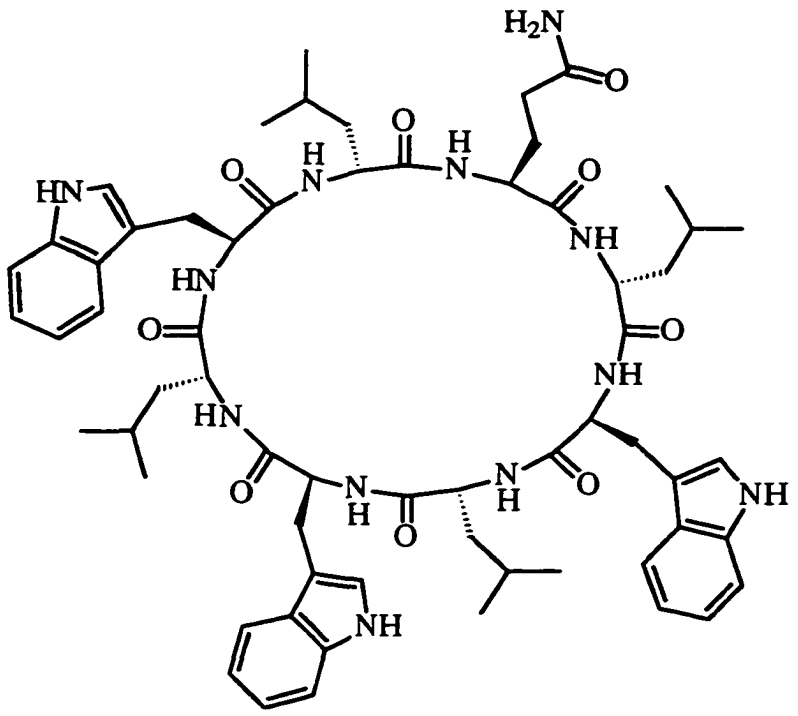

Figure 1.8: Ghadiri's cyclic peptide channel

A flexible tris-macrocyclic channel model was developed by Gokel's group[25]. Two macrocycles are used as head group anchors, and a third one in the middle is a central relay. Diaza-18-crown-6 was chosen as the macrocycle in the system due to its cation selectivity, and alkyl chains connect the three macrocycles to reach to the desired length (see Figure 1.9). In phospholipid bilayer vesicle membranes, cation flux through this channel system was assessed by a fluorescence technique using pyranine as a indicator and ^{23}Na NMR spectroscopy. The cation conduction for the channel in Figure 1.9 was as much as 40 % of the activity of gramicidin under the same conditions. Their studies also indicate that the ionophore really does not require a tunnel-like conformation in order to function[25].

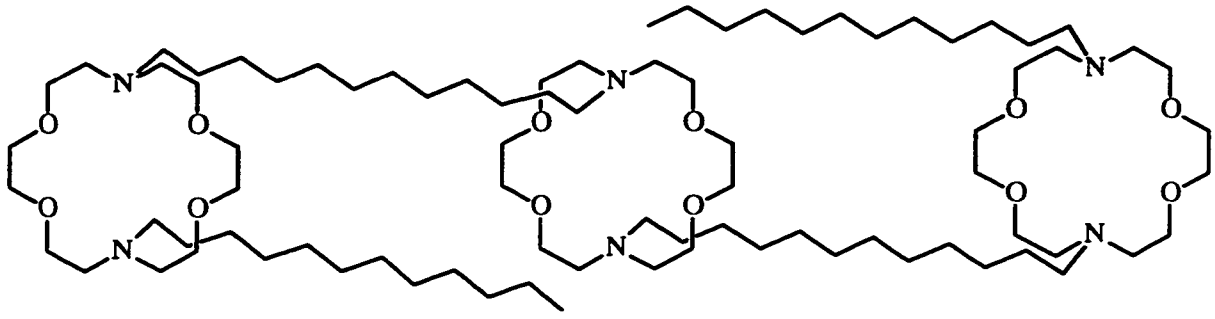

Figure 1.9: Gokel's tris-macrocyclic channel system

Fuhrhop's group was the first to use the term "bolaamphiphiles" to name amphiphilic molecules with polar head groups at both ends of a hydrophobic core[26]. They also reported a number of bolaamphiphiles capable of forming thin monolayer lipid membranes, presumably via aggregate structures. One of their typical bolaamphiphiles is shown at Figure 1.10. They found monensin pyromellitate which has both hydrophobic and hydrophilic sides could perforate the thin monolayer vesicles made from electronegative or electroneutral bola-amphiphiles and make the membrane permeable to Li^+ ions.

Another flexible channel system is an ion pair model demonstrated by Kobuke and co-workers[27]. As shown in Figure 1.11, the phosphate monoester or carboxylate terminated tetra(1, 4 - butyleneglycol) monobutyl ether combined with dioctadecyldimethylammonium cation to form an ion pair. When the ion pair was incorporated into planar lipid bilayers, a single channel recording showed stable and constant currents. They also observed an irregular voltage dependent property for the phosphate-ammonium ion pair.

However, there was no direct evidence to support the aggregation in bilayers, and there was no cation selectivity for these ion channels.

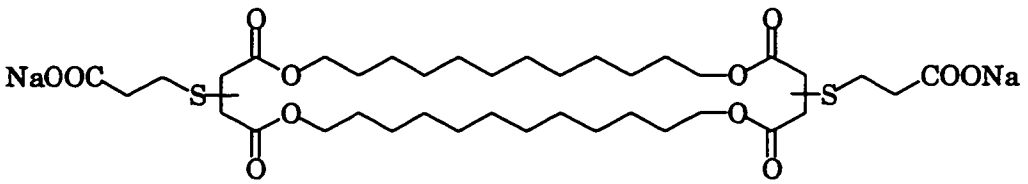

Fuhrhop's bolaamphiphile

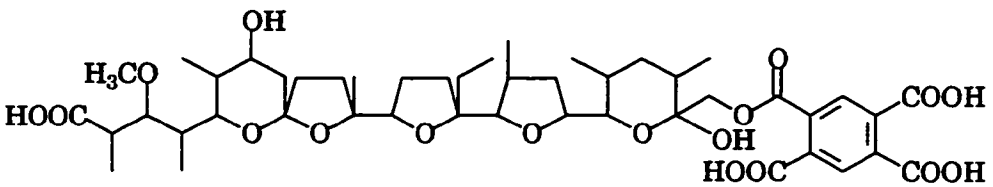

Monensin pyromellitate

Figure 1.10: Fuhrhop's monolayer system

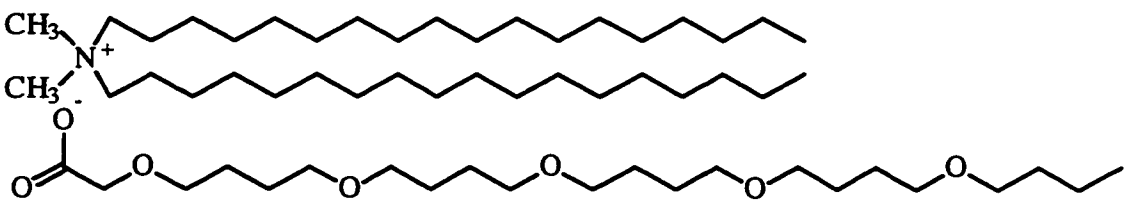

or

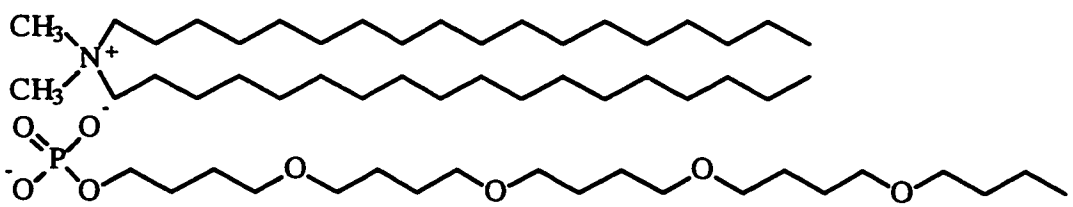

Figure 1.11: Kobuke's ion pair system

Regen and co-workers reported two series of compounds: one called bolaphiles[28] and the other called a bola-amphiphile system[29]. The former were diesters synthesized from an homologous series of linear saturated, olefinic, and acetylenic α,ω-dicarboxylic acids with hexaethylene glycol (see examples in Figure 1.12). Bilayer vesicle experiments indicated this series behaved as membrane-disrupting agents and the most active bolaphiles were three times more active than the detergent Triton X-100 [28]. The bola-amphiphile was a sterol-polyether conjugated 5-androstene derivative (Figure 1.12) designed to mimic the antibiotic amphotericin B. Using a similar method to Lehn[22], Na^+ transport was monitored by ^{23}Na NMR. LiCl was incorporated inside of egg PC vesicle bilayers. Li^+ exit (antiport) and/or Cl^- entry (symport) maintains electroneutrality on both sides of the membrane, and permits the collapse of a Na^+ concentration gradient (the transmembrane potential drives the ion transport). The experimental data indicated ion channels were formed through aggregation at high concentrations of bola-amphiphiles[29].

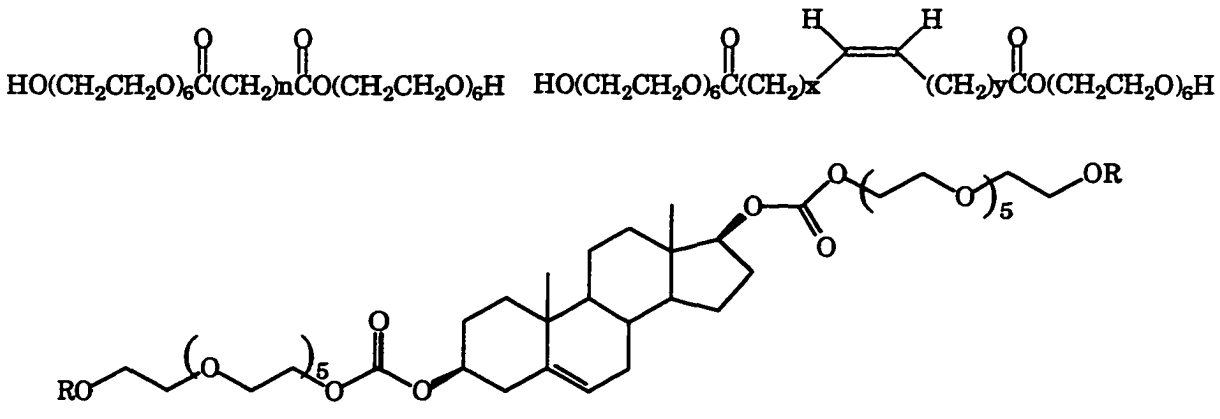

Figure 1.12: Regen's bolaphiles and bola-amphiphile compounds

1.3 The early explorations from Fyles' group

Combining information from natural and artificial ion transporters leads to the following criteria for designing membrane active transporters: The transporter should be an amphiphile, and have suitable columnar shape which combines with its hydrophobic part to incorporate into bilayers. It should span a 4 nm thick bilayer either as a monomer or as an aggregate, and it should simultaneously surround an ion of at least 0.3 nm diameter. The hydrophilic part of the transporter should provide a potential path for the ions or should provide ionophilic sites deep within the lipid core of the bilayer. During the transit of ions across the bilayer, the transporter must accommodate the ion solvation requirement either by partial replacement of the ion solvation sphere with transporter-cation interactions or by introduction of water within the lipid core of the bilayer. A final requirement for the transporter is that a feasible and efficient convergent synthesis should be possible.

In our group's early explorations there were two different types of ion channels made. One system is illustrated in Figure 1.13, and was mainly synthesized by Dr. T. James[30]. All transporters are unimolecular structures: an 18-crown-6 derivative is used as a central core, and macrocycles are linked to both sides of the crown ether to allow the transporter to span the bilayer, then polar head groups are capped on the macrocycles to create the amphiphilic character needed to contact the aqueous phases. Transporters in this system are fairly rigid due to the specific conformation of the crown ether core. They form a tunnel-like channel, and kinetic measurements verify that there was no

aggregation formed[31].

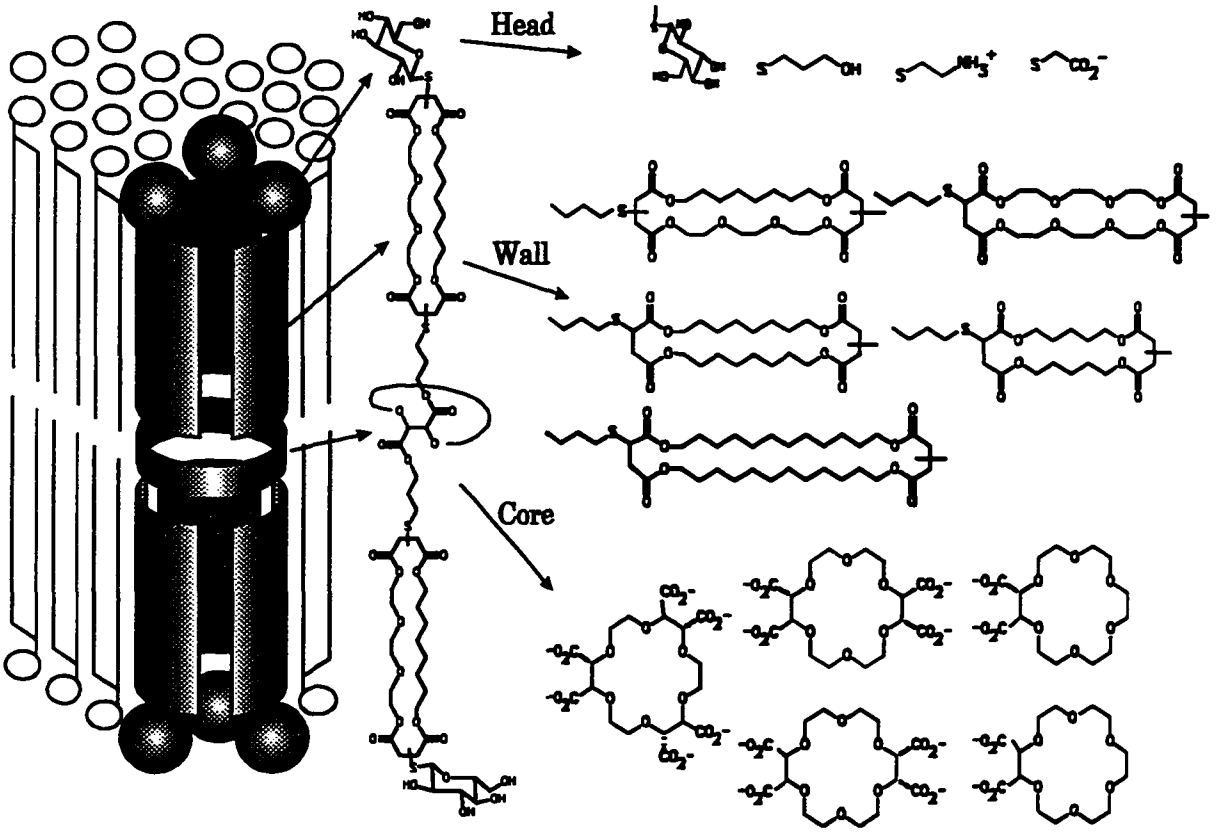

Figure 1.13: Tunnel-defined channels

The other system is illustrated in Figure 1.14, and mainly synthesized by Dr. M. Zojaji[32]. The main difference from the first system is that either propyl tartaric ester or meta-xylyl was used as central linker to form a more flexible structure. The kinetic measurements indicated that the transporters in this system form active aggregates in bilayer vesicles.

To distinguish these two systems, the former is called "channel" due to its unimolecular tunnel-like conformation, and the latter one is named of "pore-former" since it forms aggregation and its structure is quite flexible.

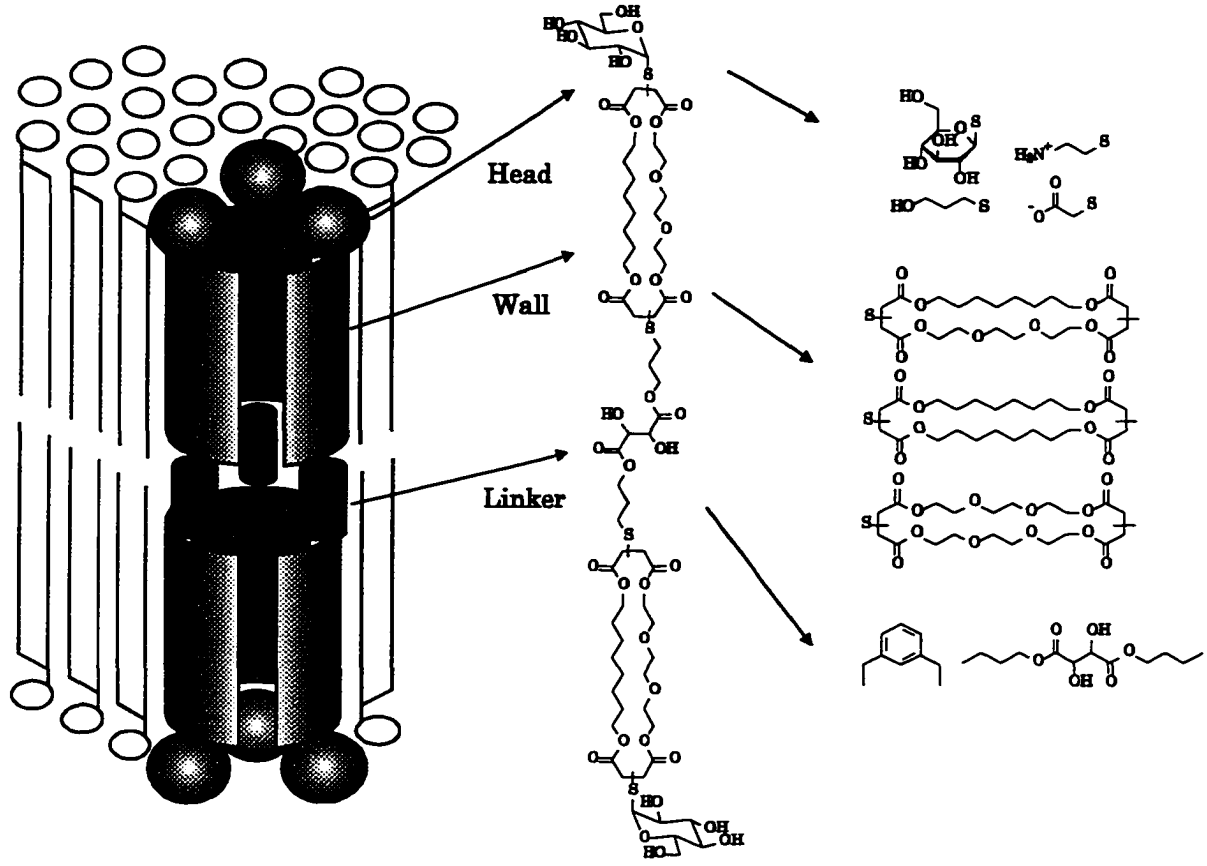

Figure 1.14: Channels formed by aggregate pores

1.4 The design of research targets in this thesis

The emphasis of this thesis is to develop a new series of bolaamphiphiles to achieve artificial voltage-gated ion channels[33] based on modular subunits developed in earlier work[32]. In essence we are looking for an artificial version of alamethicin with potential ion selectivity.

Ion selectivity of aggregated channels is different from that of carrier type of compounds, such as crown ethers, or valinomycin. In these cases the structure relates to carrier size, charge, and binding site. The aggregated channels are relatively loosely bound collections of transporter monomers, and

there are a lot of unanswered questions about their detailed structures, forming mechanism, and structurally determined factors. These remaining puzzles need to be solved gradually in the exploration of artificial channels.

In our transporter system, to achieve alkali-metal cation selectivity for aggregate bola-amphiphiles, the size of the aggregate needs to be limited. Thus we are interested in active dimers or trimers which are closely similar to lipids in both cross-sectional area and chain length.

While bolaamphiphiles span the bilayers, the central linker should be able not only to facilitate ionic passage through the channel but also to stabilize the transporter within the bilayer. This means that the central linker has to be a well balanced mixture of hydrophobic and hydrophilic character. The design proposal is illustrated on Figure 1.15. Compared with the central linkers in early work[32], it is envisaged that the new linker should be less bulky and have fewer functional groups. At the same time, the effect of central linker length on transport activity will be examined.

In order to achieve the goal of a voltage-gated channel, the other important component, the head group, has to be closely considered. When the polarity of a voltage applied to the bilayer is switched, the bola-amphiphile should respond by a reorientation in the bilayer. In other words, the head groups on two ends of the bola-amphiphile should be different to create a large molecular dipole. Therefore, our initial strategy was to synthesize bola-amphiphiles bearing one head group having a negative charge and the other head group having a positive charge (at pH=7). At the same time, two more

control bolaamphiphiles should be synthesized to compare the relative activities of symmetrical and neutral analogs. Later in this thesis work, one more head group carrying -2 charge (pH = 7) was added to this set of targets.

As described in the early work[30, 32], macrocyclic tetraesters were used as building blocks in the syntheses. Two series of bola-amphiphiles were created to test the importance of the effects of hydrophobicity and hydrophicility on transport.

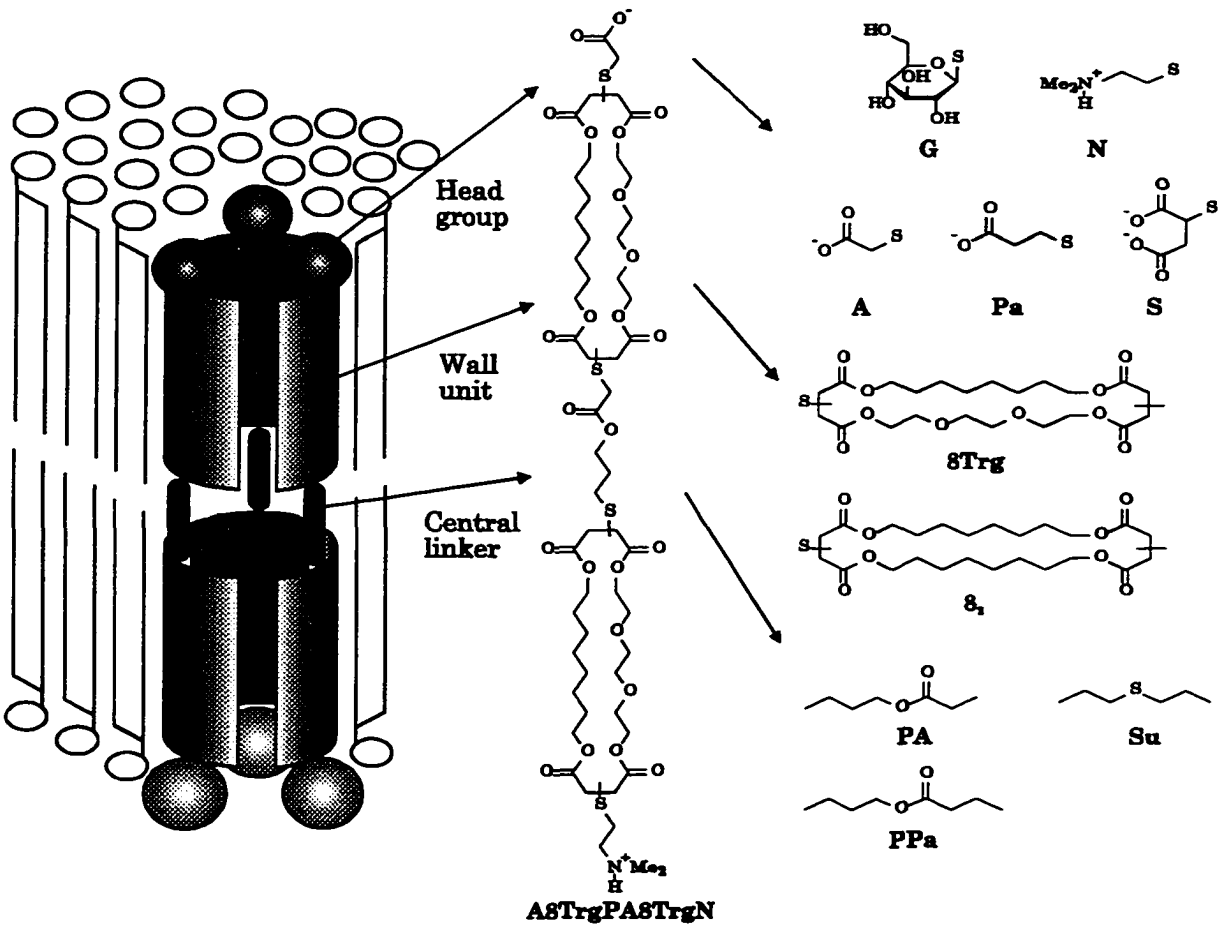

Figure 1.15: Design proposal for pore formation by aggregation of bola-amphiphiles

To get suitable structures for potential voltage-gated ion channels, molecular modeling with CAChe scientific computing program was used to assist the design. Since the present computer program cannot simulate behaviors of larger aggregates of molecules in lipid bilayer membranes, the possible global minimum conformations of candidates in gas phase were investigated to provide indirect evidence for their possible molecular shapes. The extended shapes are the potential structures expected and molecules which fold are less interesting as candidate pore-formers.

To simplify naming and give some standard information on the number of combinations possible, a structure-based semi-systematic naming system is described as follows and equated on Figure 1.15: 1) Each synthon was assigned one or two simple letter or number name: **A** = 2-mercaptoacetic acid or 2-mercaptoacetic carboxylate, **G** = 1-mercapto-β-D-glucose, **Pa** = 3-mercaptopropionic acid or 3-mercatopropionic carboxylate, **8** = from 1,8-octanediol, **Trg** = from triethylene glycol, **P** = 3-mercaptopropyl, **Su** = 2-mercaptoethyl sulfide, etc. 2) Each intermediate is named as a combination of its synthon abbreviations with the exception that the maleate esters of the wall units are implied: **8Trg** = the macrocyclic tetraester derived from 1 mole of 1,8-octanediol and 1 mole of triethylene glycol (and 2 moles of maleic anhydride), $\mathbf{8_2}$ = the macrocyclic tetraester from 2 moles of 1,8-octanediol (and 2 moles of maleic anhydride), etc. 3) The final structures are named from one head group to the other head group: head group 1 + wall unit + central linker + wall unit +

head group 2. As shown in Figure 1.15, **A8TrgPA8TrgN** represents: a mercaptoacetic acid head group + a tetraester wall unit made from 1,8-octanediol and triethylene glycol + a central linker derived from 3-mercaptopropanol and 2-mercaptoacetic acid + the same wall unit + an N,N-dimethylaminoethanethiol head group.

It can be envisaged that membrane spanning bola-amphiphile units in which the macrocycle 8Trg is used as wall unit will orient to create an aggregate in which the polar part of the 8Trg is toward the inside of the aggregates and the non-polar segment toward the lipid when transporters are incorporated into bilayers. However, when macrocycle 8_2 is used as wall unit, the possibility for forming an aggregate will be greatly decreased due to the loss of most of its hydrophicility.

The transport properties were investigated through pH-stat titration of vesicles and with a planar bilayer experiment. The pH-stat titration measured transport properties via a cation-proton antiport[34] across vesicle bilayers[31, 32]. Through data processing, the kinetic behaviors of transporters can be closely investigated. Transport rates which are normalized to the same concentration can be used to compare the transporter's relative activities and cation selectivities. The apparent kinetic order also can be obtained to look at aggregation of the transporter in bilayers[31, 32]. However, the pH-stat technique only measures the cation dependence of initiation of a transport process which rapidly equilibrates each vesicle within the time of a single opening. That means pH-stat titration does not directly probe the ion translocation process,

and it only examines the average behaviors of transporters.

The ion translocation process can be directly observed using the planar bilayer experiment[35]. This experiment measures the time dependence of the current carried across a planar bilayer formed on a small hole in a hydrophobic support barrier. It can detect the behavior of a single channel[36]. This technique provides unambiguous demonstration of a channel mechanism and can provide molecular details of the ion translocation process. More importantly it is an excellent tool to measure the voltage-gated property of an ion channel. Except for some very well defined cases, the planar bilayer experiment provides relatively little information about the initiation of channel openings. Using a combination of the two different techniques (planar bilayer and vesicle), the transport properties of a ion channel can be explored from different angles. Hopefully enough information can be obtained to lead to a composite portrait of the channel mechanism in molecular detail not only for a regular channel, but also for a voltage-gated ion channel.

CHAPTER 2 SYNTHESIS

2.1 Overview

Following earlier work in the group[30, 32] , a convergent synthesis was used in this thesis to construct transporter candidates based on modular subunits as previously explored (Figure 2.1). Commercial reagents were used whenever possible to simplify and optimize the synthesis. The synthesis started from two different macrocycles, 8Trg and 8_2, which were subsequently modified to different derivatives. The two macrocyclic derivatives, mesylate and carboxylate, then were coupled to hold one polar head group. Finally, the second polar head group was added to give a bolaamphiphile, pore-former candidate. From different combinations of wall unit, linker, and head group, it is hoped that the regulation of ion transport across bilayer membranes can be detected and controlled.

2.2 Syntheses of macrocycles

Syntheses of tetraester diene macrocycles followed the procedures reported previously[30, 32] with minor changes to improve handling and separation. 1,8-Octanediol reacted with two equivalent of maleic anhydride to give a diacid (**1**) which was esterified with either triethylene glycol or 1,8-octanediol to form the macrocycles 8Trg (**2**) or 8_2 (**3**) [30] (Scheme 2.1). The purification of macrocycles was the major challenge of this step of the syntheses. Macrocycle 8_2 is relatively easy to separate; the crude oily product of the macrocyclization can be washed with diethyl ether a few times to give an

oily solid, followed by several recrystallizations from ethyl acetate to give pure 8_2 (**3**). The total yield of the two steps was 14%.

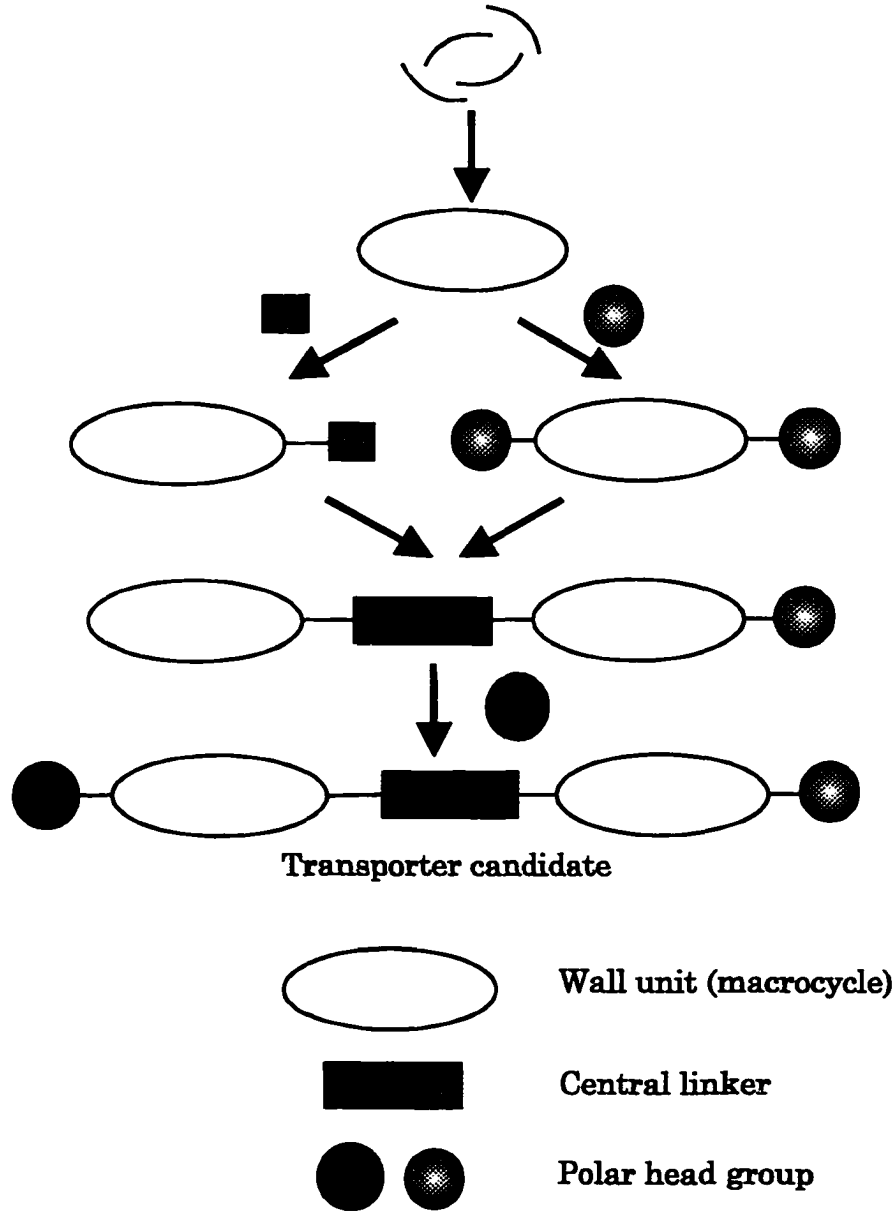

Figure 2.1: Synthetic strategy for making transporter candidates

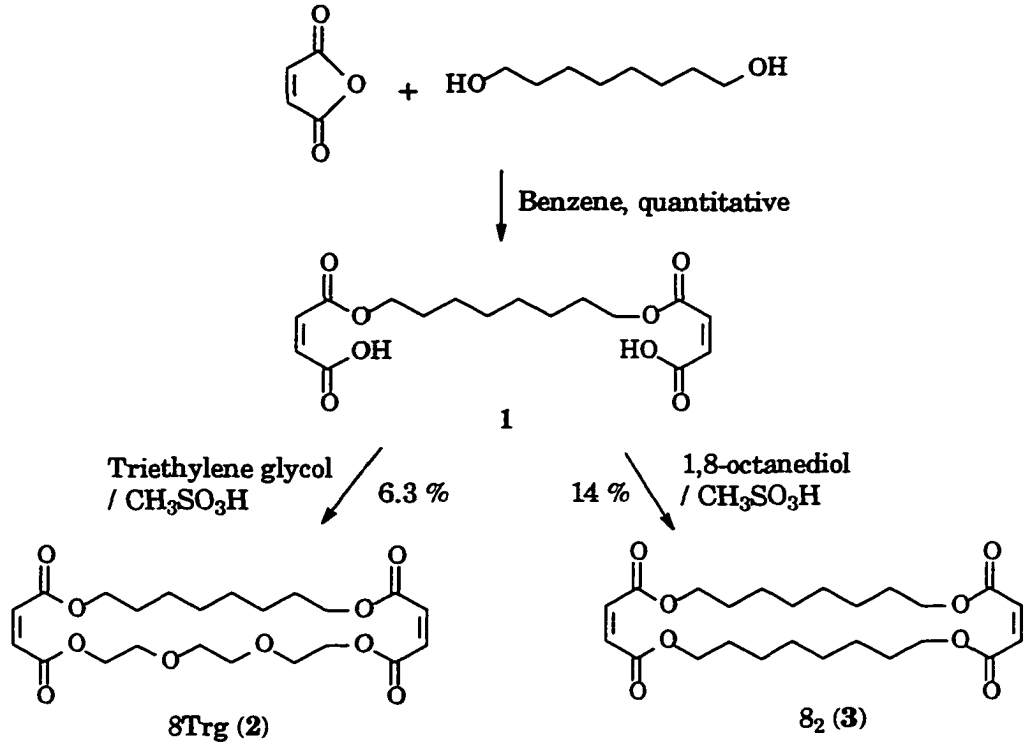

Scheme 2.1: Syntheses of macrocycles

The isolation of 8Trg is more arduous. The mixture of five compounds and polymer by-products (Scheme 2.2) was chromatographed on silica gel via pre-absorption to remove compounds **3**, **6**, and some of the polymer product. Kugelrhor distillation was then used to fractionate the product-containing chromatography fractions. Compounds **4**, **5**, and the rest of the polymer product were removed, and pure 8Trg (**2**) was obtained. Due to the various by-products and the losses in the process, the yield of **2** was only 6.3%.

The syntheses of the two macrocycles were revisited at least four times each during the course of this project. Based on the previous work done by James[30] and Zojaji[32], various improvements to the macrocyclization were

attempted. The purification of macrocycle **2** and **3** was improved over previous reports and by-products **3** and **6** were isolated in pure form from the purification process of macrocycle **2**. However, the yield of macrocycle couldn't be further improved, and the yields shown on Scheme 2.1 are unchanged from earlier reports.

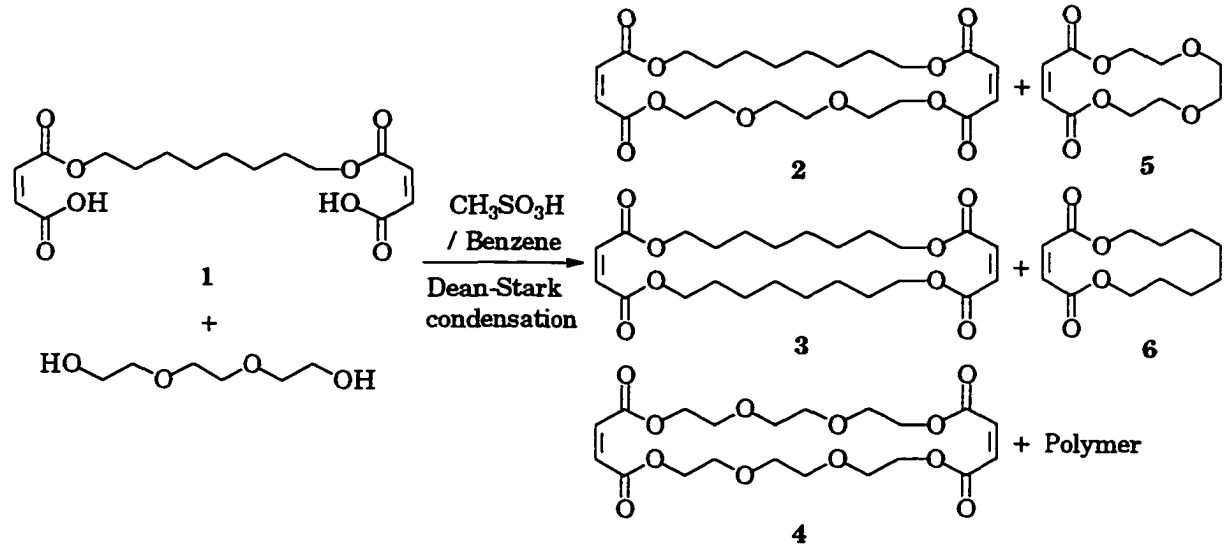

Scheme 2.2: Formation of 8Trg

2.3 Syntheses of transporter candidates in the 8Trg series

2.3.1 Syntheses of derivatives of macrocycle 8Trg

Following prior work[30, 32], the tetraester diene macrocycle 8Trg (**2**) was converted to the mono-alcohol **7** via Michael addition of 3-mercaptopropanol (Scheme 2.3). Three compounds were isolated: unreacted macrocycle 8Trg **2**, the mono-adduct **7**, and the double-adduct (not shown in Scheme 2.3). In a modification of published work, carefully controlled silica column

chromatography could separate this mixture to give pure mono-adduct **7** and recovered macrocycle **2**. Mono-alcohol **7** reacted with methanesulphonyl chloride to yield the mesylate **8** [30]. The yield of the two steps was 36%, unchanged from previous reports.

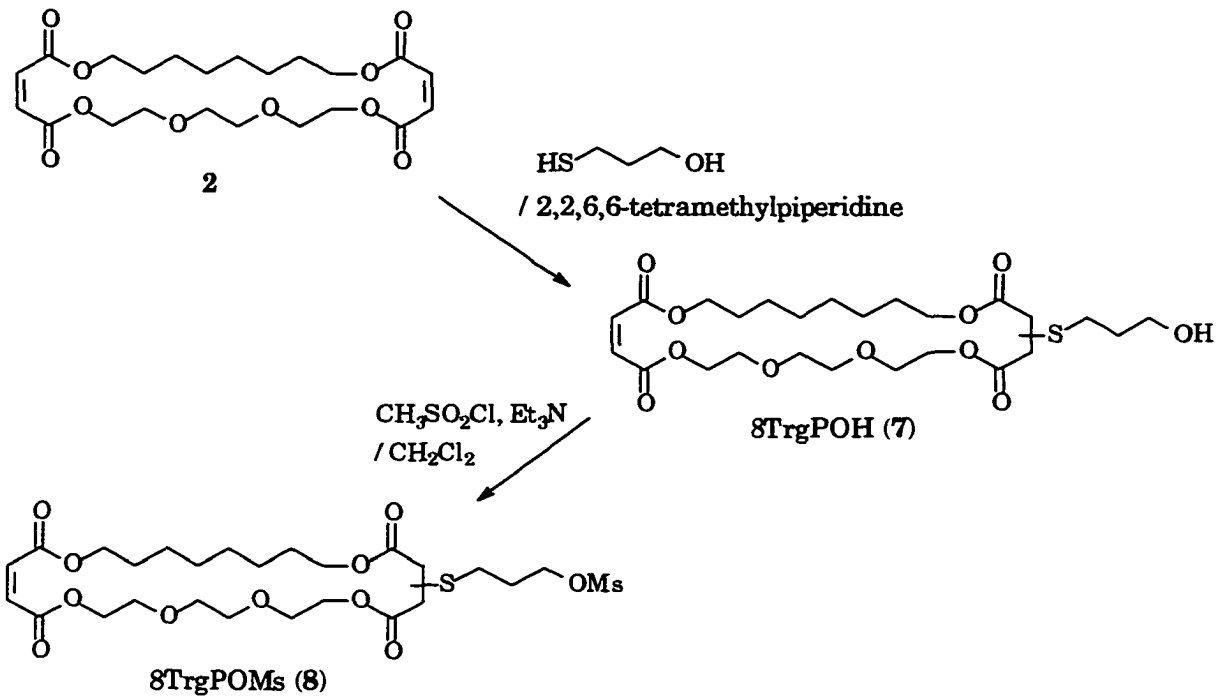

Scheme 2.3: Synthesis of mono-adduct of the macrocycle **2**

New compounds, the diacid A8TrgA (**9**) and the mono acid 8TrgA (**10**), were obtained through Michael addition of 2-mercaptoacetic acid catalyzed by 2,2,6,6-tetramethylpiperidine (Scheme 2.4). The product mixture of this reaction was dependent on the reaction time. The double Michael addition could be completed with longer reaction times, typically more than 24 h, and **9** could be obtained through a simple work up. However, after a shorter reaction time, for example 6 h, the product was a mixture of double adduct **9**, and mono

adduct **10**, plus the unreacted macrocycle **2**.

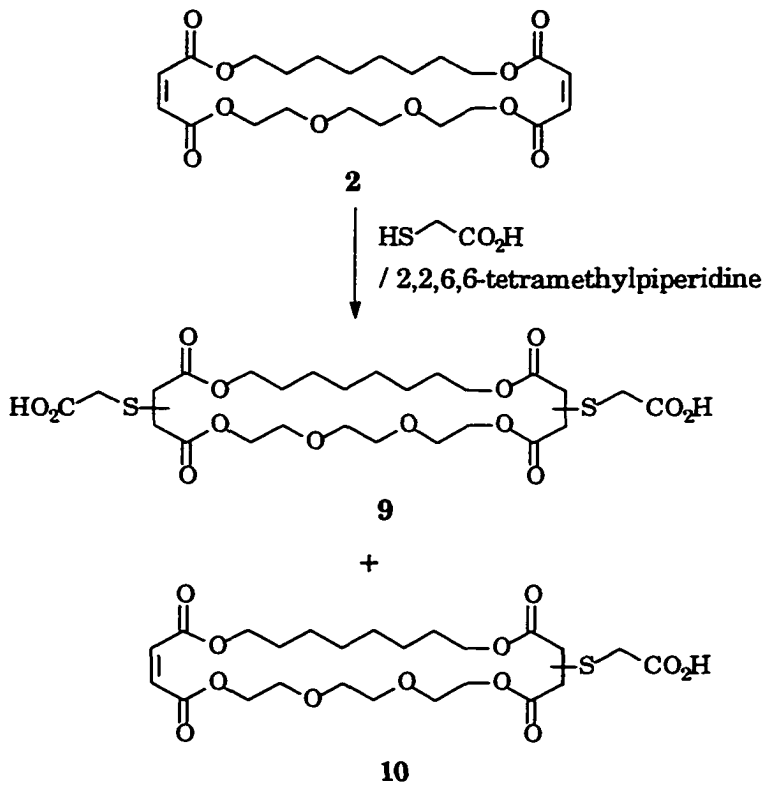

Scheme 2.4: Syntheses of new adducts **9** and **10**

Through a fortuitous accident, the separation of the mixture of **9** and **10** was found to be possible by silica column chromatography using a solvent gradient of hexanes and ethyl acetate. There was some degree of product loss on the silica column, but the separation was achieved cleanly. When the mixture of reactants was refluxed for 6 h, the yield for **10** was 12% and the yield for **9** was 69% after the purification.

Figures 2.2, and 2.3 compare the ^{1}H and ^{13}C NMR spectra of A8TrgA (**9**) and 8TrgA (**10**). In the ^{1}H NMR spectrum of A8TrgA (**9**), there was a broad singlet at 8.75 ppm due to the acidic protons (**a**). The methylene protons (**b**) adjacent to the carboxyl are seen between 4.27 ppm and 4.06 ppm as a

multiplet, and the methylene protons (**d**) adjacent to the ether group formed another multiplet between 3.69 ppm and 3.64 ppm. The two inequivalent methylene protons (**e**) on the acetic acid side chain coupled with each other. Since there were three possible regio-iosomers formed, a total of four protons gave three sets of doublets of doublets from 3.57 ppm to 3.30 ppm. The methine proton (**c**) adjacent to sulfide coupled with two inequivalent methylene protons (**f**) on the ring to form a multiplet at 3.89 ~ 3.82 ppm, and those two methylene protons (**f**) gave two sets of multiplets from 3.00 to 2.66 ppm. The methylene protons (**g**, **h**, **i**) on the hydrocarbon chain of the macrocycle gave a broad multiplet and a broad singlet at 1.61 ~ 1.59 ppm and 1.31 ppm. Note that there are sixteen possible enantiomers plus diasteromers for **9**.

In comparison with **9**, the ^{1}H NMR spectrum of 8TrgA (**10**) revealed more details about the macrocycle conformation. Both spectra had quite similar patterns for most protons, except for very small differences in chemical shifts. The acidic proton (**a**) of compound **10** moved to 8.34 ppm. Two singlets at 6.77 and 6.19 ppm were due to the methine protons (**b**) of the olefin. The former was from the *trans* conformation of the olefin, and the latter one was from the dominant *cis* conformation. The methine proton (**d**) on the ring, and two different inequivalent methylene protons (**f**, **g**) all showed doublets of doublets. One set of doublet of doublets from proton **f** was much bigger than the other one. This could be due to the selective formation of one of two possible regio-isomers at each end of the macrocycle.

For the ^{13}C NMR spectrum of **9**, the carbonyls from the carboxylic acid (**a**) showed four peaks at 173.6, 173.5, 173.4, and 173.3 ppm, and the carbonyls from the ester groups of the macrocycle (**b**) gave three peaks at 170.9, 170.8, 170.0 ppm. The methylene carbons (**c**) from the ether group were in two sets at 70.1, 70.0, 68.7, 68.6 ppm. The methylene carbons (**d**) adjacent to the carboxyl gave four lines at 65.4, 64.9, 64.3, 63.7 ppm. A pair of lines at 41.7 and 41.5 ppm was contributed from the methine carbon (**e**) adjacent to sulfide. The methylene carbons (**g**) on the acetic acid side chain were a pair of peaks at 33.1, 32.8 ppm, and the methylenes (**f**) on the ring were another pair at 35.9, 35.7 ppm. The remaining signals 28.4, 28.1, 25.2, and 25.1 ppm were due to the methylene carbons (**h, i, j**) from the hydrocarbon chain of macrocycle.

In comparison to **9**, the ^{13}C NMR spectrum of 8TrgA (**10**) had some extra peaks: 165.3, 165.0 ppm were due to the α,β-unsaturated carbonyl carbons (**c**), 133.8, 133.0 ppm were contributed from the *trans*, and 130.2, 130.1, 129.3, 129.1 ppm were from the *cis* olefin (**d**). The rest of the assignments for chemical shifts were quite similar to compound **9** except the relative ratios were different. These different ratios again verified the selective contribution from one of two possible regio-isomers indicated in the ^{1}H NMR spectrum analysis. From chemical shift considerations, the favored regio-isomer for **10** would be the one shown in Figures 2.2 and 2.3.

The successful isolation of mono-adduct 8TrgA (**10**) will allow more and different combinations of head groups of transporter candidates in future

exploration.

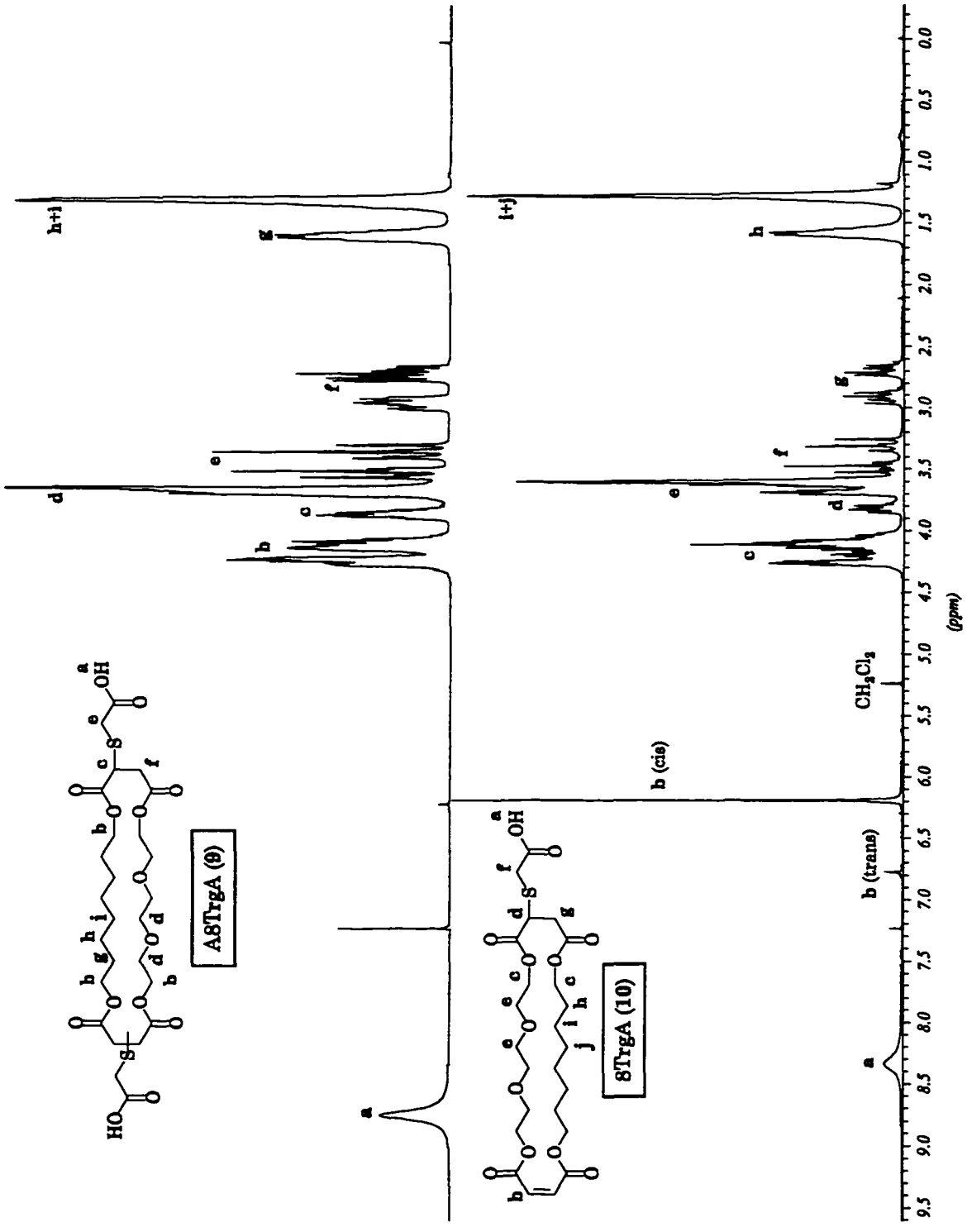

Figure 2.2: ^1H NMR ($CDCl_3$) spectra of A8TrgA (**9**) and 8TrgA (**10**)

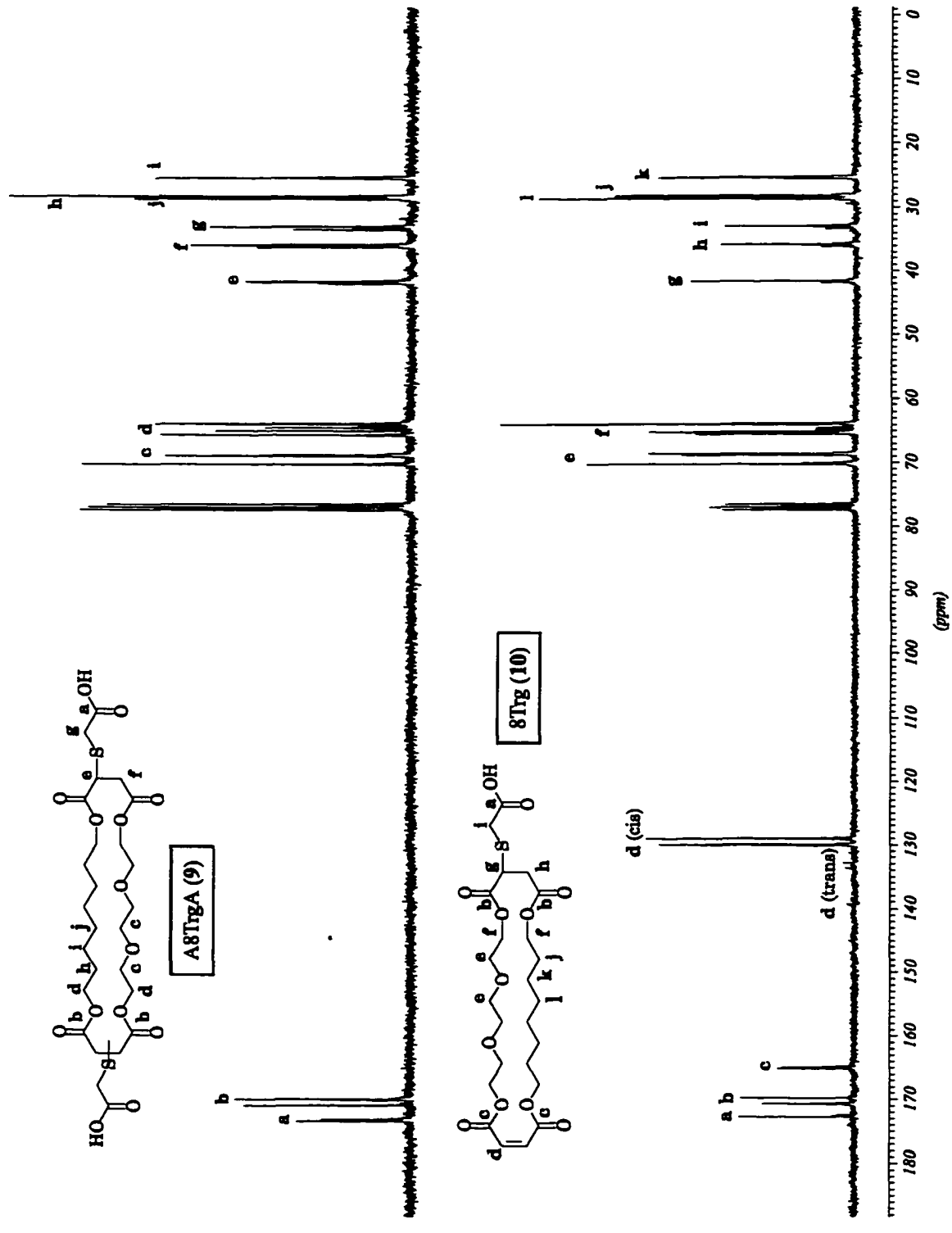

Figure 2.3: ^{13}C NMR ($CDCl_3$) spectra of A8TrgA (**9**) and 8TrgA (**10**)

2.3.2 Coupling reaction to make bis-macrocycles

The coupling of the two macrocyclic derivative **8** and **9**, was carried out using tetramethylammonium hydroxide pentahydrate in DMSO to form the ester bond as the middle linker. Once again, separation was the main obstacle in the synthesis. Statistically, the products formed from this mono-alkylation are the desired bis-macrocycle, 8TrgPA8TrgA (**11**), and a by-product tris-macrocycle 8TrgPA8TrgAP8Trg (**12**), plus unreacted starting materials (Scheme 2.5). Due to their comparable polarity, silica or alumina column chromatography is not able to separate bis-macrocycle (**11**) from tris-macrocycle (**12**). In consideration of the molecular weight difference between them, gel permeation chromatography, also called size exclusion chromatography, was used to explore the separation. After several different types and pore-sizes of gel were investigated, Lipophilic Sephadex LH-20 was finally chosen as the most suitable one, and the mixed solvent, chloroform : 2-propanol = 4 : 3, was used as packing solvent and eluent. However, the mixture could not be separated in a single step. Therefore, after each separation, the mixed fractions were combined, and carried over to a subsequent separation step. Since TLC was not good enough for monitoring to detect mixed fractions, HPLC equipped with an analytical gel permeation column was used to determine the composition of each fraction. Usually the pure transporter precursor, bis-macrocycle 8TrgPA8TrgA (**11**), could be obtained through a cycle of ten stages of gel permeation chromatography.

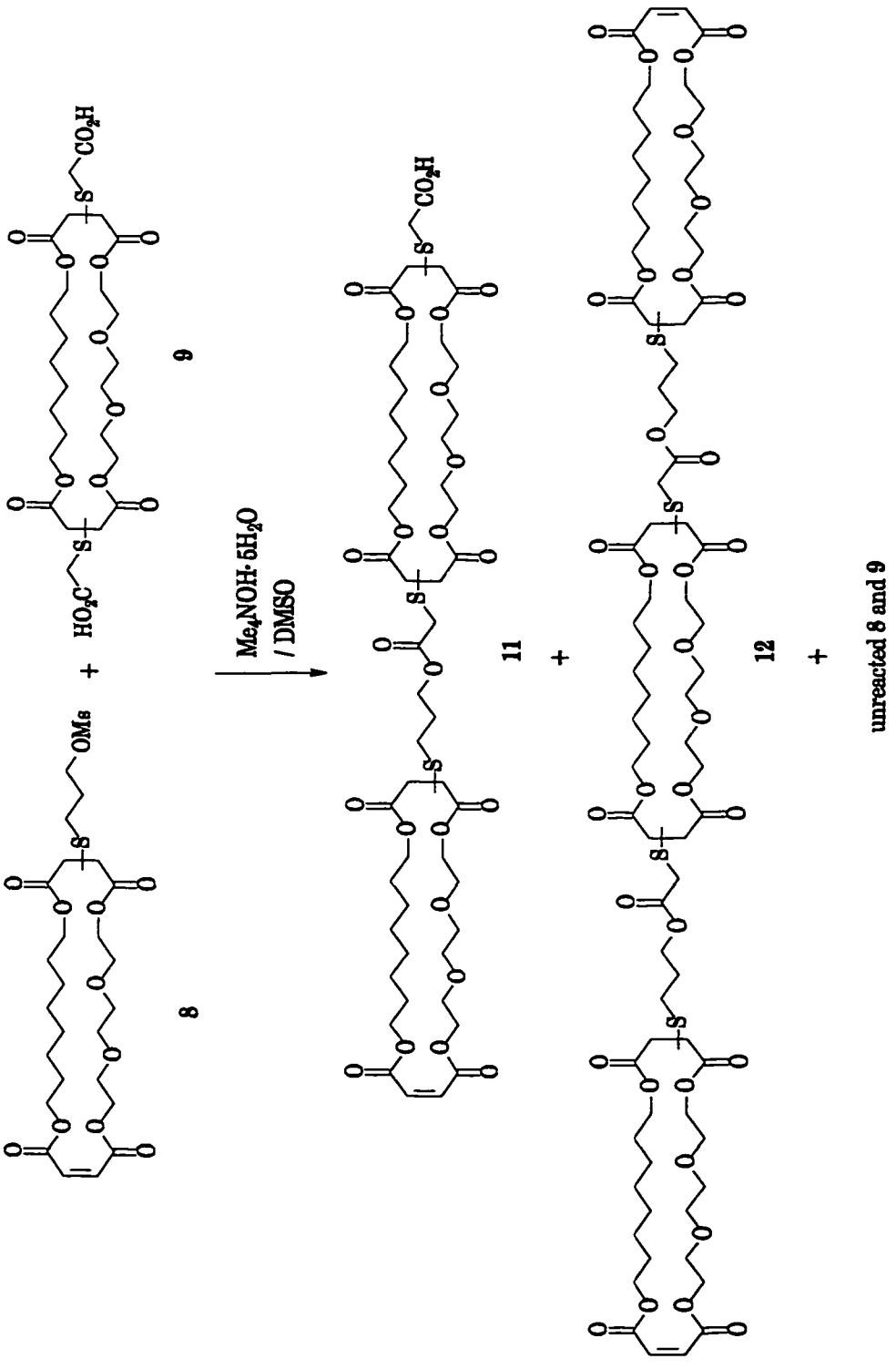

Scheme 2.5: The carboxylate coupling reaction with mesylate

Figure 2.4 shows the analytical GPC detection before and after purification, the negative LSIMS spectrum for the bis- macrocycle, and the positive LSIMS spectrum for the tris-macrocycle. Figures 2.5 and 2.6 give ^{1}H and ^{13}C NMR spectral comparisons for **11** and **12**. Figures 2.7 and 2.8 give 2D NMR spectra for 8TrgPA8TrgA (**11**), this key precursor.

The ^{1}H NMR spectrum of compound **11** is well resolved. The acidic proton (**a**) was a very broad singlet at 7.82 ppm. Two singlets at 6.76 and 6.17 ppm were the *trans* and *cis* methine protons (**b**) of the olefin. The methylene protons adjacent to carboxyl which were sixteen from two macrocycles plus two from the middle linker (**c**) formed a multiplet from 4.26 to 3.94 ppm. The methylene protons (**e**) from the ether groups of the macrocycles gave another multiplet between 3.68 and 3.53 ppm. Two sets of two isolated inequivalent methylene protons (**f**) adjacent to the carboxylate coupled with each other to form three sets of doublets of doublets from 3.50 ~ 3.23 ppm. Three methine protons (**d**) adjacent to sulfide had two sets of multiplets at 3.84 ~3.71 ppm and 3.68 ~ 3.53 ppm, and the methylene protons (**g**) gave two sets of multiplets each for one type of protons in 2.95 ~ 2.84 ppm and 2.72 ~ 2.55 ppm. The methylene protons (**h**) from the propyl linker adjacent to sulfide showed a multiplet overlapped with one of the protons **g** in range 2.72 ~ 2.55 ppm, and protons (**i**) of the middle methylene group gave another multiplet at 1.86 ppm. Twenty four methylene protons (**j**, **k**, **l**) from the hydrocarbon chain of two macrocycles had a multiplet at 1.55 ppm and a broad singlet at 1.24 ppm.

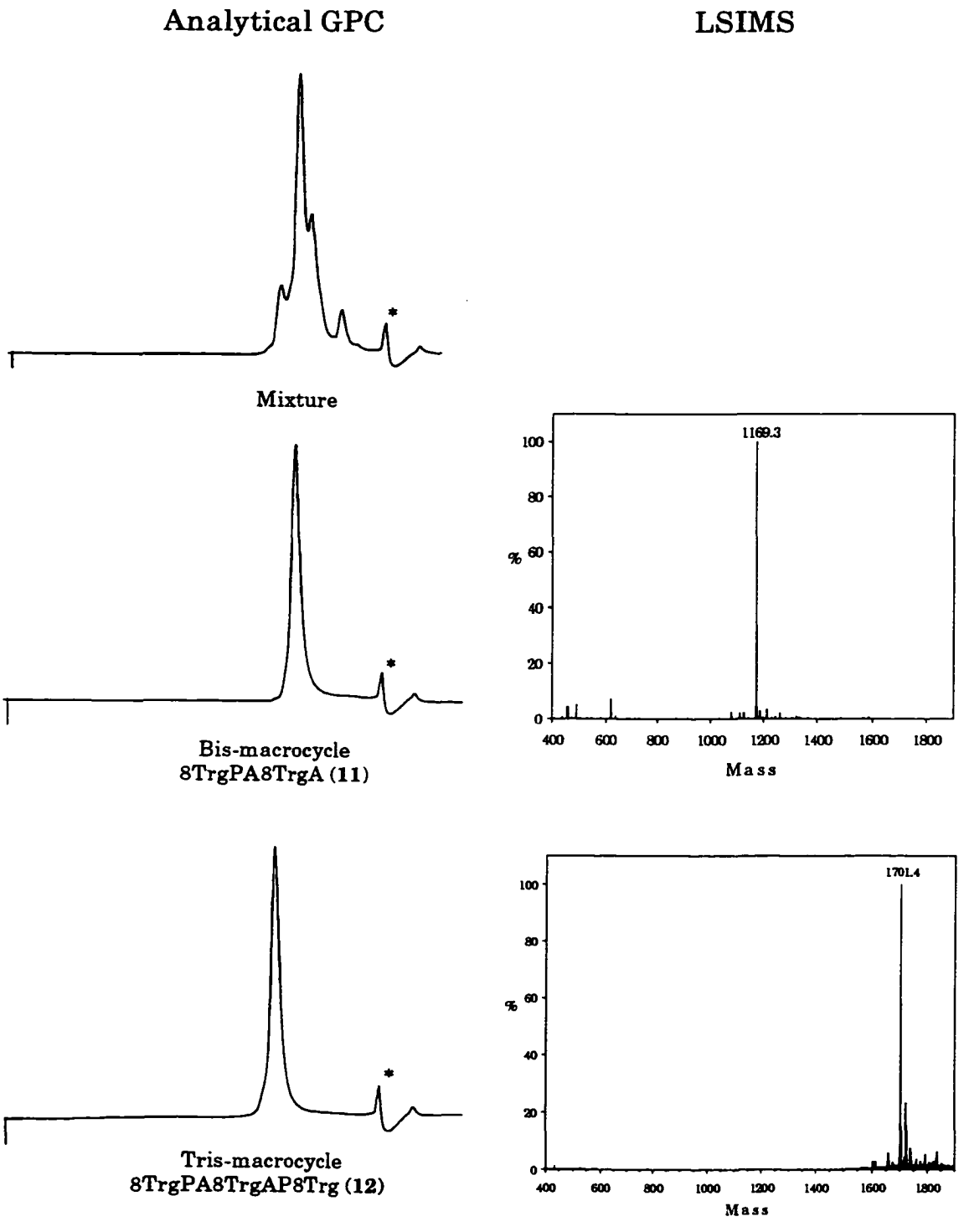

* : 2-propanol used as an internal reference

Figure 2.4: The analytical GPC measurements and LSIMS spectra

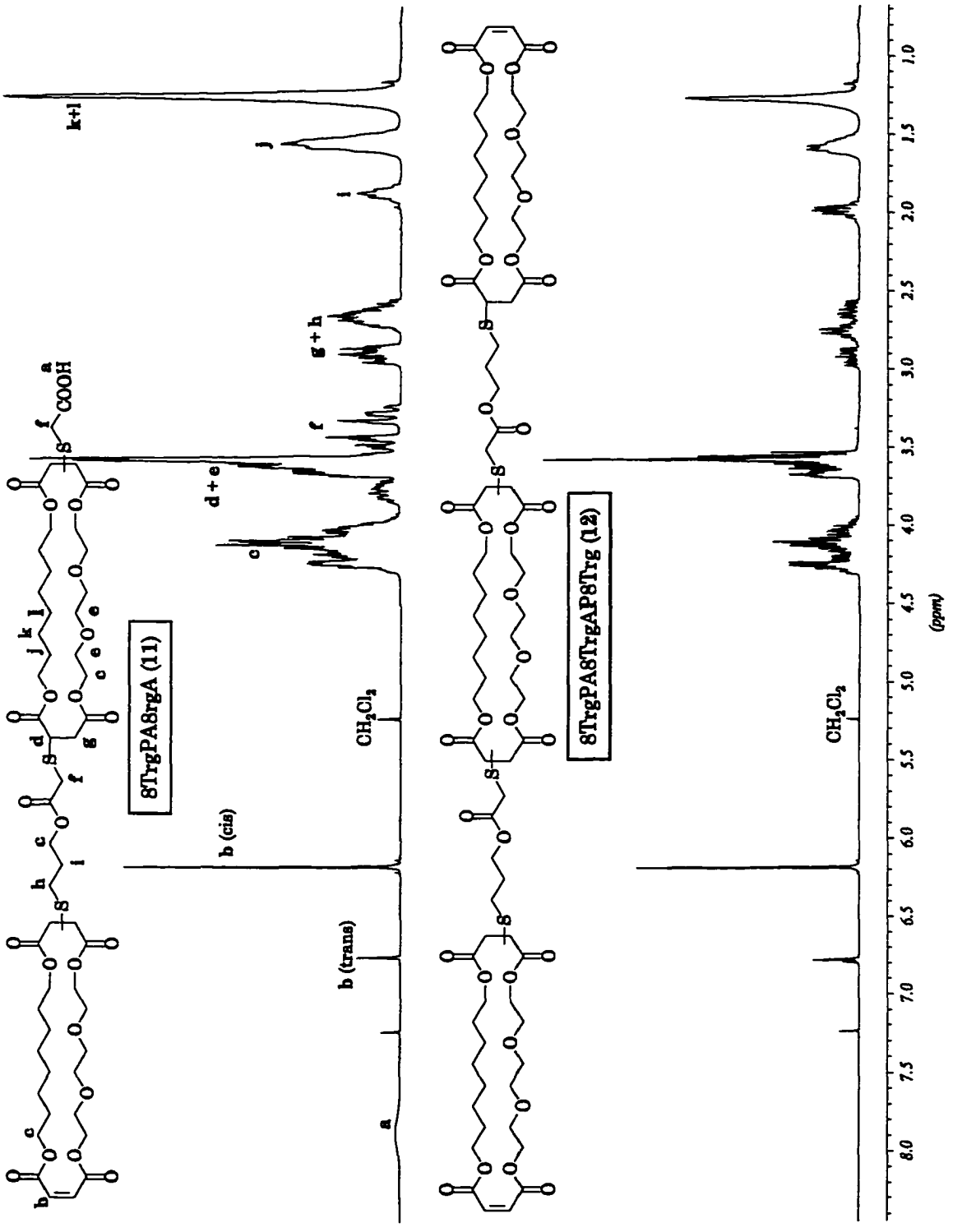

Figure 2.5: ^{1}H NMR ($CDCl_3$) of 8TrgPA8TrgA and 8TrgPA8TrgAP8Trg

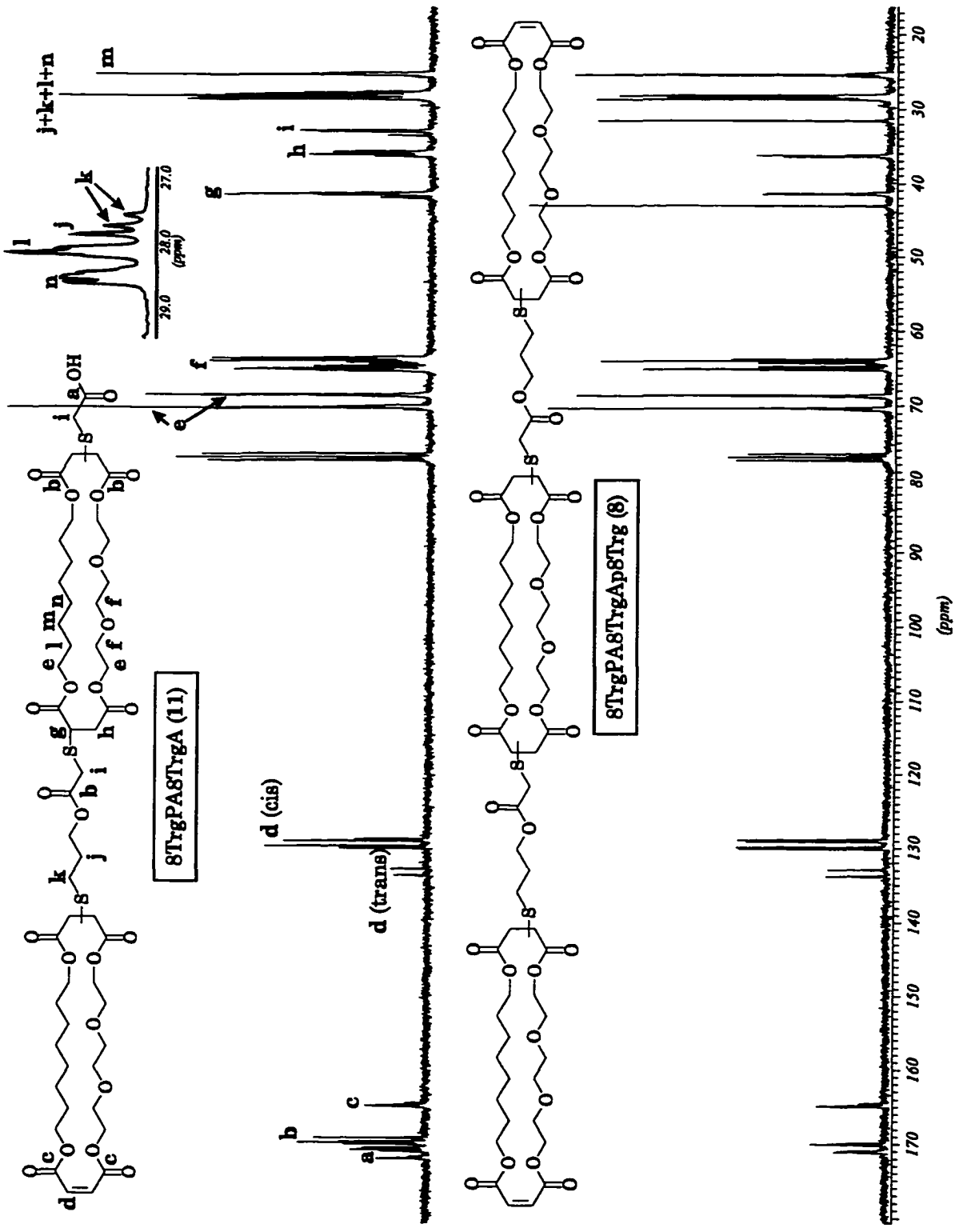

Figure 2.6: ^{13}C NMR ($CDCl_3$) of 8TrgPA8TrgA and 8TrgPA8TrgAP8Trg

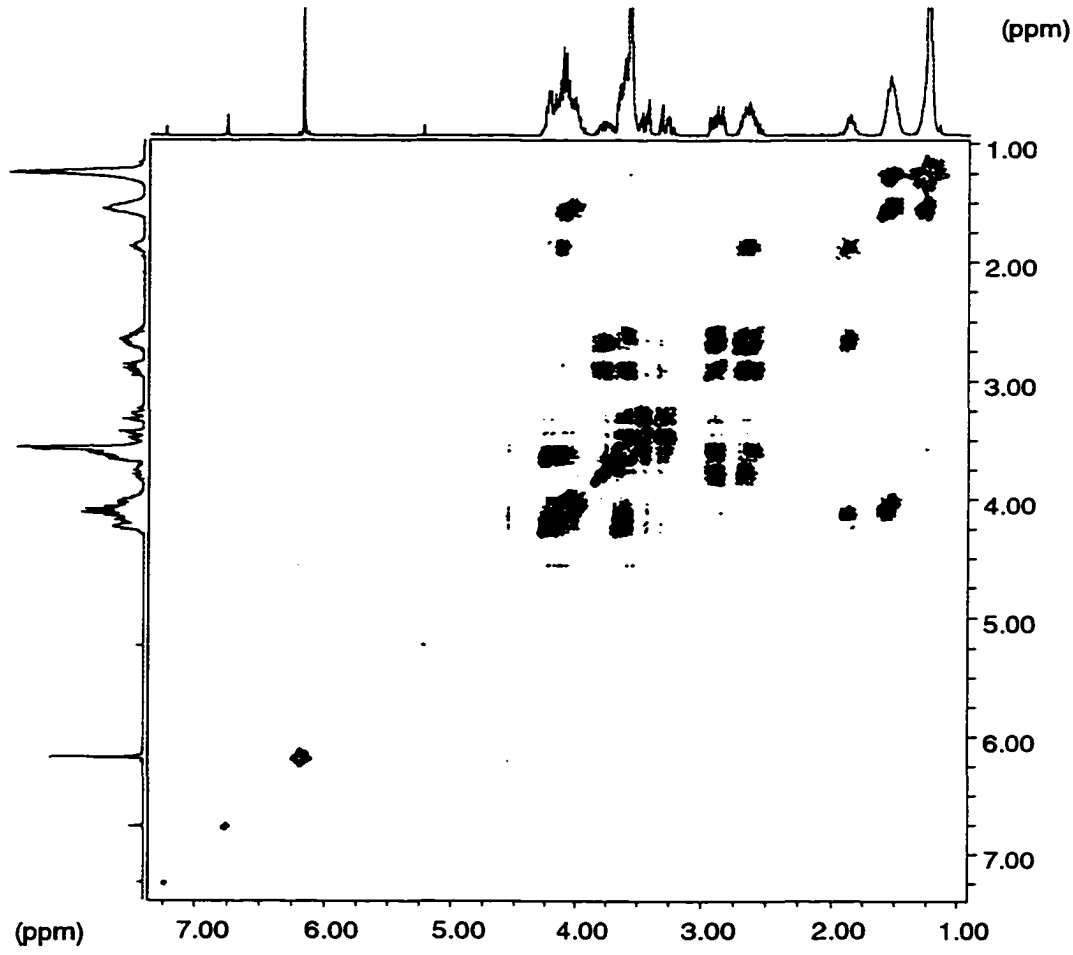

Figure 2.7: COSY NMR of 8TrgPA8TrgA

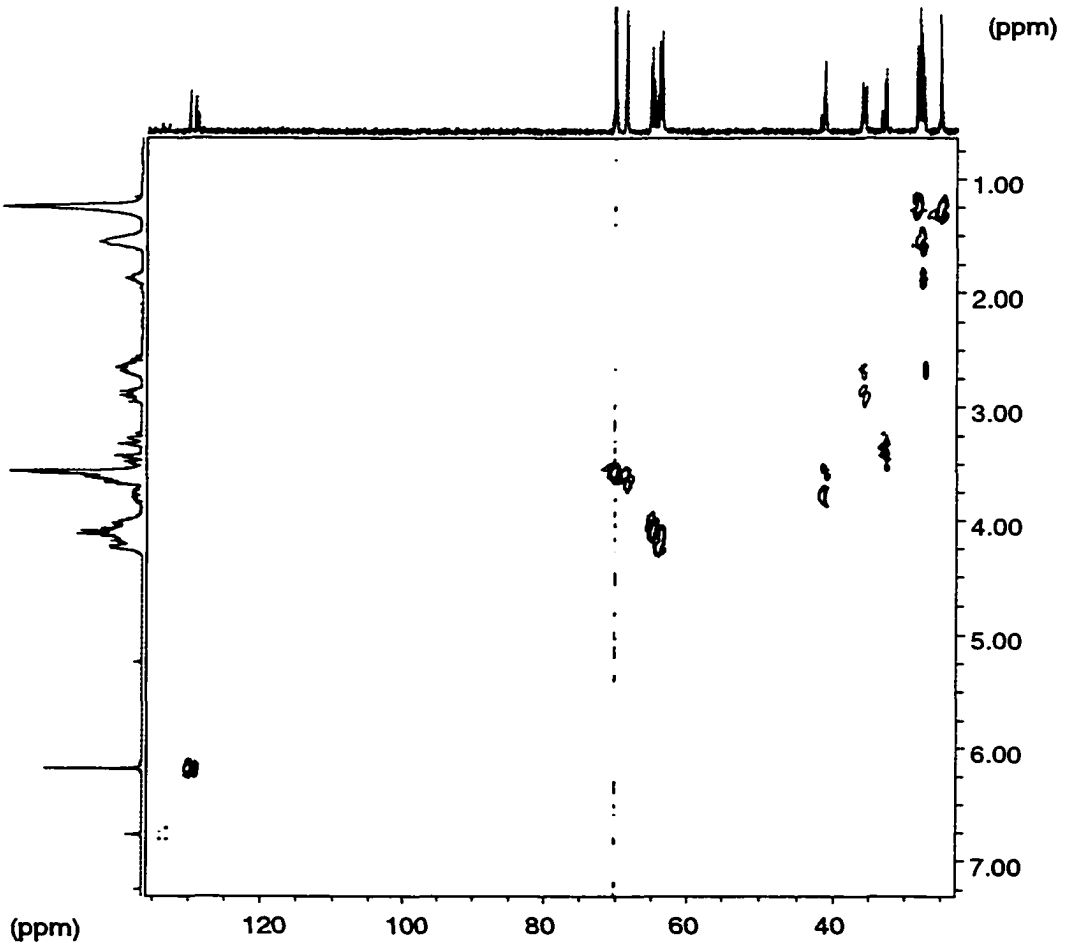

Figure 2.8: ^{1}H-^{13}C Heterocorrelation NMR of 8TrgPA8TrgA

The assignment of the ^{13}C NMR spectrum for **11** is also well established. Three peaks at 172.1, 171.9, 171.8 ppm represented the carbonyl carbon (**a**) of the carboxylic acid. The other twelve peaks from 171.2 to 169.3 ppm were from seven carbonyl carbons (**b**) from two macrocycles and the middle linker. The leftover two α, β- unsaturated carbonyl carbons (**c**) gave five peaks from 165.2 to 164.6 ppm. Signals at 133.8 and 132.9 ppm were from the *trans* olefin (**d**), and 130.1, 129.9, 129.1, and 128.9 ppm were *cis* olefin (**d**). The eight methylene carbons (**e**) of the ether groups gave eight peaks in the range between 70.5 and 68.6 ppm, and the nine methylene carbons (**f**) adjacent to carboxyl (including the one from the linker) formed eleven peaks from 65.3 to 63.6 ppm. The signals at 41.9, 41.5, 41.4, and 41.2 ppm revealed three methine carbons (**g**) adjacent to the sulfide substituent, and three nearby methylene carbons (**h**) gave signals at 36.3, 36.1, 35.9, and 35.7 ppm. Two methylene carbons (**i**) from the sulfide methyl carboxyl group occurred at 33.5, 33.0, 32.9 ppm. The signal at 27.8 ppm was the methylene carbon (**j**) of propyl group adjacent to sulfide, and the other methylene carbon (**k**), in the middle position of the propyl group, was revealed at 27.7, 27.5 ppm. All of methylene carbons (**l**, **m**, **n**) on the hydrocarbon chain of macrocycles gathered in two ranges of 29.4 ~ 28.1 and 25.5 ~ 25.2 ppm.

All of the 1D NMR assignments for **11** were supported by 2D NMR (COSY and ^{1}H-^{13}C HETCOR[37]) data. In HETCOR spectrum (Figure 2.8), the carbons at 33.5, 33.0, 32.9 ppm coupled with the protons having a multiplet at

3.50 ~ 3.23 ppm which didn't couple with other protons except self-coupling, this indicated these protons and carbons were the methylene groups between sulfide and carboxyl. Combining the data from COSY and HETCOR, it was found that the methine protons (**d** in Figure 2.5) gave two multiplets between 3.84 ~3.71 ppm and 3.68 ~ 3.53 ppm due to their coupling with two inequivalent protons (**g**) indicated in the COSY spectrum. The COSY spectrum also indicated that the multiplet at 1.86 ppm (proton **i**) coupled individually with two multiplets in 4.26 ~ 3.94 ppm and 2.68 ~ 2.53 ppm (proton **c** and **h**) which clearly revealed the proton **i** was from the middle methylene group in the propyl linker.

Since the tris-macrocycle has a symmetrical structure, its ^{1}H and ^{13}C NMR spectra were simpler than the spectra of bis-macrocycle **11** in Figures 2.5 and 2.6. The detailed assignments of ^{1}H and ^{13}C NMR spectra of **12** do not follow directly from the well established spectra of **11**. The overall chemical shift groups are however consistent with the structure. The positive LSIMS spectrum indicated the signal at 1701.4 was the molecular ion $(M + H)^{+}$ for **12**, and the structure proof rests principally on this MS result.

2.3.3 Syntheses of transporter candidates in the 8Trg series

The last step in the synthesis of transporter candidate was to add the second head group on the precursor 8TrgPA8TrgA (**11**) by Michael addition. The reaction was catalyzed by 2,2,6,6-tetramethylpiperidine in THF or DMF. The desired product was acidified by washing with 1M HCl and purified by Lipophilic Sephadex LH-20 column chromatography. By using 2-

mercaptoacetic acid, N, N'-dimethylaminoethanethiol, or 1-thio-β-D-glucose as different combinations of head groups, a negatively charged (pH 7), positively charged (pH 7), or neutral head group on one side of a transporter were obtained (Scheme 2.6).

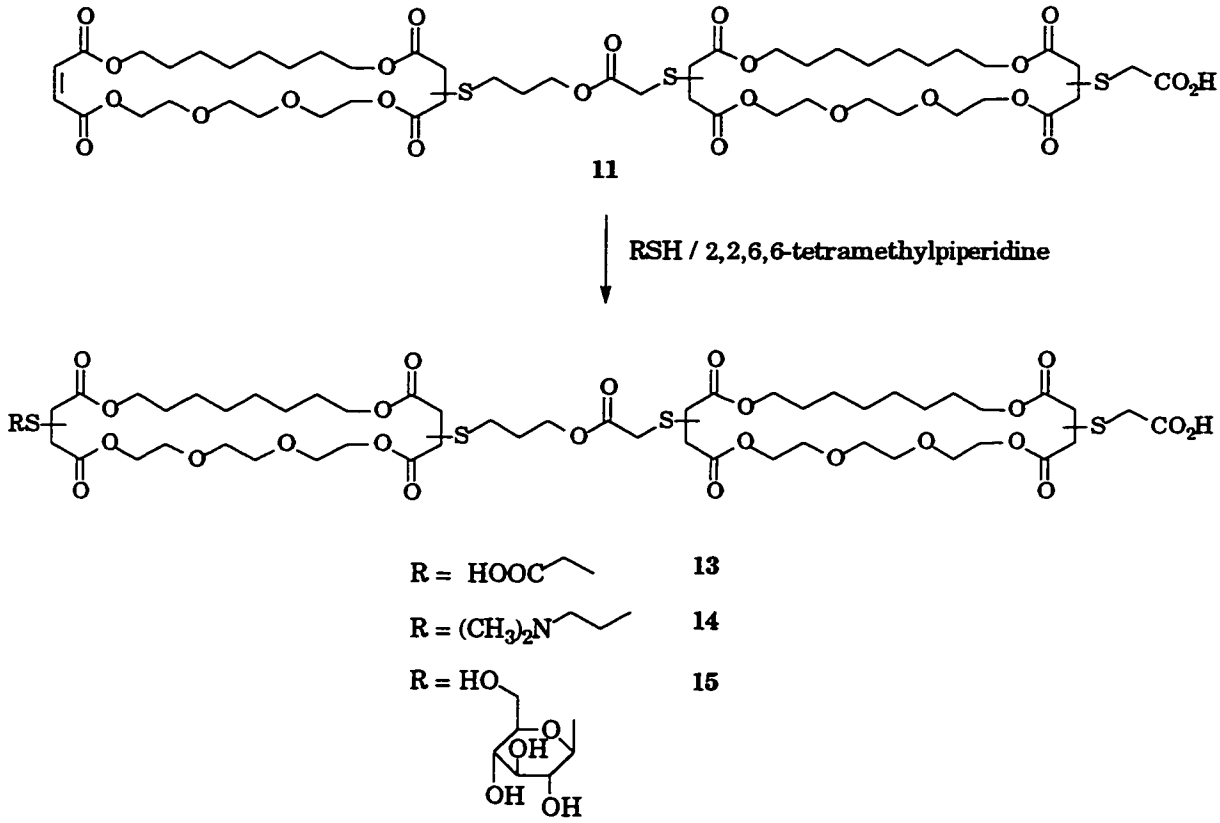

Scheme 2.6: Syntheses of transporter candidates in 8Trg series

The ^{1}H and ^{13}C NMR spectra are compared in Figures 2.9 and 2.10. The ^{1}H NMR spectra of these three compounds are quite similar except for some specific chemical shifts due to the different head groups. For **13**, the broad singlet at 5.14 ppm was due to the carboxylic acid proton. Compound **14** had a singlet at 3.61 ppm and a multiplet at 2.83 ppm contributed from the N,N-

dimethylamino ethyl head group. Compound **15** gave a very broad multiplet between 5.33 ~ 4.65 ppm caused by four hydroxyl protons of the D-glucose head group. Two peaks at 1.24 and 1.22 ppm of **13** indicated a low level of contamination by formation a 2-propyl ester from 2-propanol and the carboxylic acid during the work-up.

The differences among the three compounds were also clearly indicated in their ^{13}C NMR spectra. Compound **14** had three distinct peaks, 43.0 ppm for the methyl carbon, and 56.9, 34.1 ppm for the two methylene carbons between nitrogen and sulfur in the head group, which verified the structure. Compound **15** gave seven peaks at 78.1, 72.8, 70.8, 70.7, 66.5, 66.2, and 62.1 ppm for the D-glucose head group. Due to the two identical carboxylic acid head groups of **13**, the new head group only gave some overlapping peaks in the spectrum. The 2-propyl ester contamination was clearly seen at 22.6, 21.7, and 14.1 ppm, and the negative LSIMS also verified the analysis.

The negative LSIMS spectra of these three candidates, **13**, **14** and **15**, individually gave their molecular ion $(M - H)^-$ at 1261.4, 1274.6 and 1365.4. All of the evidence indicated these three candidates in 8Trg series had been successfully synthesized. In the second phase of the program, these different transporters will be compared each other for their physical properties.

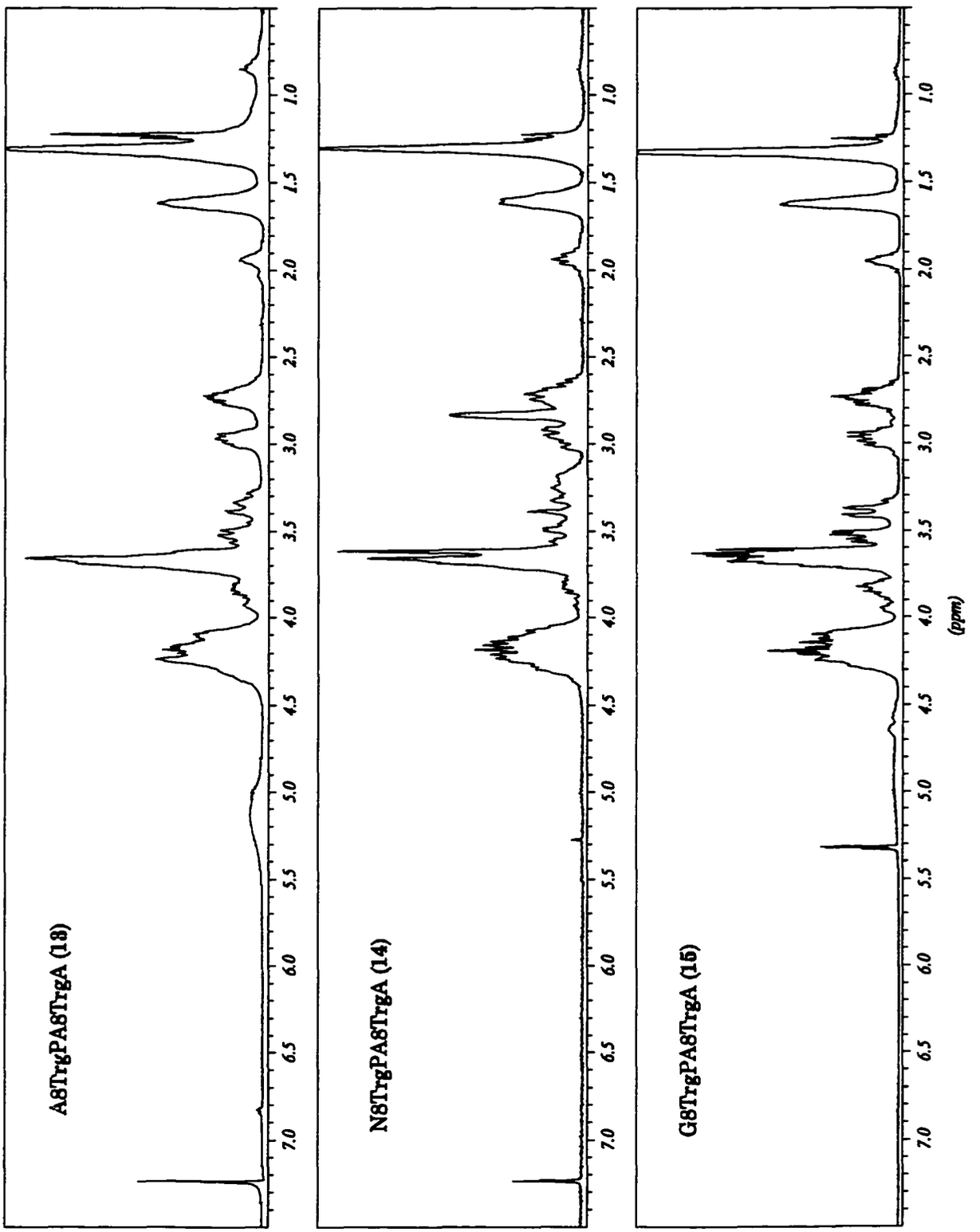

Figure 2.9: ^{1}H NMR spectra of compound **13**, **14**, and **15**

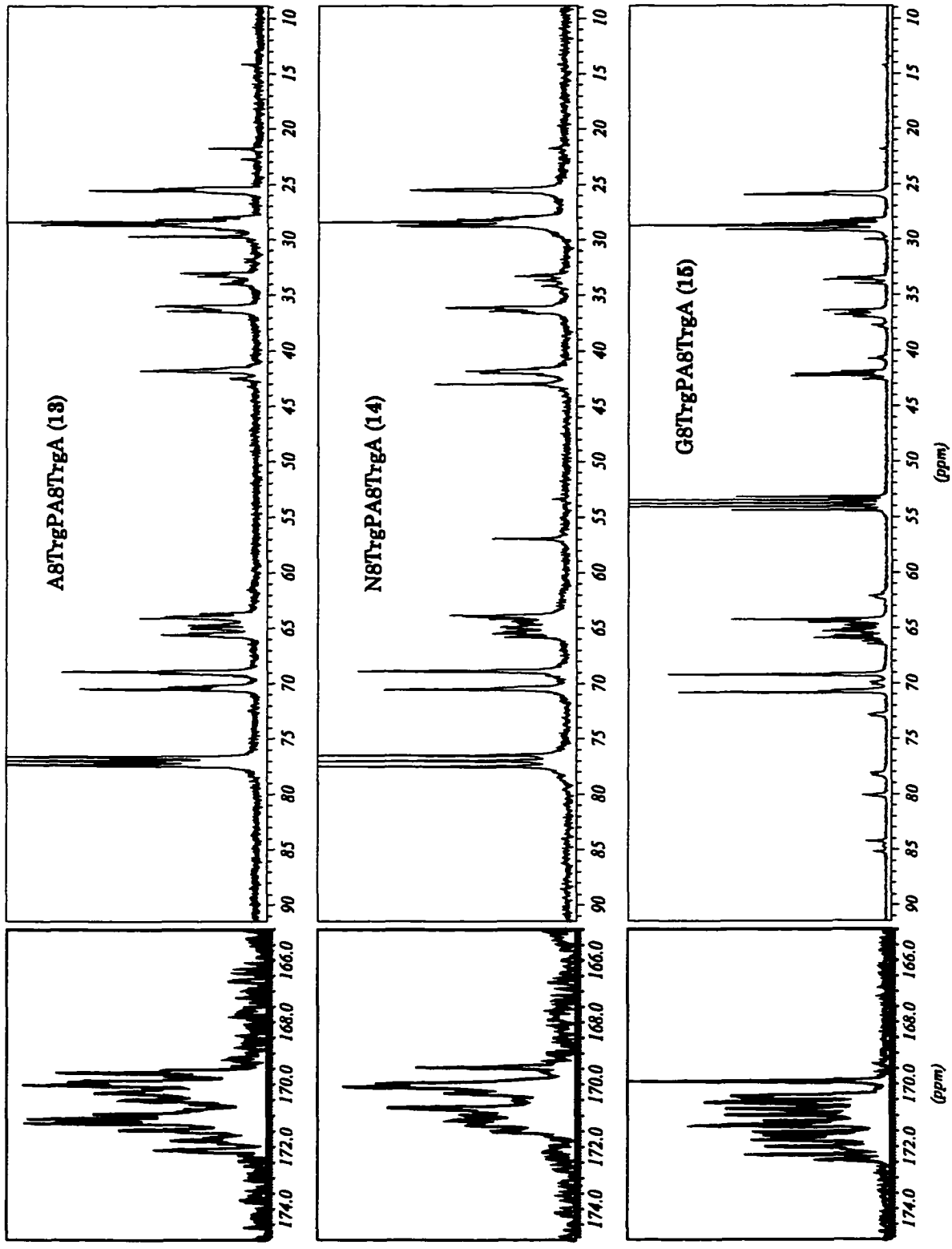

Figure 2.10: ^{13}C NMR of compound **13**, **14**, and **15**

2.4 Syntheses of transporter candidates in the 8_2 series

2.4.1 Synthesis of A8_2PA8_2A

The difference between macrocycles 8Trg (**2**) and 8_2 (**3**) is that the former has one hydrophobic side and one hydrophilic side, and the latter has two hydrophobic sides on the macrocycle. The macrocycle 8_2 can be used as a wall unit on a transporter to compare with 8Trg to investigate the importance of hydrophobic / hydrophilic effects. Based on this idea, the synthesis of new transporter candidates in the 8_2 series was explored.

The syntheses of transporters using macrocycle 8_2 as the wall unit was directly similar to the synthesis in the 8Trg series. The mono-adduct 8_2POMs (**17**) was made following the previous work[30] as shown in Scheme 2.7.

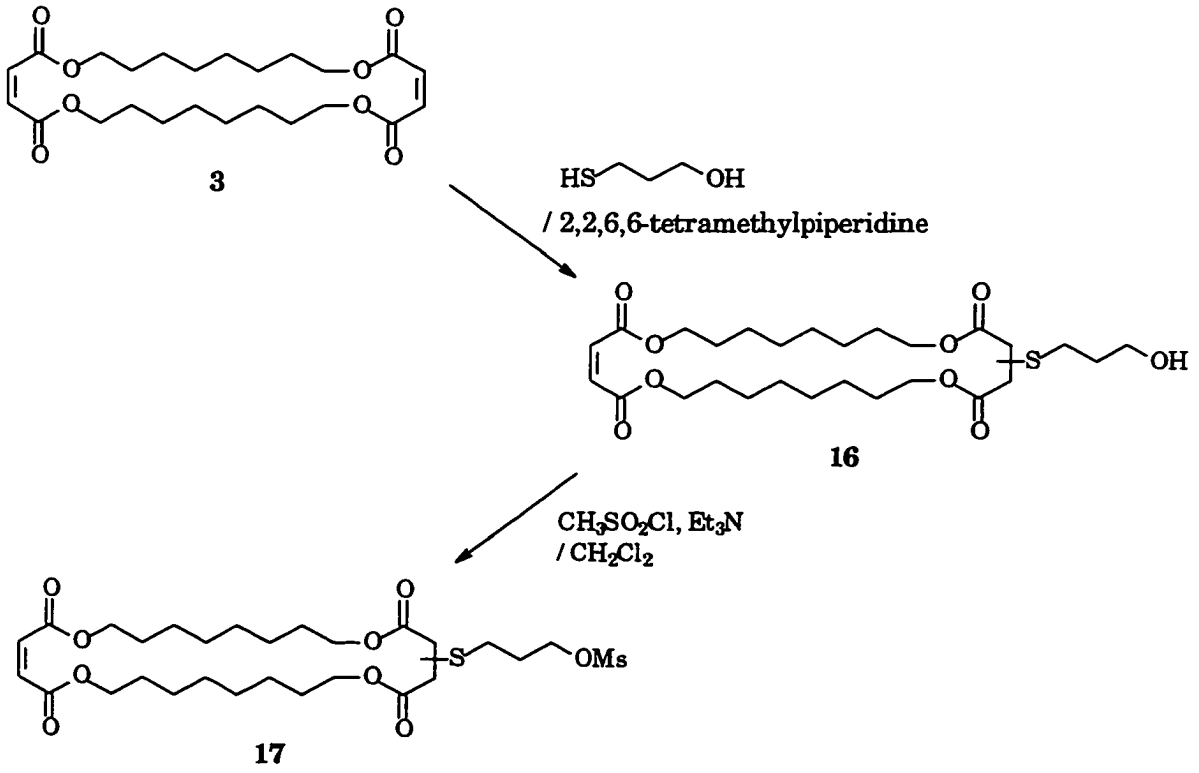

Scheme 2.7: Synthetic route of 8_2POMs (**17**)

The new diacid, A8$_2$A (**18**) was synthesized by double Michael addition of 2-mercaptoacetic acid to macrocycle 8$_2$ (Scheme 2.8). After the reagents were kept at 64°C for 26 h and workup, diacid **18** was obtained quantitatively. A mono-adduct is possible, but in the early stages it was not seen as an important target. Early trials did show that the double Michael addition was not completed if the reaction time was less than 16 h. The mono-acid from macrocycle 8$_2$ will be discussed in a later section.

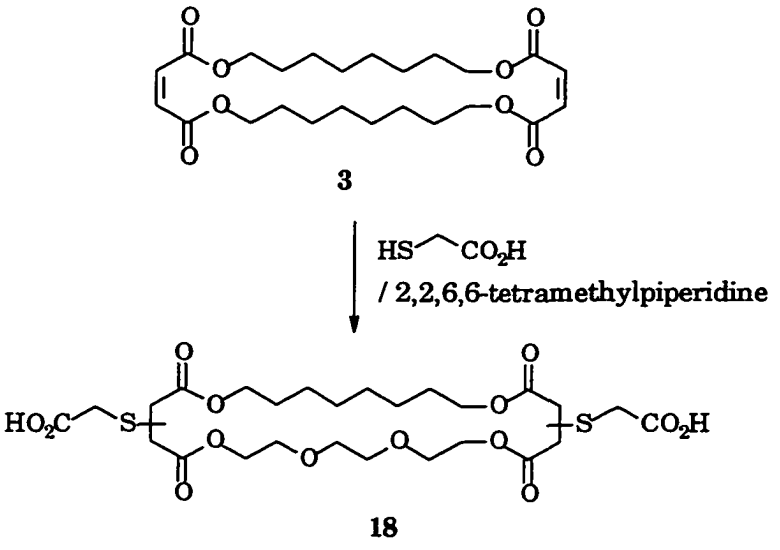

Scheme 2.8: Synthesis of A8$_2$A (**18**)

Figures 2.11 and 2.12 give the ^{1}H and ^{13}C NMR spectra of diacid **18**. Comparing with the ^{1}H NMR spectrum of diacid A8TrgA (**9**) (Figure 2.2), the ^{1}H NMR spectrum of A8$_2$A (**18**) had a quite similar pattern despite the differences between them. One difference was that there wasn't a multiplet between 3.72 and 3.60 ppm, because the polyether chain was replaced by hydrocarbon chain in the 8$_2$. The other difference was that **18** had a relatively

simpler spectrum and a different relative ratio of protons, but the ratio fitted the assigned structure.

Also comparing with the ^{13}C NMR spectrum of A8TrgA (**9**) (Figure 2.3), the ^{13}C NMR spectrum of **18** was simpler but offered the same general pattern. The only significant difference was **18** didn't have four lines around 70 ppm, because it didn't have methylene carbons next to the ether group on 8_2.

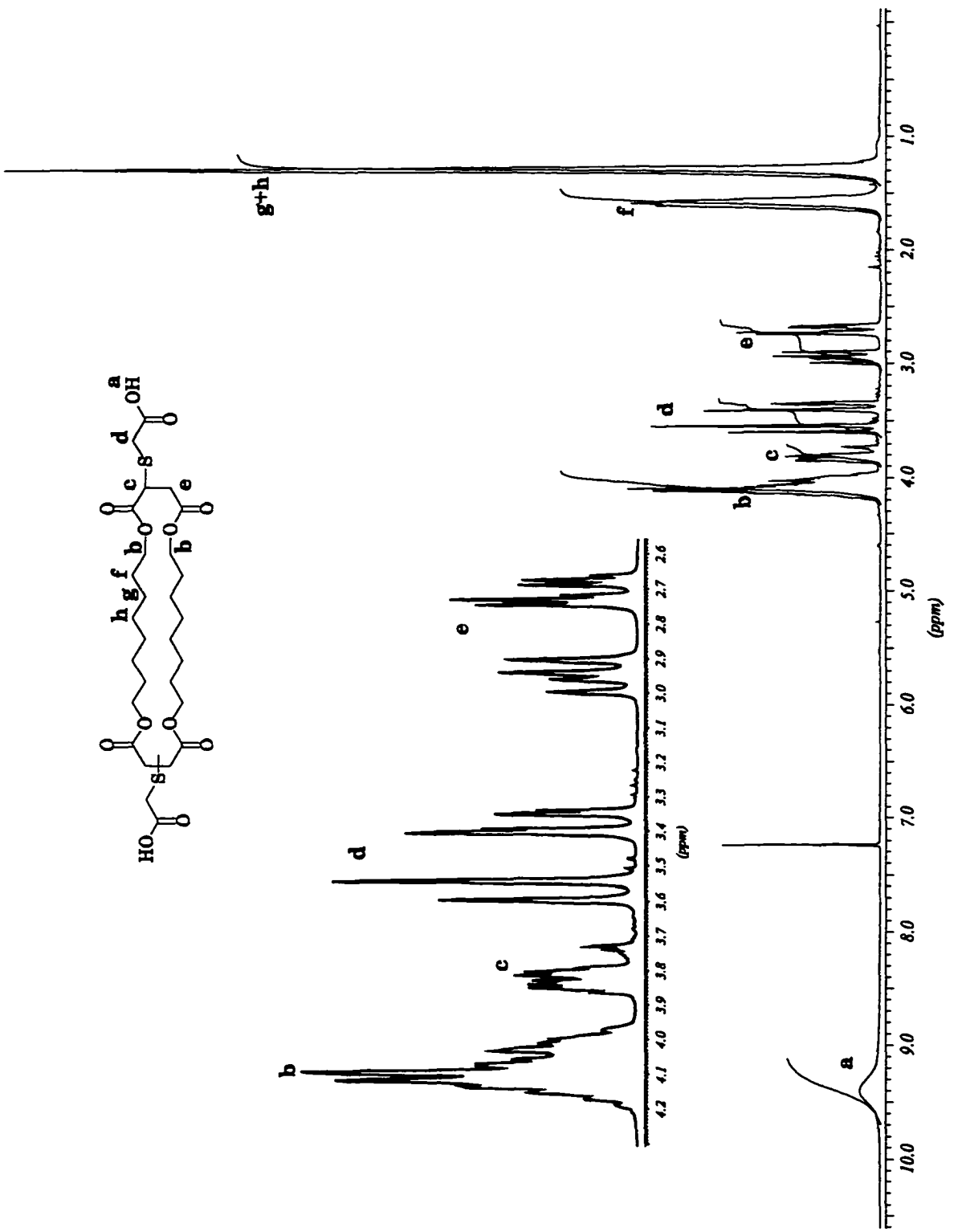

Figure 2.11: The ^{1}H NMR spectrum ($CDCl_3$) of $A8_2A$ (**18**)

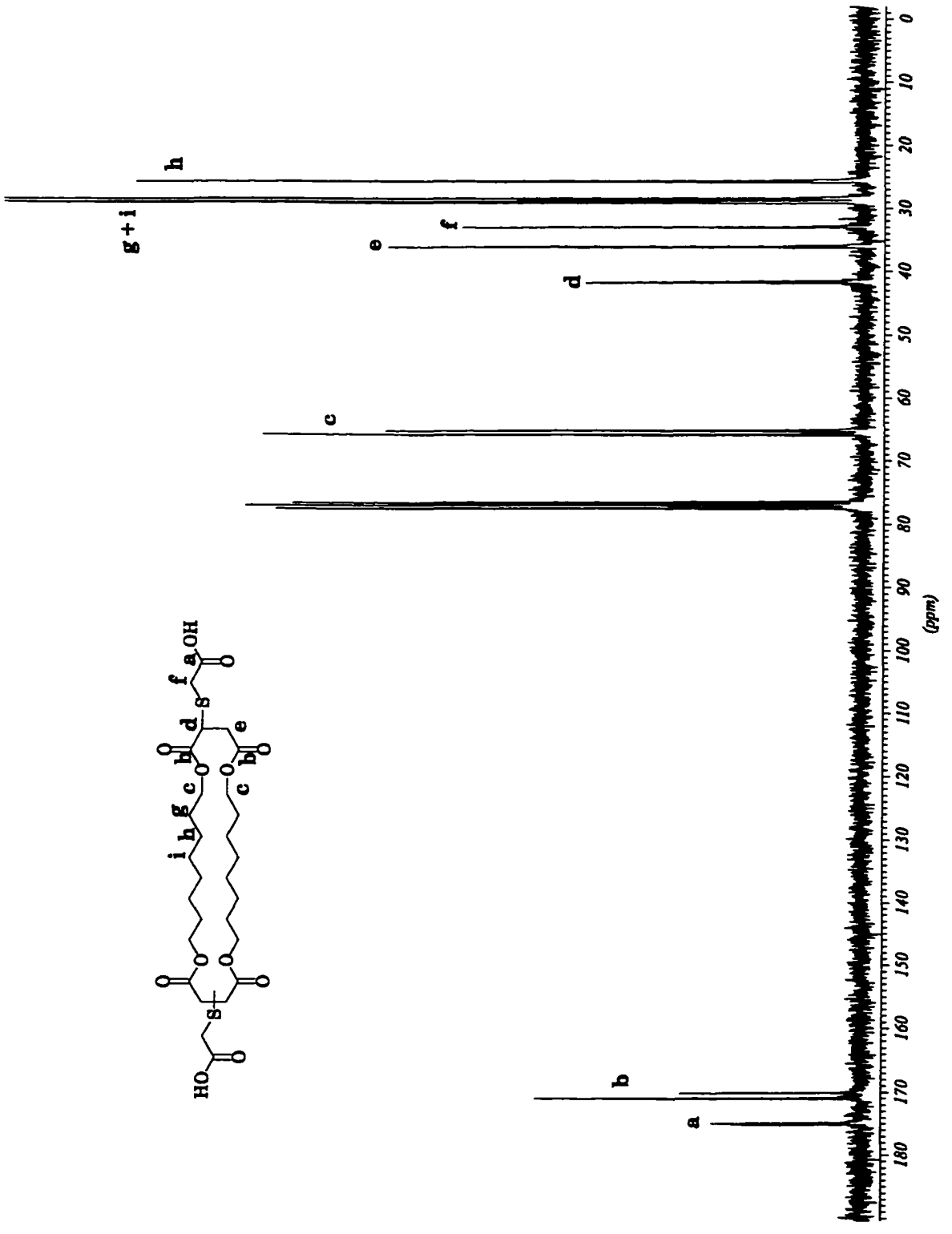

Figure 2.12: The ^{13}C NMR spectrum ($CDCl_3$) of $A8_2A$ (**18**)

Using the same reaction conditions as in the 8Trg series, the mesylate 8_2POMs (**17**) was coupled with diacid A8_2A (**18**) catalyzed by tetramethylammonium hydroxide pentahydrate in DMSO (Scheme 2.9). Following the same work-up procedures as used in the 8Trg series, the crude mixture was chromatographed on a gel permeation column (LH-20) half a dozen times to remove the bigger molecule (possible tris-macrocycle) and small molecule impurities. However, the separated transporter precursor 8_2PA8_2A (**19**) was always found to be contaminated by one of the desired final compounds A8_2PA8_2A (**20**). Due to the closeness of their molecular weights, they could not be separated adequately by the preparative gel permeation column. The negative LSIMS spectra (Figure 2.13) clearly identified that the separated product was a mixture of compounds **19** and **20.**

After further study, it was found that the contamination was caused by the occurrence of a retro-Michael addition (Scheme 2.10). When the carboxylate was formed from the carboxylic acid by reaction with tetramethylammonium hydroxide, it can substitute the mesylate group to form a ester bond joining two macrocycles. However, at the same time, it also could behave as a base to remove an adjacent acidic proton to form olefin and an intermediate sulfide anion. The free sulfide might then execute a Michael addition to another precursor molecule (**19**) to form A8_2PA8_2A (**20**). Scheme 2.10 gives a proposed mechanistic explanation for the retro-Michael addition via an intramolecular seven membered ring.

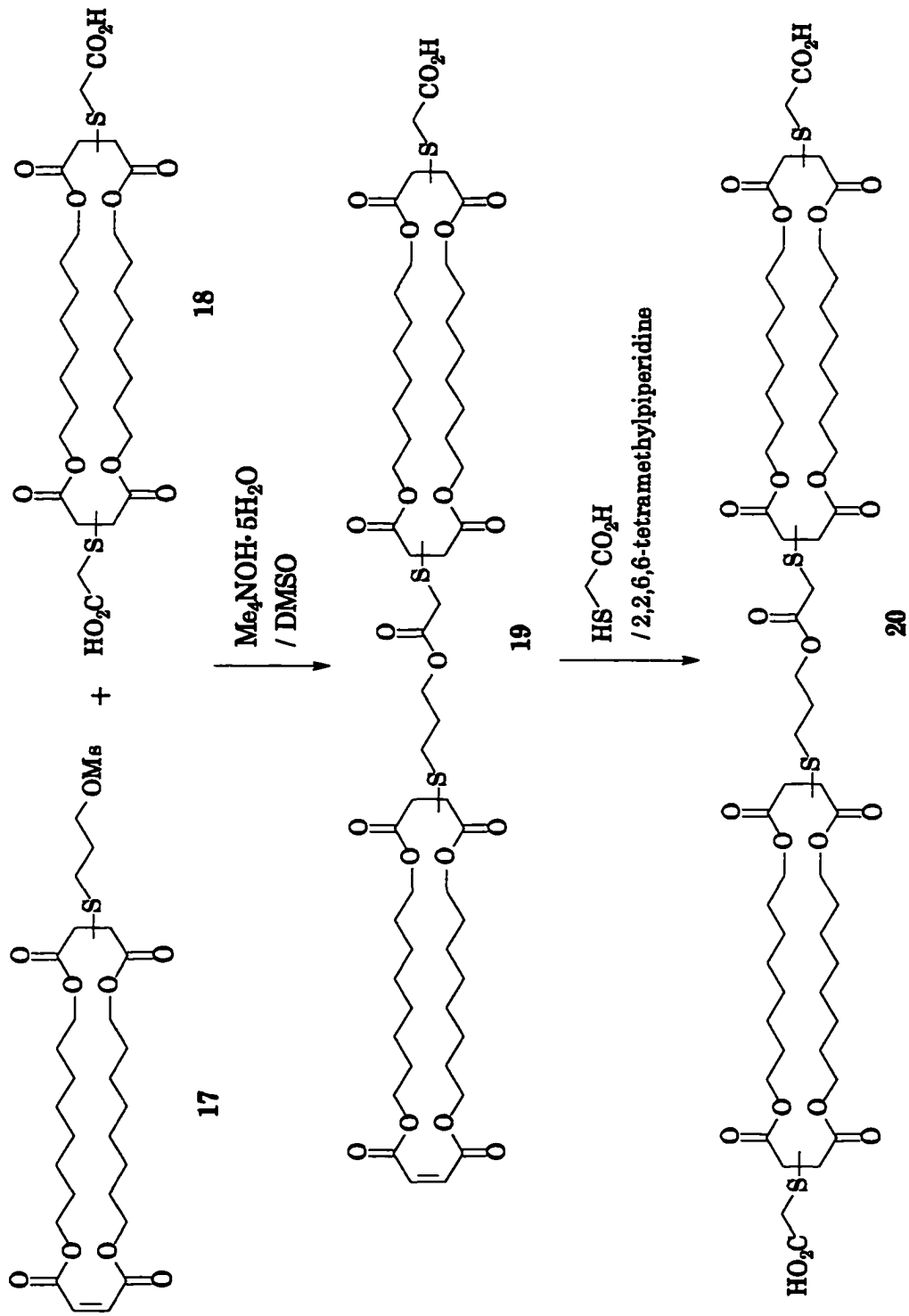

Scheme 2.9: Syntheses of 8_2PA8_2A (**19**) and $A8_2PA8_2A$ (**20**)

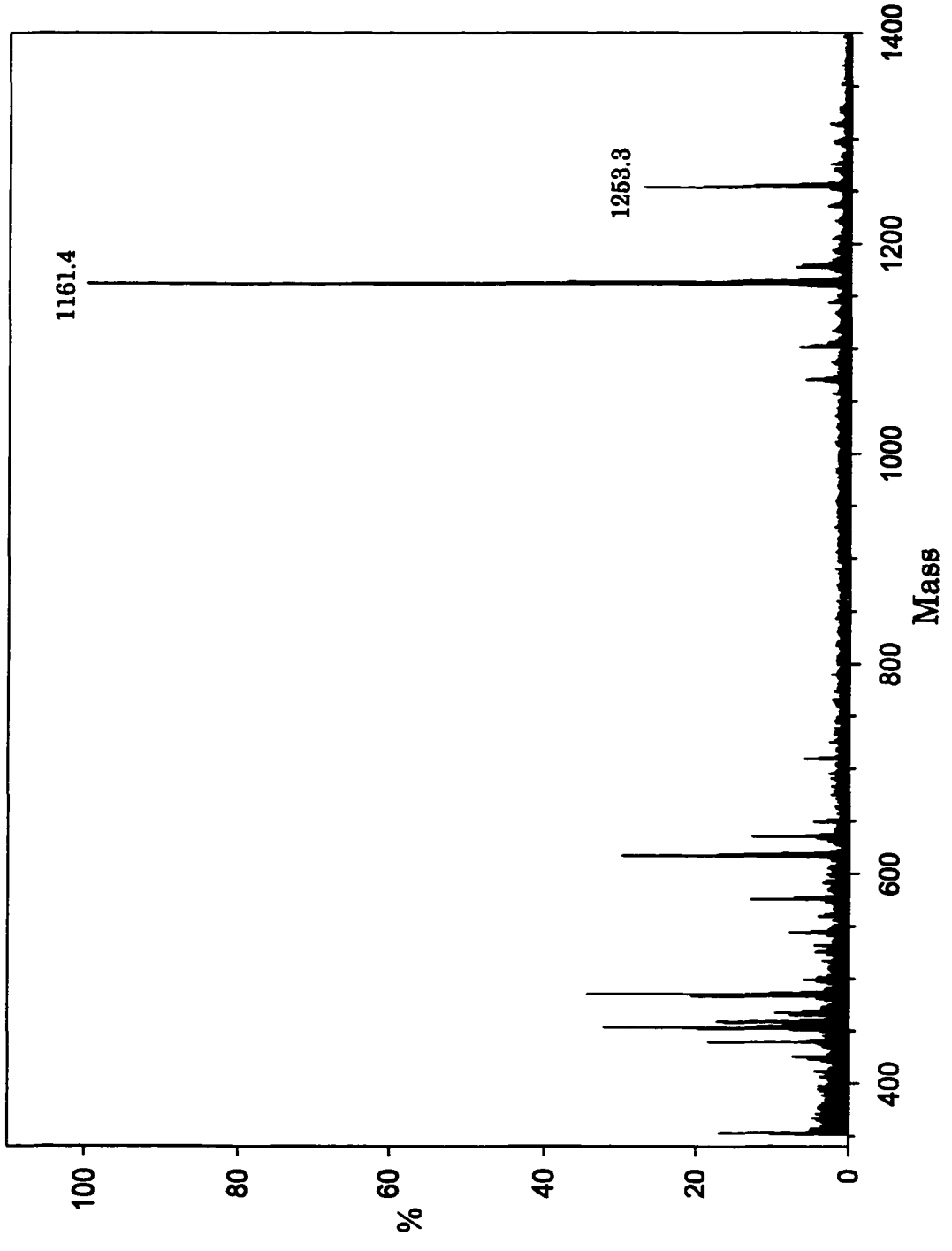

Figure 2.13: The negative LSIMS spectra of 8_2PA8_2A (**19**)

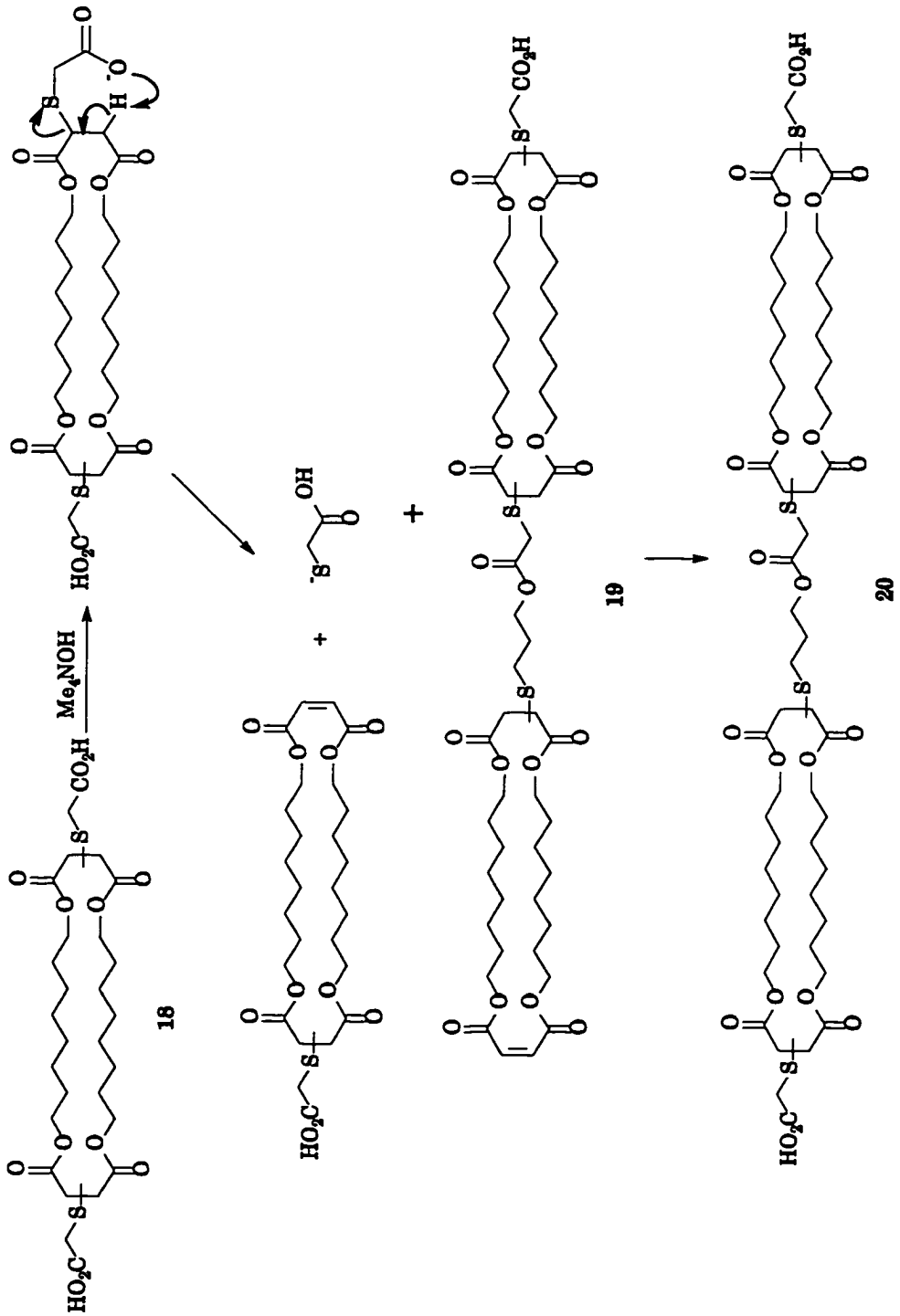

Scheme 2.10: The proposed mechanism for intramolecular retro-Michael addition

Due to the impure precursor 8_2PA8_2A, 2-mercaptoacetic acid became the only choice for the second head group to add to the mixture to form a transporter candidate $A8_2PA8_2A$ in the 8_2 series. The mixture of **19** and **20** was treated with 2-mercaptoacetic acid and 2,2,6,6-tetramethylpiperidine in THF for 22 h. After acidification with aqueous 1M HCl and purification by gel permeation column LH-20, pure $A8_2PA8_2A$ (**20**) was obtained.

Its ^1H NMR (Figure 2.14) spectrum was assigned with no difficulty. A broad singlet at 9.05 ppm belonged to the acidic protons (**a**). Eighteen methylene protons (**b**) next to the carboxylate formed a multiplet from 4.19 to 3.94 ppm. Four methine protons (**c**) adjacent to the sulfide substituent gave two multiplets between 3.84 ~ 3.72 ppm and 3.63 ~ 3.58 ppm (3:1 ratio) because three of them are adjacent to sulfide acetate and the final one is next to the propyl sulfide. Eight (four sets) neighboring methylene protons (**e**) coupled with the adjacent methine protons and with each other to form two multiplets (4:4 ratio) from 2.98 to 2.59 ppm. The methylene protons (**d**) between sulfide and carboxylate coupled with each other to reveal two sets of doublets of doublets in the range of 3.59 to 3.31 ppm. The methylene protons (**f**) of the propyl group next to the sulfide had a overlap with protons **e** from 2.78 to 2.59 ppm, and the neighboring methylene protons (**g**), the middle methylene in propyl group, had a multiplet at 1.91 ppm. The remaining methylene protons (**h, i, j**) from the hydrocarbon chain of the macrocycles gave a multiplet at 1.58 ppm and a broad singlet at 1.27 ppm.

The ^{13}C NMR spectrum (Figure 2.15) was well assigned for **20**. The carbonyls of carboxylic acid (**a**) gave a chemical shift at 174.3 ppm, and the remaining carbonyls (**b**) from the macrocycles and the linker formed seven peaks between 171.3 to 169.5 ppm. Nine methylene carbons (**c**) adjacent to carboxyl had chemical shifts at 65.6, 65.5, 65.1, 63.9 ppm. Four methine carbons (**d**) gave two peaks at 41.7 and 41.5 ppm in a 3:1 ratio corresponding to the same ratio in the ^{1}H NMR, and the peaks at 36.5, 36.2, and 36.1 ppm were contributed by the neighboring methylene carbons (**e**). Similarly to the 8Trg series, the methylene carbons (**f**) between the sulfide and the ester group were at 33.1 and 33.0 ppm, and the methylene carbon of the propyl group which was adjacent (**g**) and subsequent (**h**) to the sulfide had a chemical shift at 27.8 and 28.0 ppm. The remaining methylene carbons (**i**, **j**, **k**) from the hydrocarbon chain of the macrocycles gave chemical shifts at 29.1, 29.0, 28.4, 25.7, and 25.6 ppm. The analysis of the ^{1}H and ^{13}C NMR spectrum of compound **20** was supported by 2D NMR (COSY and HETCOR).

The clean negative LSIMS spectrum (Figure 2.16) also verified that the dominant peak at 1253.3 was the molecular ion $(M - H)^-$ of **20**.

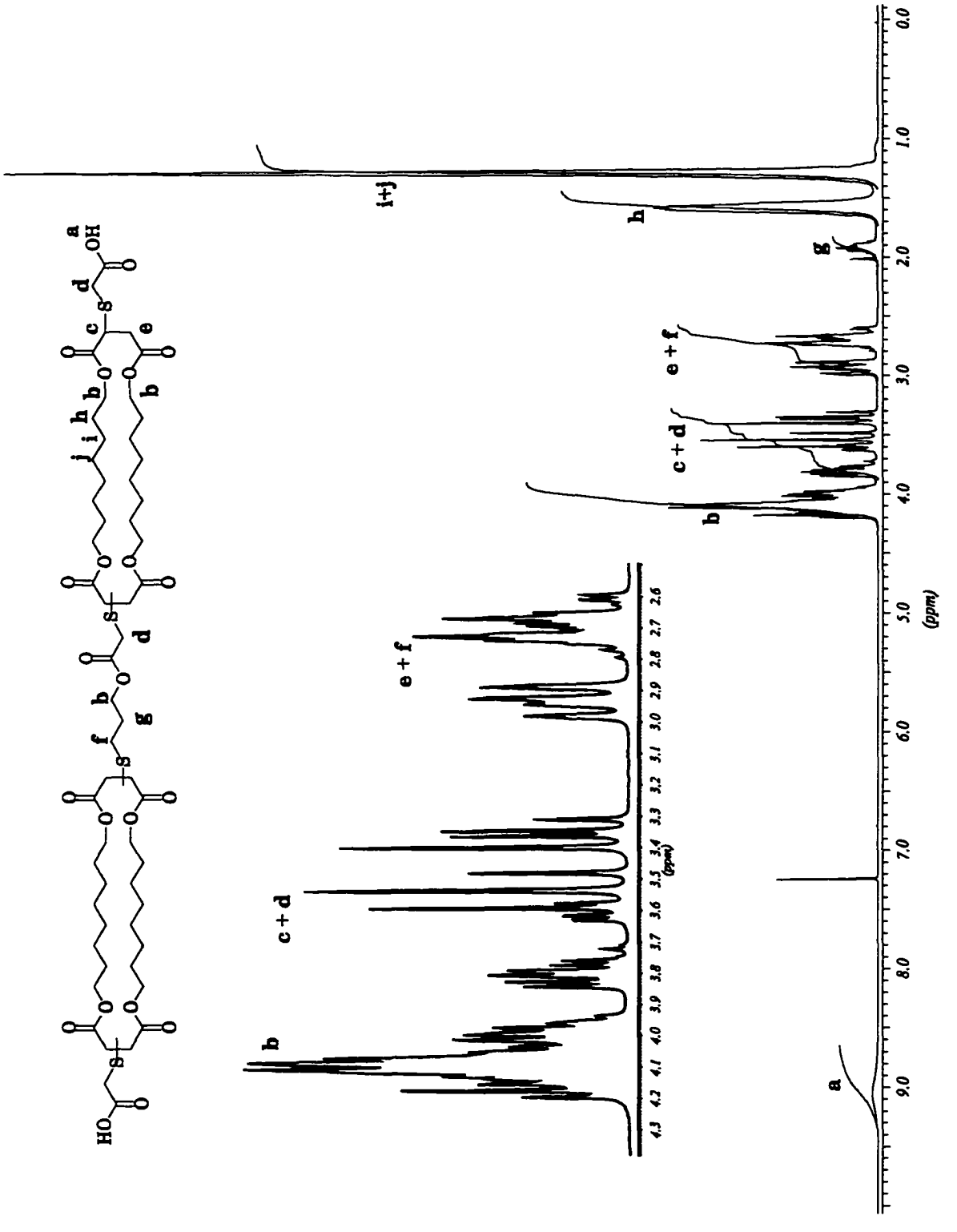

Figure 2.14: ^{1}H NMR ($CDCl_3$) spectrum of $A8_2PA8_2A$ (**20**)

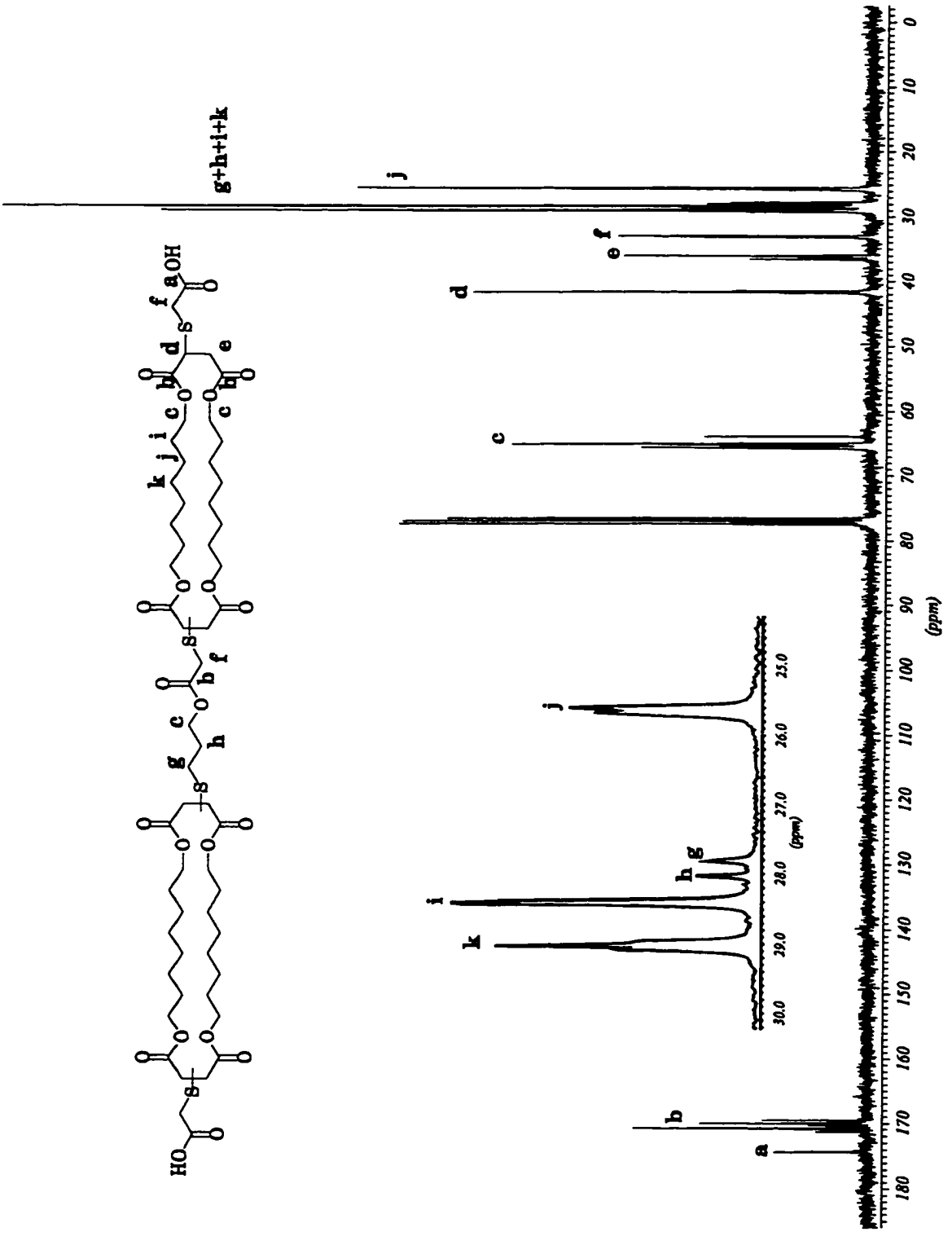

Figure 2.15: ^{13}C NMR ($CDCl_3$) spectrum of $A8_2PA8_2A$ (**20**)

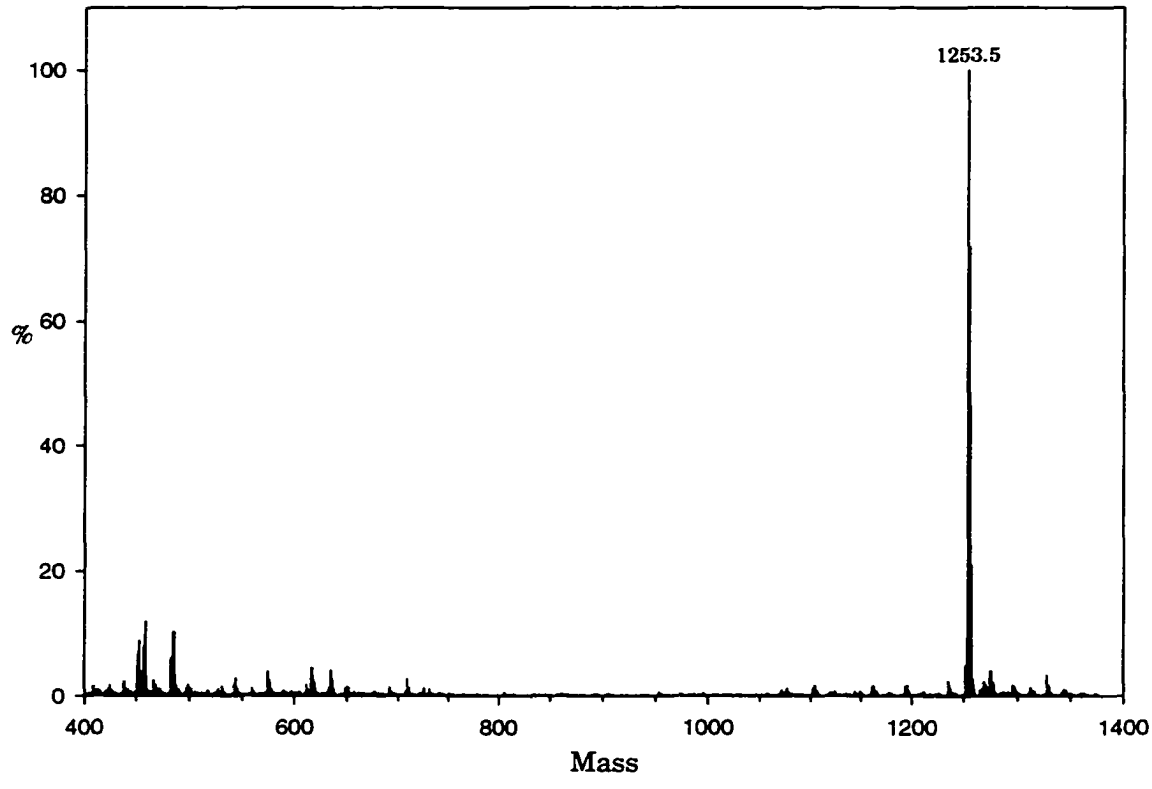

Figure 2.16: Negative LISMS spectrum of A8$_2$PA8$_2$A (**20**)

2.4.2 Synthesis of Pa8$_2$PPa8$_2$Pa

Due to the unexpected difficulty in getting pure precursor **19** for the 8$_2$ series, the original design goal for examining the head group effects on the 8$_2$ as wall units could not be accomplished. In order to minimize the retro-Michael addition occurring as proposed in Scheme 2.10, 3-mercaptopropionic acid was used to replace 2-mercaptoacetic acid. If the intramolecular process is a significant factor, it should be much less efficient for a larger ring and the indiscriminate competitor would be minimized. Similar synthetic routes were followed to obtain diacid Pa8$_2$Pa (**21**) (Scheme 2.11), and mesylate 8$_2$POMs

(**14**). The new compound **21** was synthesized using the previous method used for A8$_2$A. Macrocycle 8$_2$ reacted with 3-mercaptopropionic acid catalyzed by excess 2,2,6,6-tetramethylpiperidine to give a mixture of diacid, Pa8$_2$Pa (**21**), mono-acid, 8$_2$Pa (**22**), and unreacted 8$_2$ (Scheme 2.11). The complete addition could not be achieved even though the solution was refluxed in THF for two days. The mixture was separated by silica column chromatography with a solvent gradient of hexanes and ethyl acetate to give a 30% yield for **21** and a 16% yield for **22**.

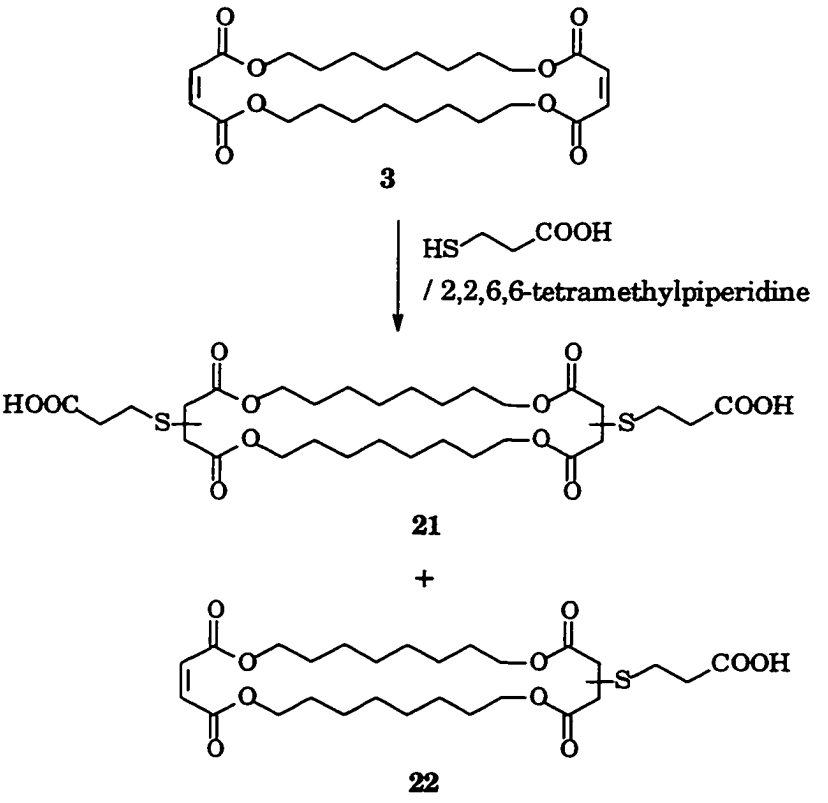

Scheme 2.11: Synthesis of Pa8$_2$Pa (**21**)

Figures 2.17 and 2.18 are the ^{1}H and ^{13}C NMR spectra comparison of diacid Pa8$_2$Pa (**21**) and mono-acid 8$_2$Pa (**22**).

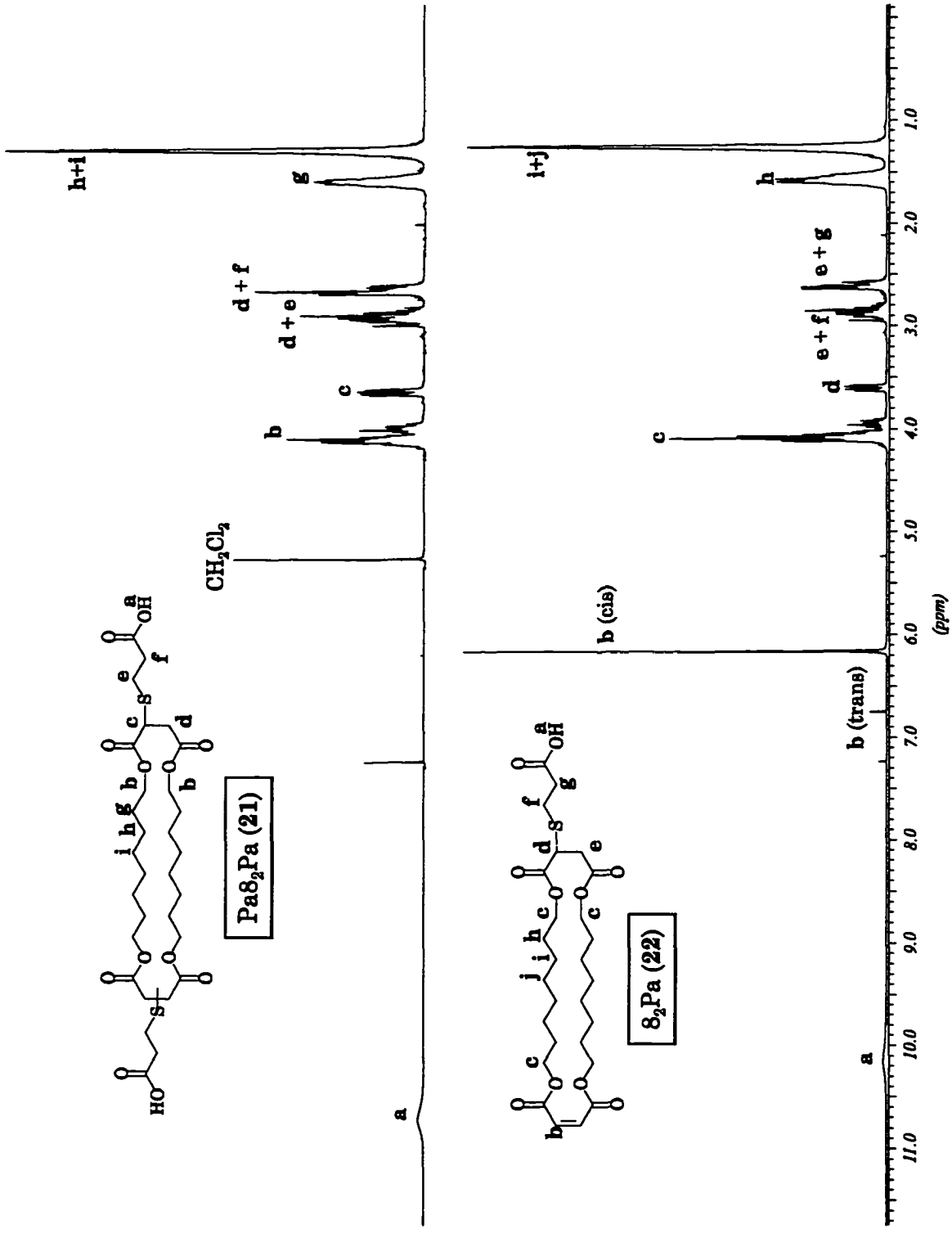

Figure 2.17: ^{1}H NMR ($CDCl_3$) spectra of compound **21** and **22**

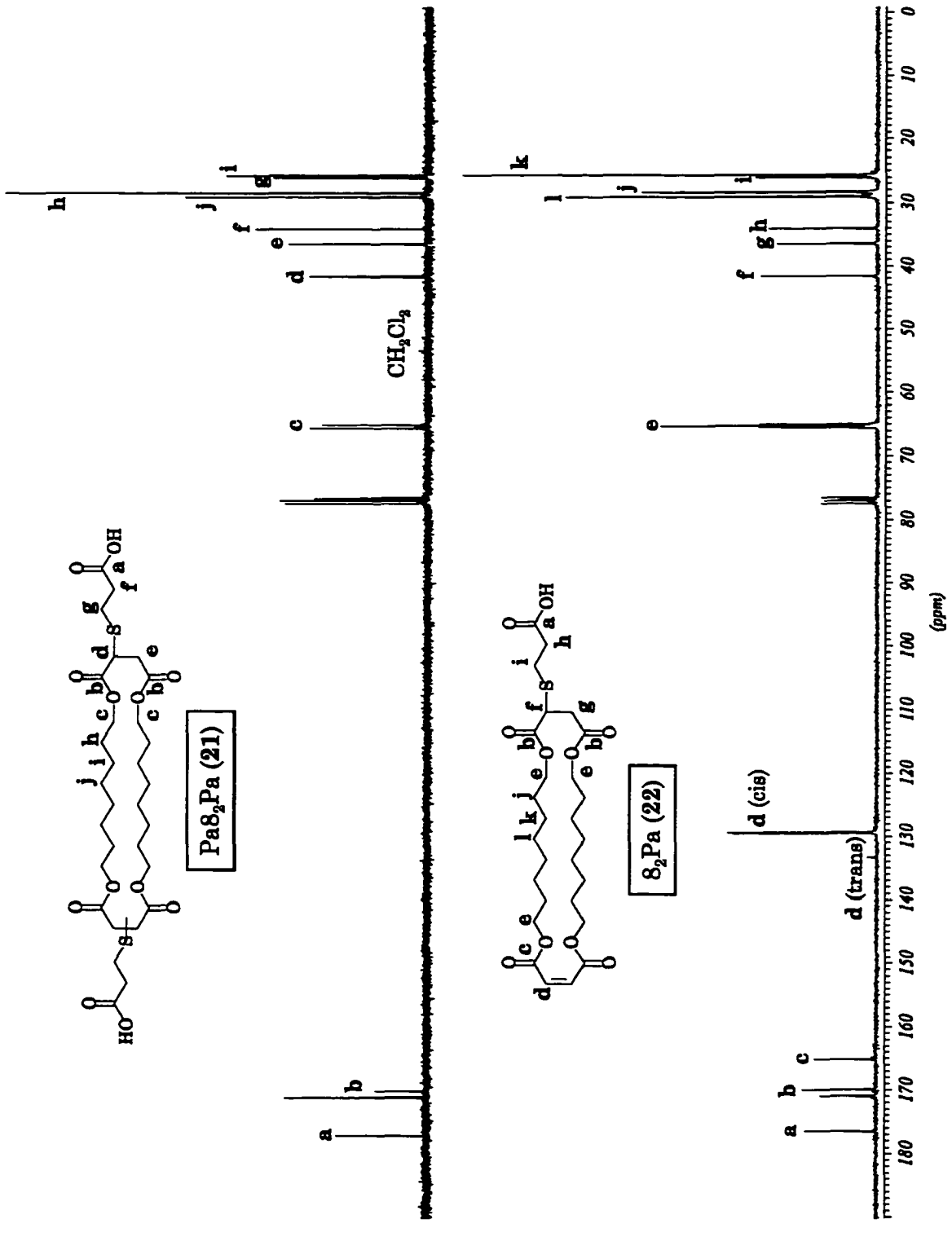

Figure2.18: ^{13}C NMR ($CDCl_3$) spectra of compound **21** and **22**

Comparing with the ^{1}H NMR spectrum of diacid A8$_2$A (**18**) (Figure 2.11), the ^{1}H NMR spectrum of Pa8$_2$Pa (**21**) in Figure 2.17 had several different assignments despite their structural similarities. First of all, the acidic proton (**a**) moved downfield to 9.91 ppm. Second, the methine proton (**c**) moved upfield to 3.64 ppm to give a perfect doublet of doublets which verified that proton **c** was coupled with the two inequivalent neighboring methylene protons (**d**). Lastly, on the side chain the methylene protons (**e**) adjacent to sulfide moved to 2.90 ppm, and the methylene protons (**f**) next to carboxylic acid shifted to 2.66 ppm, where they both overlapped with methylene protons (**d**) on the ring to form two sets of multiplets.

The ^{1}H NMR spectrum of the mono-acid, 8$_2$Pa (**22**) was comparable with the spectrum of diacid **21** (Figure 2.17). Besides the acidic proton (**a**) downfield a bit further to 10.16 ppm, the other difference was two singlets at 6.75, 6.16 ppm caused by *trans* and *cis* olefin protons. Like diacid **21**, the integration of **22** fitted the structure well.

The ^{13}C NMR spectrum of diacid **21** (Figure 2.18) again had some differences with the ^{13}C NMR spectrum of A8$_2$A (**18**). As in the ^{1}H NMR spectrum, the carbonyl (**a**) of carboxylic acid moved downfield to 177.3 ppm. The methylene carbon (**f**) adjacent to carboxylic acid moved downfield to 34.1 ppm, and the methylene carbon (**g**) next to sulfide went to 26.1 ppm.

The ^{13}C NMR spectrum of **22** was also similar to the spectrum of diacid **21**. The two differences were caused by the olefin present in mono-acid **22**.

One was the α,β-unsaturated carbonyl (**c**) at 165.2 ppm, and the other one was the *trans* and *cis* olefin revealed at 133.4 and 129.5, 129.4 ppm.

The successful isolation of mono-acid **22** suggested that the mono-acid 8_2A also could be made by controlling the reaction time. This provides the possibility of different combinations of polar head groups for 8_2 as a wall unit.

The coupling of two derivatives of macrocycle 8_2, **14** and **21** was catalyzed by tetramethylammonium hydroxide pentahydrate (Scheme 2.12) as before. After work-up and purification with gel permeation chromatography (LH-20), it was found that the coupled bis-macrocycle, 8_2PP$a8_2$Pa (**23**), was contaminated by one of the final products, Pa8_2PPa8_2Pa (**24**). This indicated that the same problem of retro-Michael addition still existed, although the ratio of contamination was decreased from 28% to 12% in comparison to 8_2PA8_2A (**19**) based on their negative LSIMS spectra. The mechanistic explanation for the retro-Michael addition as an intramolecular elimination mentioned earlier would require the transition state to form an eight membered ring. The same elimination could also be accomplished via an intermolecular process. The latter explains why the retro-Michael addition couldn't be prevented by the longer thioacid (Scheme 2.13). Another transporter candidate Pa8_2PPa8_2Pa (**24**) was made from contaminated precursor (**23**) through Michael addition of 3-mercaptopropionic acid.

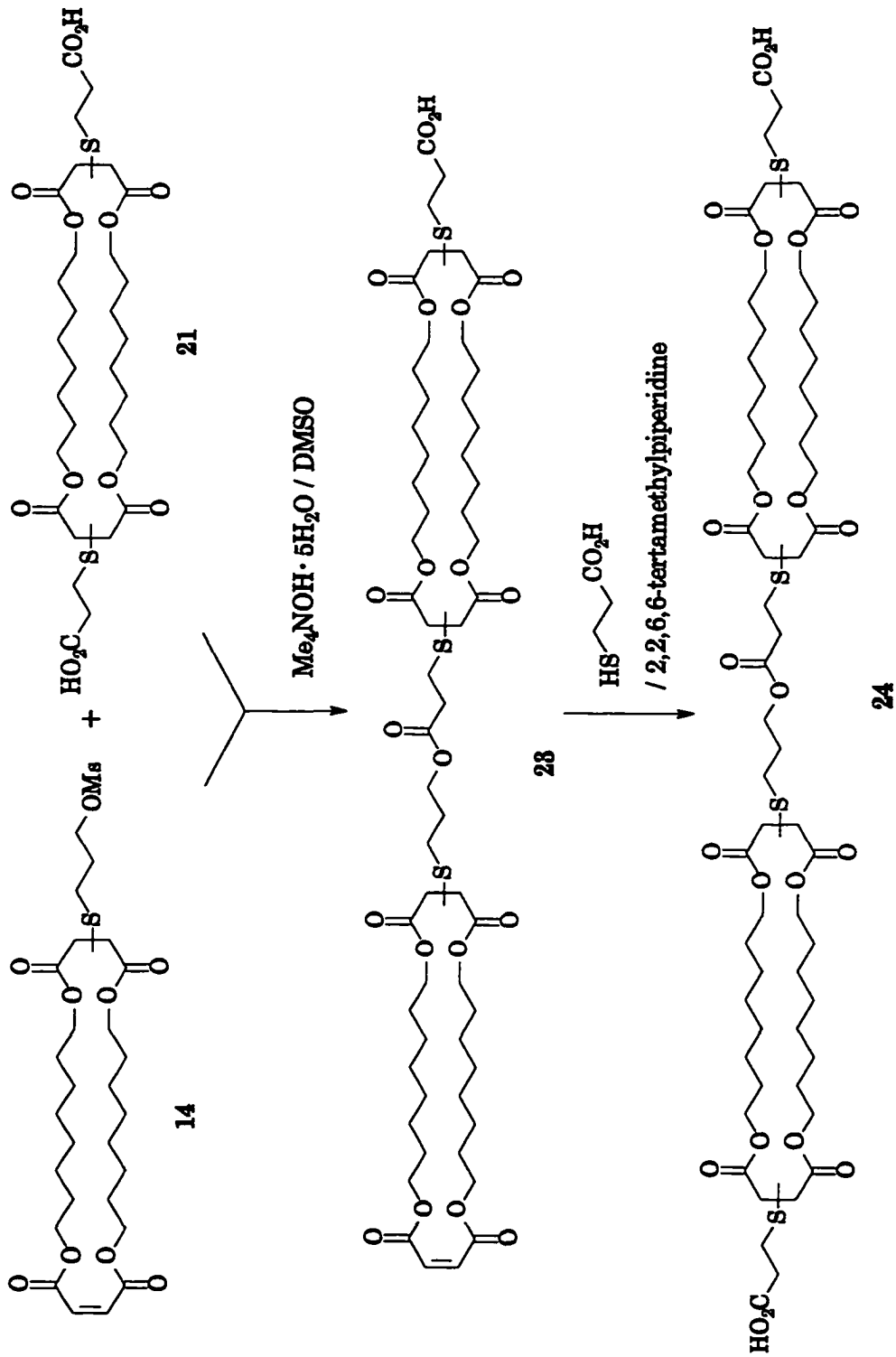

Scheme 2.12: Synthesis of Pa8$_2$PPa8$_2$Pa (24)

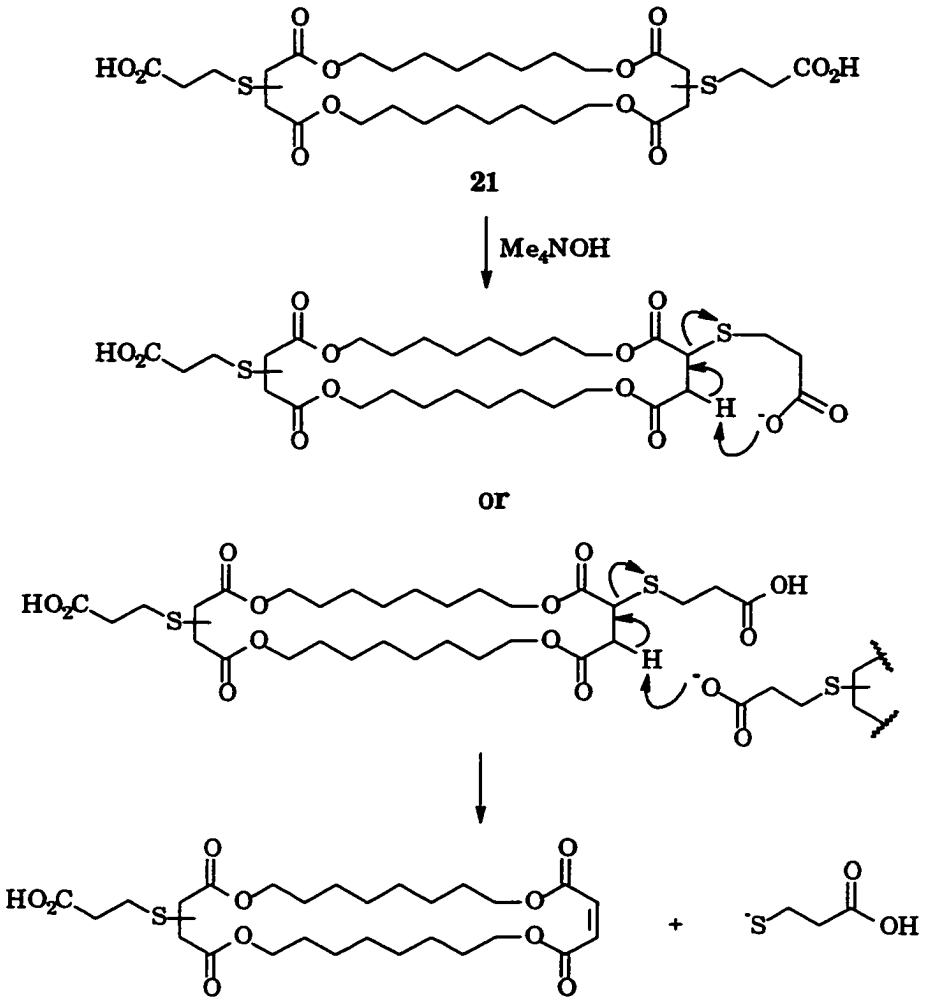

Scheme 2.13: Retro-Michael addition for Pa8$_2$Pa (**21**)

Figures 2.19 and 2.20 are the ^{1}H and ^{13}C NMR spectra of Pa8$_2$PPa8$_2$Pa (**24**). In comparison to the ^{1}H NMR spectrum of A8$_2$PA8$_2$A (**20**), the spectrum of **21** was also resolved without difficulty. The significant differences in **24** are that the methylene protons **f** appeared in the range 2.98 ~ 2.81 ppm and **g** shifted upfield to 2.73 ~ 2.60 ppm. Both of them overlapped with other methylene protons (**d** and **e**) to form two multiplets.

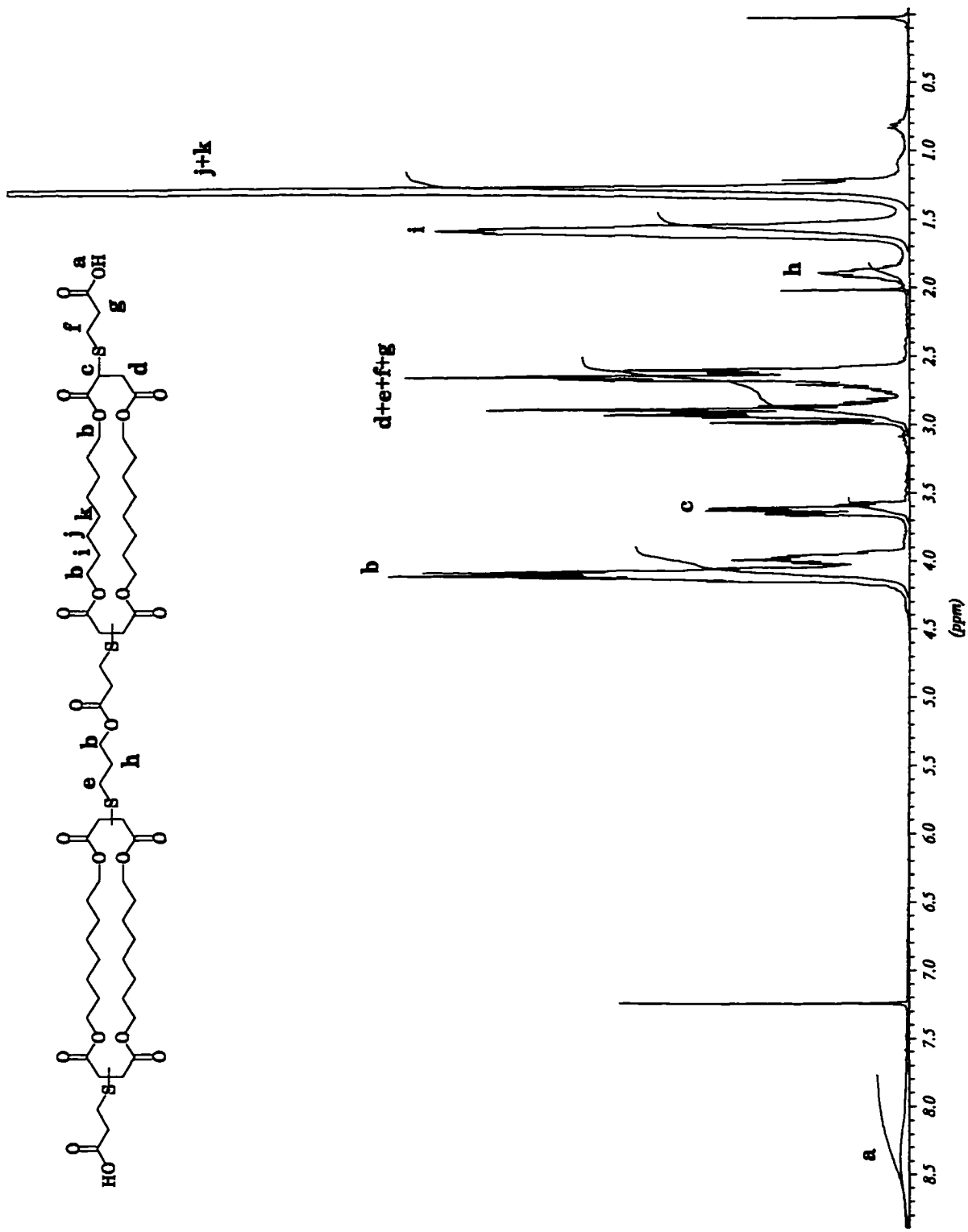

Figure 2.19: ^{1}H NMR spectrum of Pa8$_2$PPa8$_2$Pa (**24**)

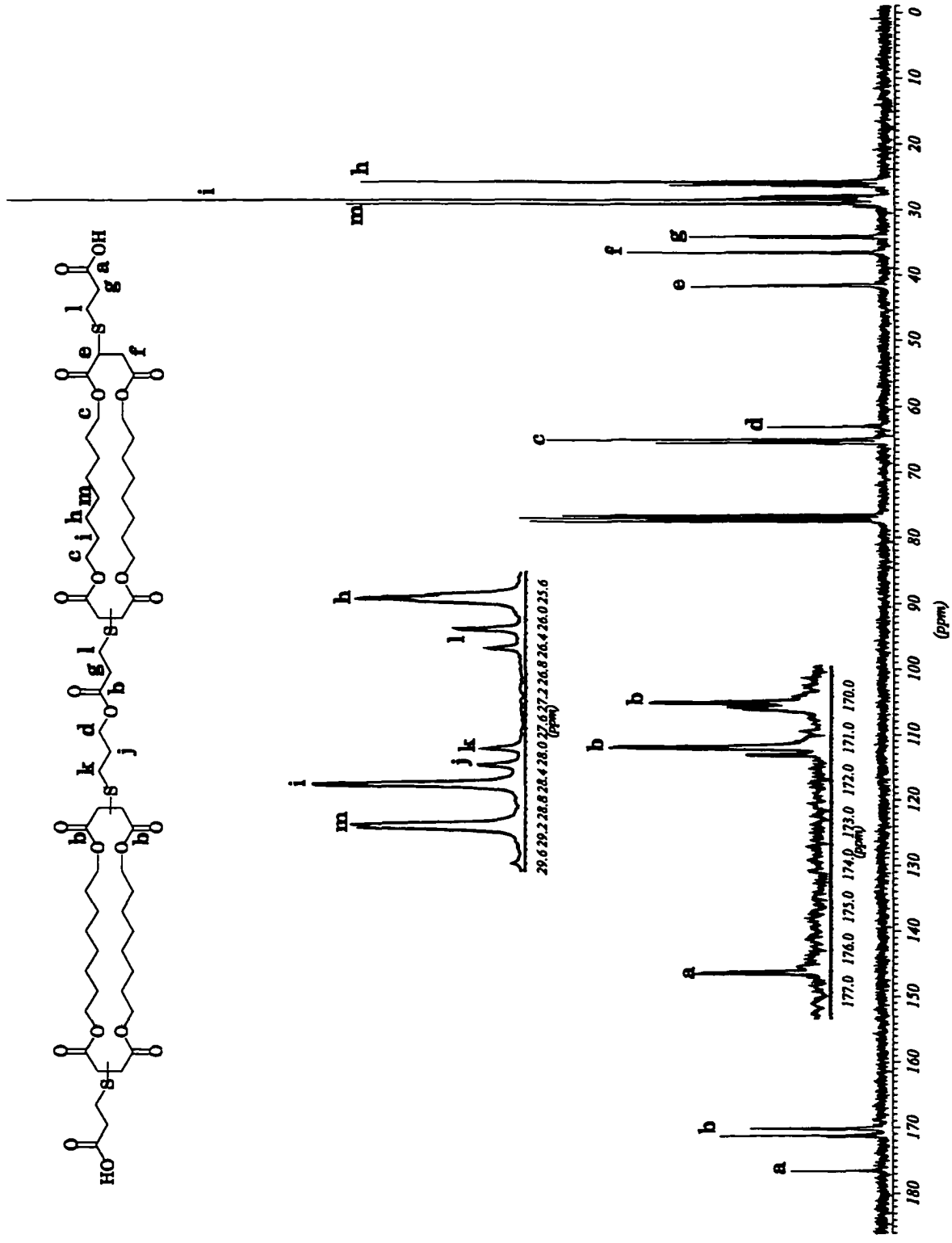

Figure 2.20: ^{13}C NMR spectrum of Pa8$_2$PPa8$_2$Pa (**24**)

The ^{13}C NMR spectrum of **24** was also quite similar to **20**. The only difference was the extra peaks from methylene carbons (**1**) on the side chain, which appeared at 26.4 and 26.1 ppm. The negative LSIMS spectrum indicated that the molecular ion $(M - H)^-$ was 1295.4 which verified the structure of **24**.

2.4.3 Syntheses of the redesigned two transporter candidates in the 8_2 series

Since $Pa(8_2)PPa(8_2)Pa$ (**24**) is three carbons longer than $A8_2PA8_2A$ (**20**), another perspective, the length of transporter, can be used to examine the effect on the properties of the transporter. To accomplish the same goal more directly, two more candidates were added in the 8_2 series: $A8_2Su8_2A$ (**26**), and $N8_2Su8_2N$ (**27**) (see Scheme 2.14). In the central link of these two compounds, the usual carboxyl (two atoms) is replaced by sulfide (one atom) to form a bit shorter transporter.

The syntheses of compound **26** and **27** are apparently relatively easier than ones of asymmetrical coupling compounds (Scheme 2.14). 2-Mercaptoethyl sulfide reacted with two equivalent of macrocycle 8_2 catalyzed by 2,2,6,6-tetramethylpiperidine to give a mixture of compound **25**, some unresolved bigger molecules (one possibility is $8_2Su8_2Su8_2$), plus unreacted macrocycle 8_2. A silica gel column with a gradient solvent of hexanes and ethyl acetate was used to separate unreacted 8_2. The rest of the mixture was purified

by gel permeation column (LH-20) eluted with a mixed solvent of 2-propanol and chloroform (3:4). After two cycles of separation, pure **25** was obtained from the middle fractions in 24% yield. Since the early fractions were still a mixture, the existence of $8_2Su8_2Su8_2$ could not be unambiguously verified.

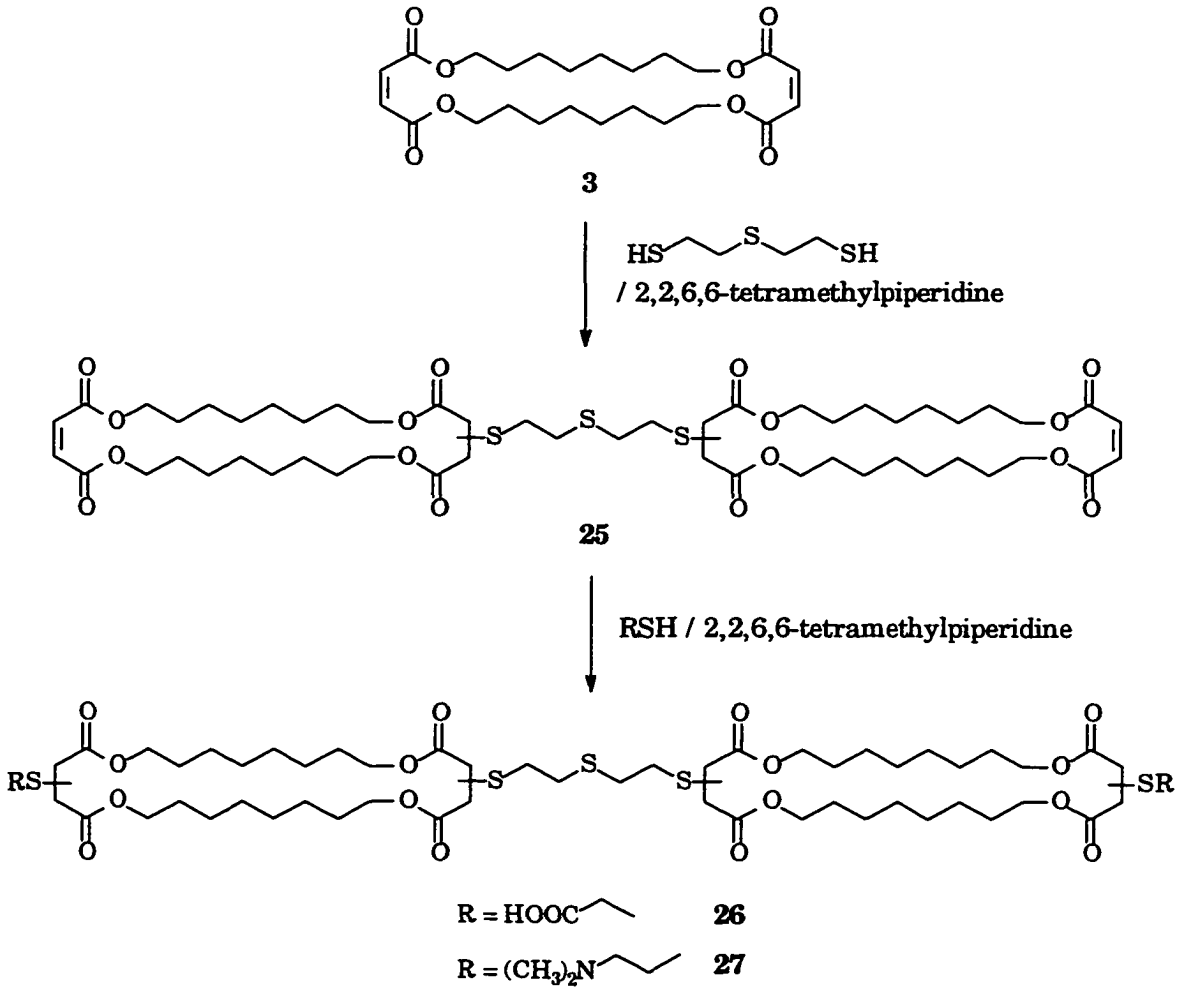

Scheme 2.14: The synthetic routes for $A8_2Su8_2A$ (**26**) and $N8_2Su8_2N$ (**27**)

Figures 2.21 and 2.22 are the ^1H and ^{13}C NMR spectra of precursor, 8_2Su8_2 (**25**). Its ^1H NMR spectrum is simpler than the asymmetrical precursor 8_2PA8_2A **19**. Due to the introduction of a symmetrical central linker, the

methine protons next to the sulfide (**c**) clearly gave a doublet of doublets. The methylene protons from the linker (**e** and **f**) might form two multiplets overlapped with protons **g** in 2.95 ~ 2.58 ppm. All of the chemical shifts and multiplicity for macrocycle remained the same as those of **19**.

The ^{13}C NMR spectrum of **25** is simpler that the one of **19** because of the symmetrical structure. There was only one regio-isomer formed, so the carbonyl carbons (excluding the α, β-unsaturated carbonyl) gave only two peaks at 171.0 and 170.0 ppm. The methylene carbons on the central linker (**h**) shifted up-field to 31.5 ppm in comparison to **19**. The negative LSIMS spectrum gave the molecular ion at 1058.4 for $(M - H)^-$ which also verified the compound is **25** as assigned.

This precursor 8_2Su8_2 then reacted with either 2-mercaptoacetic acid or N,N-dimethylaminoethanethiol via Michael addition again to add two head groups on the both end of the precursor. After work-up with 1M HCl and purification with gel permeation chromatography on Sephadex Lipophilic LH-20 using 2-propanol : chloroform (3:4), compounds **26** or **27** were obtained in 63% and 74% yield respectively. Figures 2.23 and 2.24 compare the ^1H and ^{13}C NMR spectra of $A8_2Su8_2A$ (**26**) and $N8_2Su8_2N$ (**27**).

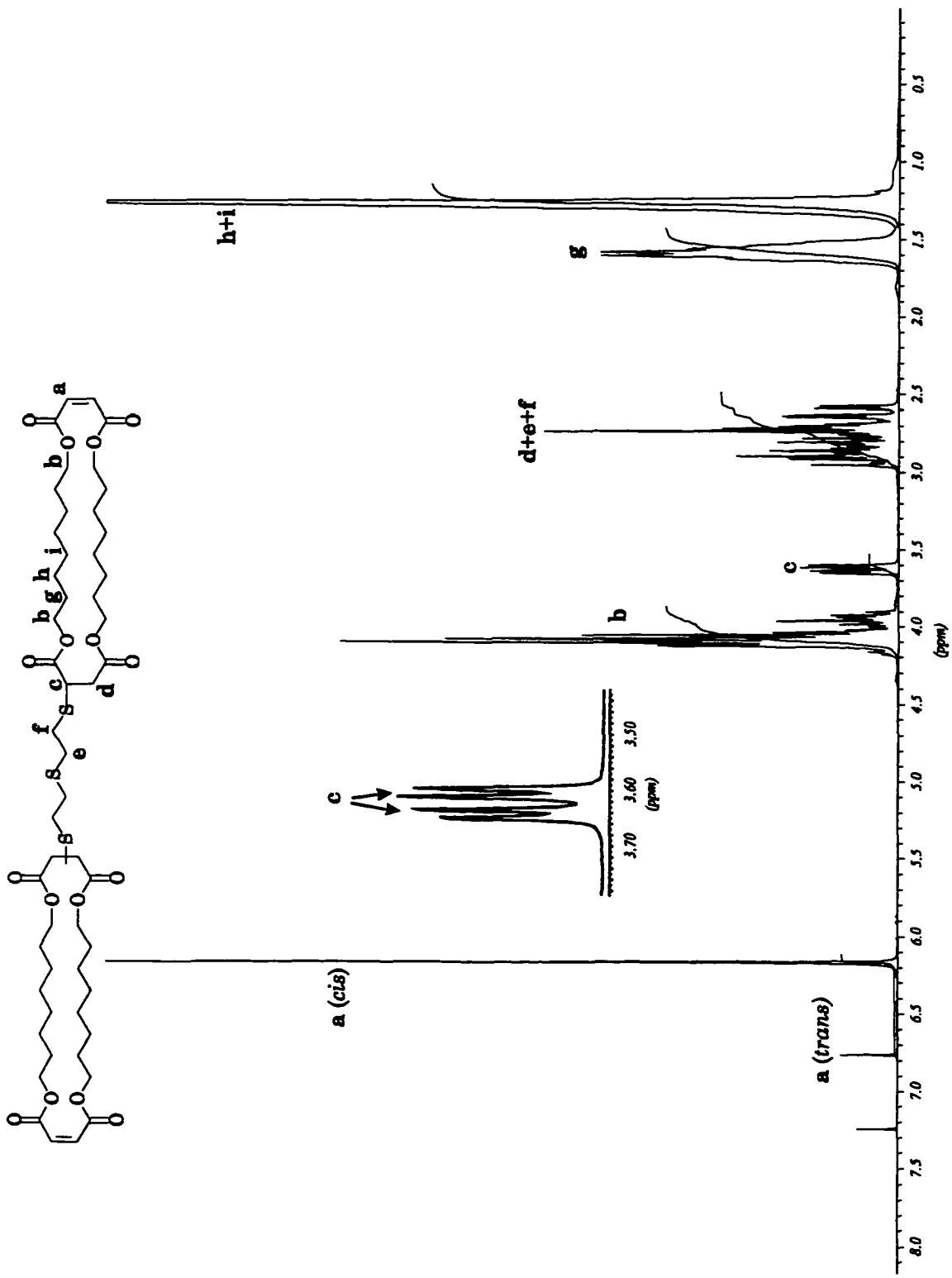

Figure 2.21: ^{1}H NMR spectrum of 8_2Su8_2 (**25**)

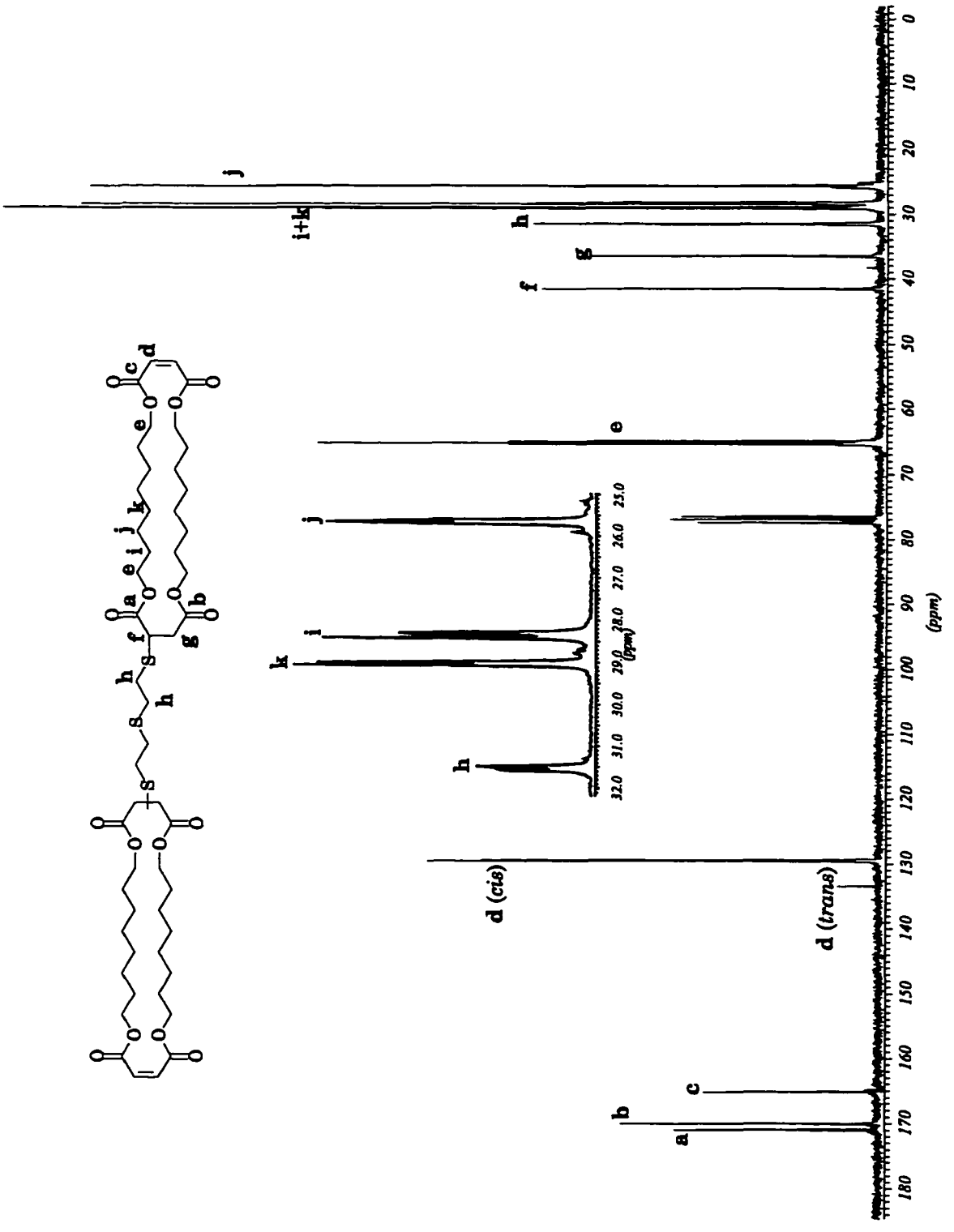

Figure 2.22: ^{13}C NMR spectrum of 8_2Su8_2 (**25**)

The ^{1}H NMR spectra of the two candidates indicated their differences in the head groups. For **26**, the broad singlet (**a**) at 7.61 ppm and a doublet of doublets (**d**) at 3.46 ppm clearly showed that acetic acid was the head group. The bigger sharp singlet (**g**) at 2.52 ppm and the multiplets in 2.91 ~ 2.56 ppm, plus the nearly perfect integration ratio indicated that N, N-dimethylaminoethyl was the head group in **27**. The methine proton next to the sulfide was changed from a clear doublet of doublets to a multiplet when the head group switched from the acetic acid to the N, N-dimethylaminoethyl.

The ^{13}C NMR spectra of **26** and **27** corresponded to their different head groups. The carbonyl of the carboxylic acid (**a**) at 174.1 ppm and the isolated methylene carbons (**f**) at 33.0 ppm were the evidence for the acetic acid head group in **26** which was mentioned in earlier synthetic discussion. The methyl carbons (**e**) at 43.4 ppm, the methylene carbons (**d** and **k**) at 57.1 and 26.6 ppm, plus the signals from the precursor **25** verified the assigned structure of **27**. Moreover, the clean negative LSIMS spectrum for **26** (molecular ion $(M - H)^-$ at 1241.4) and positive LSIMS spectrum for **27** (molecular ion $(M + H)^+$ at 1269.4) also help to confirm the structures.

At the end, four transporter candidates in the 8_2 series (**20**, **24**, **26**, and **27**) were synthesized. Their transport properties will be evaluated by two transport experiments and will be discussed in the later section of this thesis.

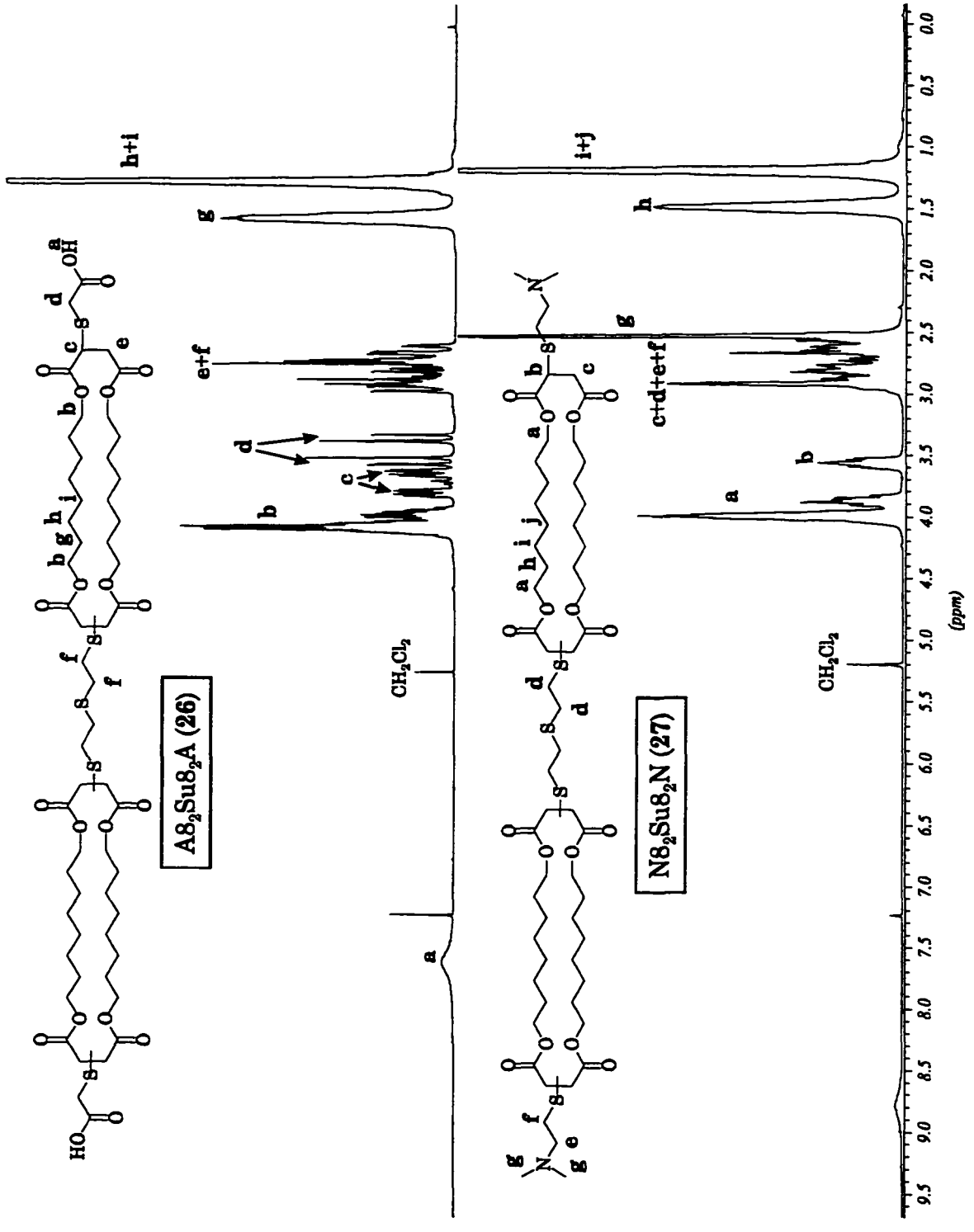

Figure 2.23: ^{1}H NMR spectra of **26** and **27**

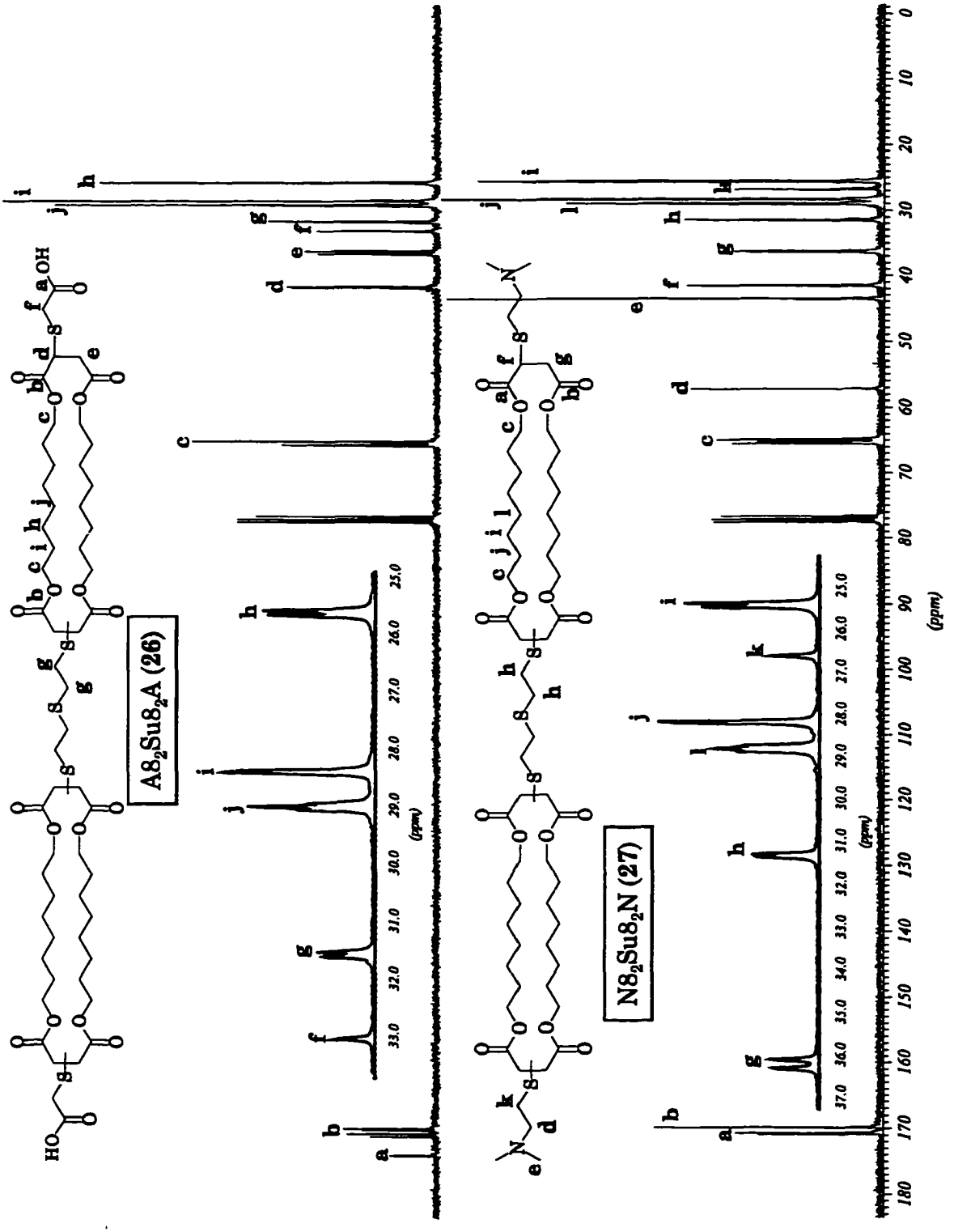

Figure 2.24: ^{13}C NMR spectra of **26** and **27**

2.5 "Second generation" in the 8Trg series

After the suite of transporter candidates was synthesized, two transport sets of experiments were conducted. One set was pH-stat titration of a vesicle bilayer system which will be discussed in a later section of this thesis. The other set was a planar bilayer experiment and was done by D. Loock. The information obtained from these experiments then was combined to evaluate the function of the targets. For the 8Trg and 8_2 series of compounds synthesized above, none of the transporters behaved as a voltage-gated ion channel. Although compounds **11**, **13**, **14**, and **15** in the 8Trg series created aggregates in bilayer membranes, they gave the same type of channel behaviors when the polarities of the potential applied to the bilayers was switched. Thus all head groups (neutral, negatively or positively charged at pH=7) must be able to penetrate bilayers from the outer to the inner aqueous phase. That redistribution allowed the transporter to adapt to any direction of potential applied. To prevent reorientation and create a voltage-gated ion channel, one head group must be modified to make it either bulky, or more hydrophilic, or both. These changes will "anchor" one head group of the transporter on one face of the bilayer, and will only allow the other small, less charged head group to "flip-flop" across the bilayer. The asymmetrical distribution should then produce a voltage-gated channel.

The simplest candidate is S8TrgPA8TrgA (**28**) (Scheme 2.15) which directly follows the synthetic route used with A8TrgPA8TrgA (**13**). The only difference was that 2-mercaptosuccinic acid was used to replace 2-

mercaptoacetic acid in the final Michael addition step. Due to the poor solubility in THF for 2-mercaptosuccinic acid, 2-propanol was used as a solvent. The reaction solution was refluxed for almost 3 h under nitrogen protection. After washing with 1M HCl and gel permeation chromatography (LH-20), S8TrgPA8TrgA **28** was obtained in 36% yield.

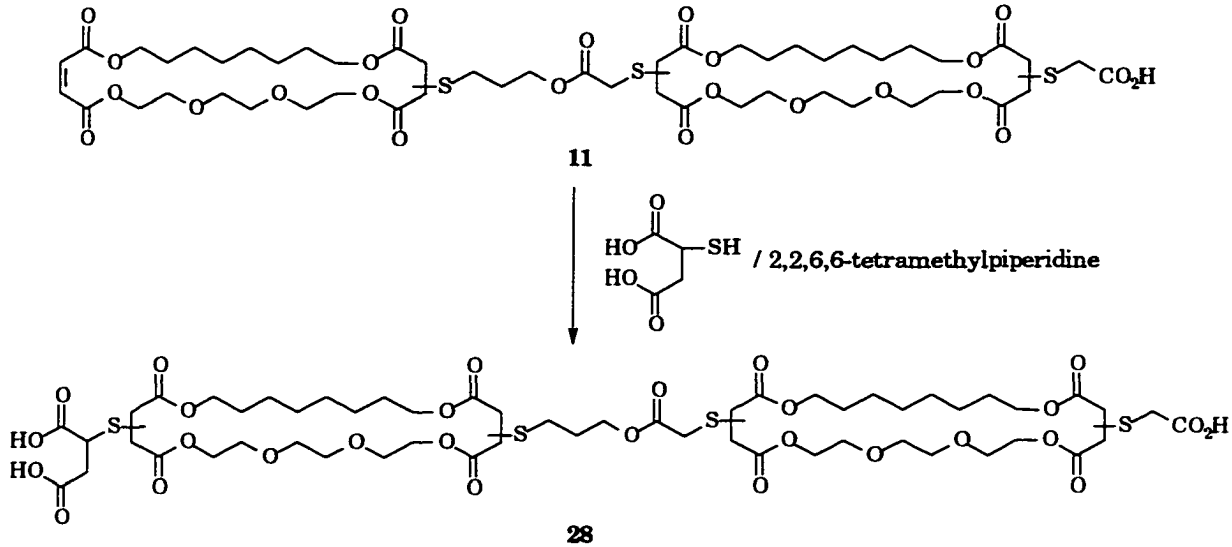

Scheme 2.15: Synthesis of S8TrgPA8TrgA (**28**)

Figures 2.25 to 2.27 are the ^{1}H, ^{13}C NMR and negative LSIMS spectra of **28**. The ^{1}H NMR spectrum of **28** has basically a similar pattern with other candidates in the 8Trg series. Its acidic protons (**a**) were at 7.37 ppm as a broad singlet. It had five methine protons (**d**) instead of four as in the other compounds (one more from the succinic acid group) which gave two multiplets in the range 3.90 ~ 3.61 ppm. Five sets of inequivalent methylene protons (**f**) coupled with each other and with the methine proton (**d**) to form two multiplets in the range 3.00 ~ 2.66 ppm. The integration matched the structure of **28** as expected.

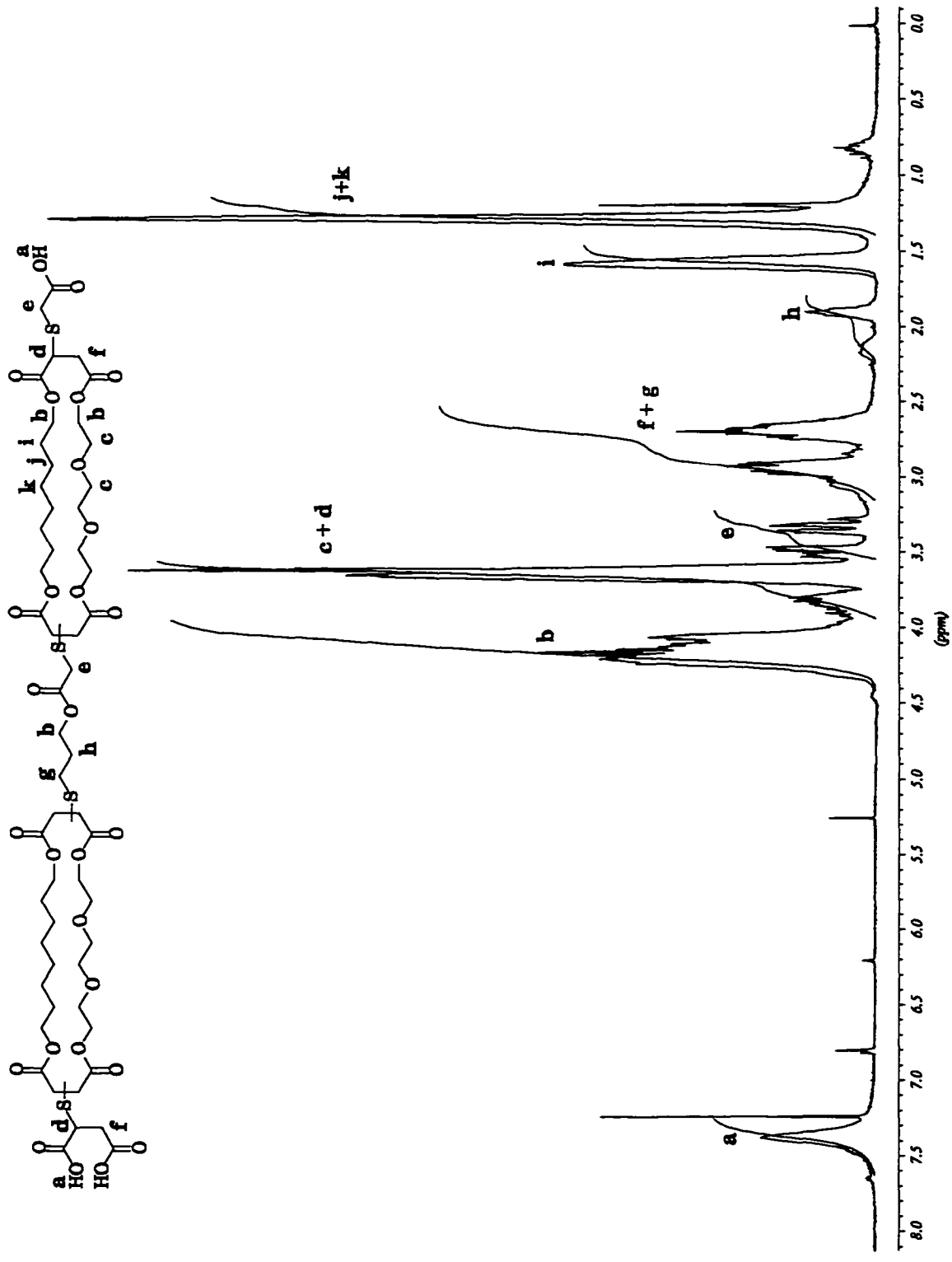

Figure 2.25: ^{1}H NMR ($CDCl_3$) of S8TrgPA8TrgA (**28**)

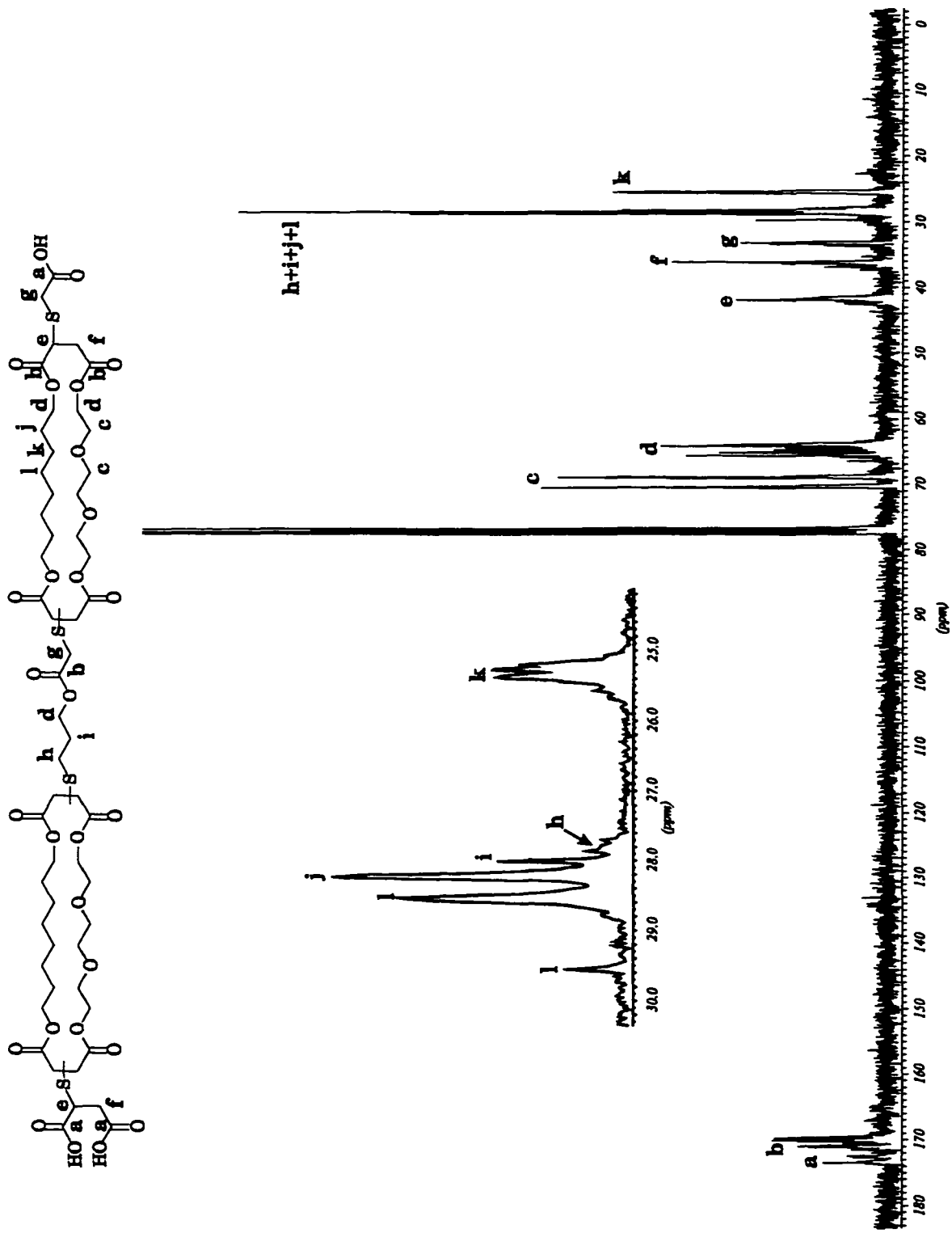

Figure 2.26: ^{13}C NMR ($CDCl_3$) of S8TrgPA8TrgA (**28**)

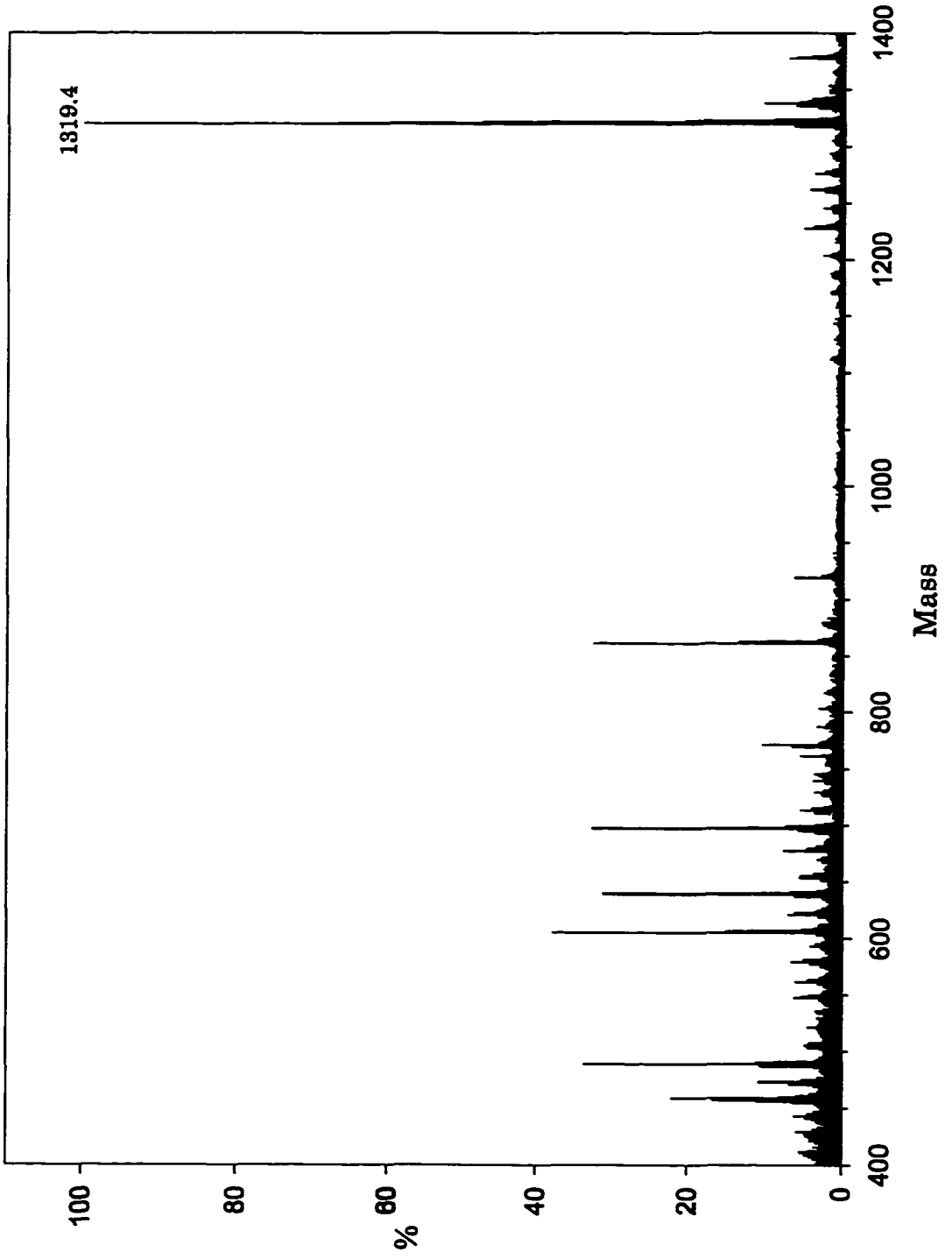

Figure 2.27: Negative LSIMS of S8TrgPA8TrgA (**28**)

The ^{13}C NMR spectrum of **28** was relatively simple. The chemical shifts from the newly added head group were overlapped with the precursor and its whole spectrum was almost same as the spectrum of **13**.

The negative LSIMS spectrum gave a dominant peak at 1319.4 which clearly indicated the molecular ion $(M - H)^-$ for S8TrgPA8TrgA (Figure 2.27).

2.6 Modification with bulky and/or hydrophilic head group

The synthesis of S8TrgPA8TrgA exhausted the commercially available bulky and hydrophilic thiols. Thus we looked at the syntheses of other thiols which could be used as potential head groups.

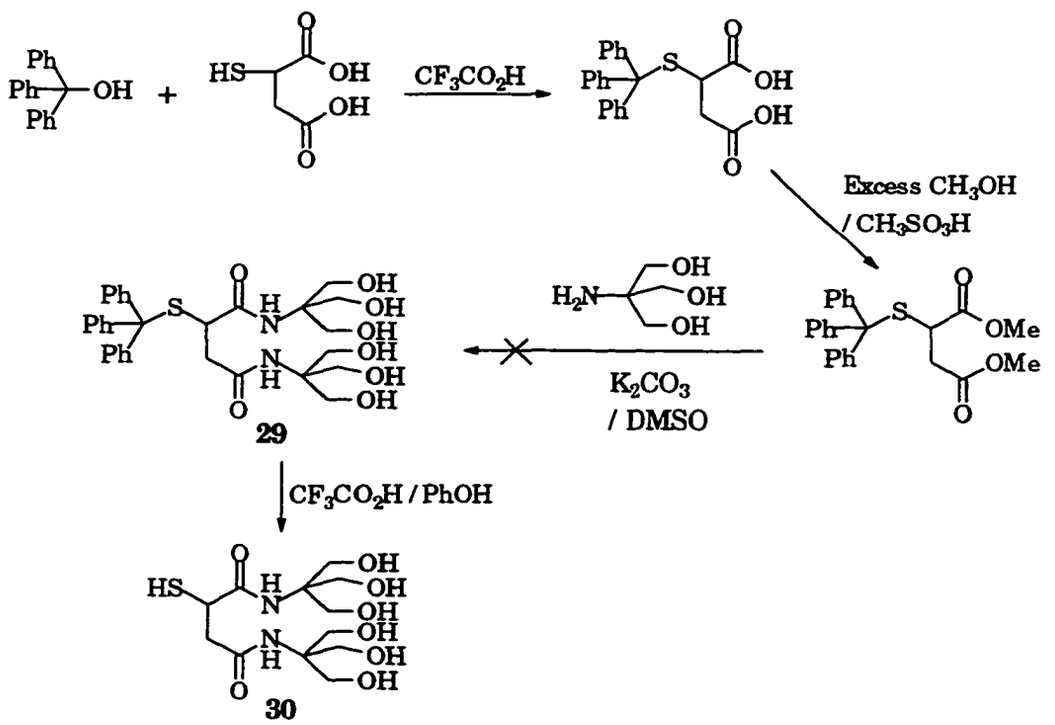

Scheme 2.16: Synthetic route for making dendrimeric type of head group

The first attempt was to make a neutral, dendrimeric type of head group as shown in Scheme 2.16. First 2-mercaptosuccinic acid was protected by triphenylmethanol to give a thiolether[38]. This carboxylic acid was treated with excess methanol to form a ester. Following the literature[39], the ester was then reacted with Tris (trishydroxymethylaminomethane) catalyzed by potassium carbonate in DMSO to give a diamide. However, the difficulties with the reaction were never worked out, and there was always a messy mixture formed in each trial which could not be separated. There was no sign that compound **29** was formed.

The second attempt was to make a derivative of a crown ether as sketched in Scheme 2.17. This head group will be bulky enough and bear a negative charge. The commercially available 2-aminoethanethiol hydrochloride reacted with diphenylethanol to form a thiolether[40]. The 1,2-18C6-dicarboxylic acid[41] was treated with acetyl chloride to undergo intramolecular dehydration and give the 18C6-anhydride[42]. The thiolether and anhydride were combined in the presence of excess triethylamine with the expectation that an amide would form. Unfortunately, the reaction always gave a mixture and no compound **31** could ever be separated. Some 1,2-18C6-dicarboxylic acid was recovered in some trials.

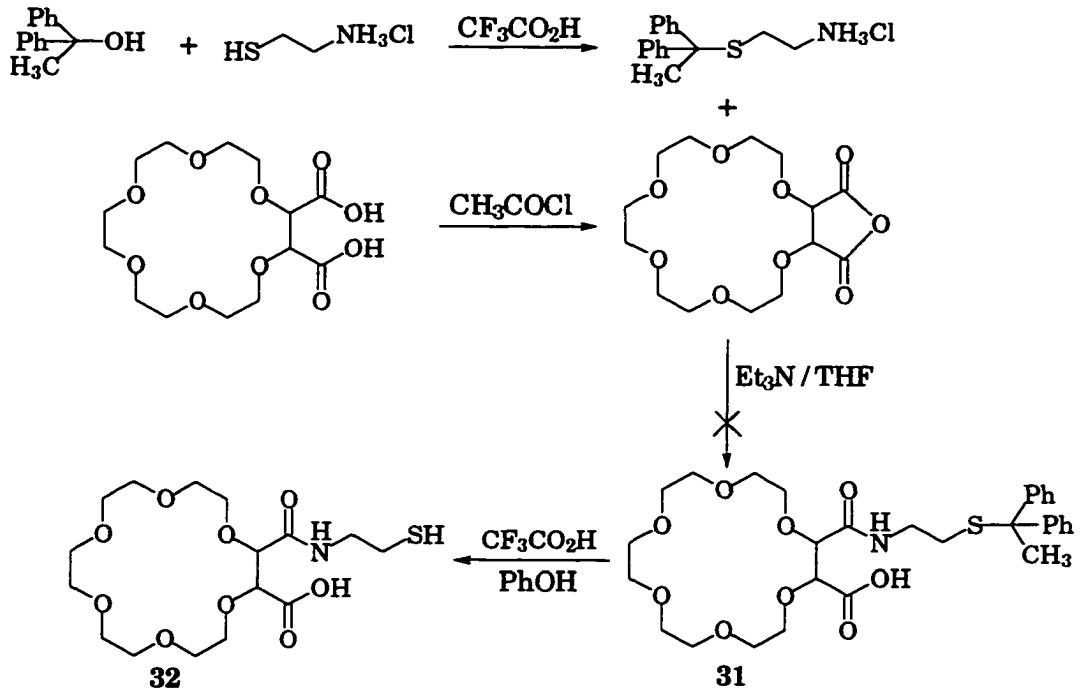

Scheme 2.17: Synthetic route for making a 18C6 derivative head group

The third exploration was directed to make a transporter with a net -2 charged head group. The head group candidate was chosen as a short peptide having three amino acid residues Cys-Asp-Asp. This peptide is commercially available through custom synthesis, and it was made at the Tripartite Microsequencing Center[43]. An LSIMS spectrum and an amino acid analysis confirmed that the peptide was synthesized. However, free thiol is easily oxidized in solution and it couldn't be fully characterized. To what degree the sample of Cys-Asp-Asp was contaminated by Asp-Asp-Cys-S-S-Cys-Asp-Asp is unknown.

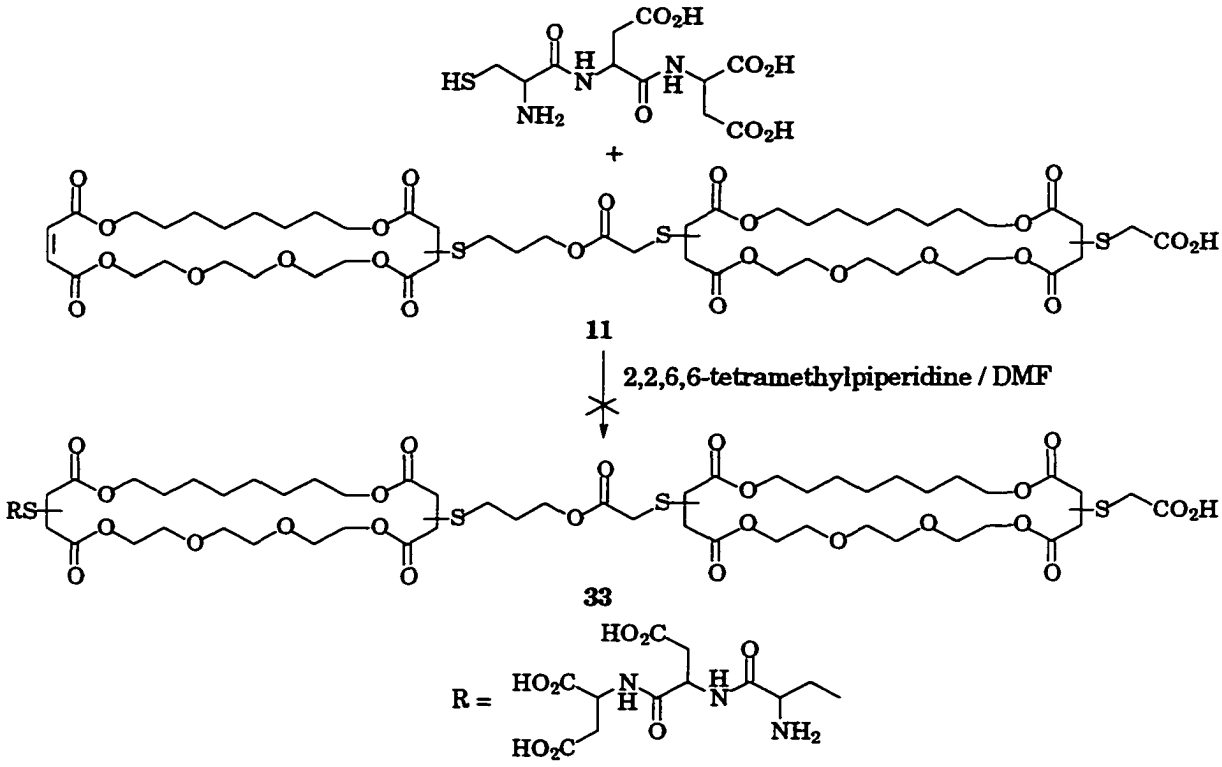

Scheme 2.18: Designed synthesis of compound **33**

As described in Scheme 2.18, the peptide Cys-Asp-Asp reacted with precursor, 8TrgPA8TrgA (**11**), using the catalyst 2,2,6,6-tetramethylpiperidine. The solution was heated at 70°C for 2 days in DMF protected by nitrogen. Unfortunately after work up and purification, the only compound obtained was unreacted **11**. In a model study, cysteine monohydrochloride monohydrate completely reacted with precursor, 8_2PA8_2A (**19**) under the same reaction conditions.

These three failed explorations clearly indicate the extra difficulty in working with thiols. Even when protected by either triphenylmethyl or diphenylethyl, the thiolether is still such a good nucleophile that it could not be prevented from interfering with the main reaction desired. As the third trial showed the thiol group is so easily oxidized to form disulfide that Michael

addition was unable to compete with it. This oxidation for forming disulfide also could happen in the other Michael addition steps, but it was compensated by adding a large excess of thiol, usually 3 ~ 4 times the equivalent amount. However, in the case of **33**, preparation of a larger amount of Cys-Asp-Asp is too costly, plus the difficulty for characterization of the peptide thiol hindered the synthesis of this interesting compound.

2.7 Summary

One conclusion to be drawn from these endeavors is that although thiol is a very good nucleophilic reagent, there is an unavoidable disadvantage of manipulating thiol groups: thiol is so active that it will participate in the main reaction, even it is protected in a thiolether form. The future development of similar construction systems should try to avoid using thiol.

In the whole exercise of the synthesis, although there were a few disappointments, the most exciting and important achievement was that simple voltage-gated ion channel **28** was successfully synthesized. From a synthetic efficiency point of view, the macrocyclizations and derivative manipulations are far from perfect, especially the mono-addition on the symmetrical olefins and the asymmetrical couplings which both significantly bring down the total yield. To maintain both the hydrophilicity and the hydrophobicity of macrocycle, and to simplify synthetic effort, the investigation of other macrocycle candidates was explored by L. Cameron[44]. The synthetic efficiency for the different macrocycles and derivatives was compared in her thesis.

CHAPTER 3. TRANSPORT MEASUREMENTS AND PROPERTIES DISCUSSION

Following previous studies[30, 32, 45] by former members of the group, pH-stat titration of vesicles is used to evaluate the transport capabilities of all of transporters synthesized. Furthermore, the planar bilayer experiment provides a powerful tool to examine single channel behavior and detect a voltage-gated ion channel. These two techniques will give a survey of transport activity and can be used to make mechanistic inferences.

3.1 Preparation and characterization of unilamellar vesicles

The assay depends on a source of unilamellar vesicles prepared under standard conditions to ensure maximum reproducibility. A phospholipid mixture composed of egg phosphatidylcholine (PC), egg phosphatidic acid (PA) and cholesterol in molar ratio 8 :1 :1 was used. The mixing of PA and cholesterol into egg PC will increase the packing density so that the stability of the bilayer membranes will be increased and slow self-leaking in the pH-stat titration can be controlled at a negligible level. The lipid mixture was stored in a refrigerator as a stock solution in chloroform. Batches were prepared directly from pure lipids shipped from Avanti in Dry Ice and handled under an argon atmosphere.

In a typical procedure, 3 mL of the chloroform solution containing 50 mg PC was evaporated to give a dry lipid film. The lipid film was then dissolved in diethyl ether, an internal buffer solution at pH = 6.6 (formed by bis-tris and D-mannitol) was added, and the two-phase mixture was sonicated to give a

homogeneous solution. The ether was removed by evaporation at a controlled pressure[46] and an external solution of unbuffered isoosmolal choline sulfate solution was added to give vesicles in which the internal buffer solution was entrapped. The vesicles were sized by filtration through Nucleopore membrane filters (1.0 μm and 0.4 μm) to give a reproducible size distribution. Gel filtration using unbuffered eluent removed the residual buffer solution on the outside of the vesicles together with small multillamellar vesicles. Particle sizing by dynamic light scattering[47] typically showed a bimodal distribution of vesicle sizes: 75 ~ 80% of the entrapped volume was associated with 350 nm diameter vesicles and the remainder with 130 nm diameter vesicles. A melittin assay typically showed 85% of the buffer contents are trapped in unilamellar vesicles.

3.2 pH-stat titration

In a pH-stat titration, the unilamellar vesicles containing entrapped buffer solution (pH=6.6) were first diluted with an isoosmolal choline sulfate solution. A base, choline hydroxide, was then added to adjust the pH to 7.6, and this created a unit pH gradient across the vesicle bilayer. A proton carrier, FCCP (carbonyl cyanide 4-(trifluoromethoxy)phenylhydrazone), was added to ensure proton release could occur rapidly in response to other cation fluxes. As indicated in Figure 3.1, an electroneutral cation-proton antiport was formed to follow the transport kinetics. An alkali metal cation concentration gradient was established by addition of a cation sulphate salt solution to the system.

Under these conditions of opposing pH and cation gradients, the pH evolves only slowly with a "drift" corresponding to about 10^{-10} mol·H^+·s^{-1}. When a transporter was added, the proton and cation gradient began to rapidly collapse. As the gradients collapse, protons are released into the bulk solution and the external pH drops. Choline hydroxide was continuously added to maintain fixed pH of 7.6 using a pH-stat controlled automatic burette. The volume of base added versus time data was accumulated until the transport event was completed.

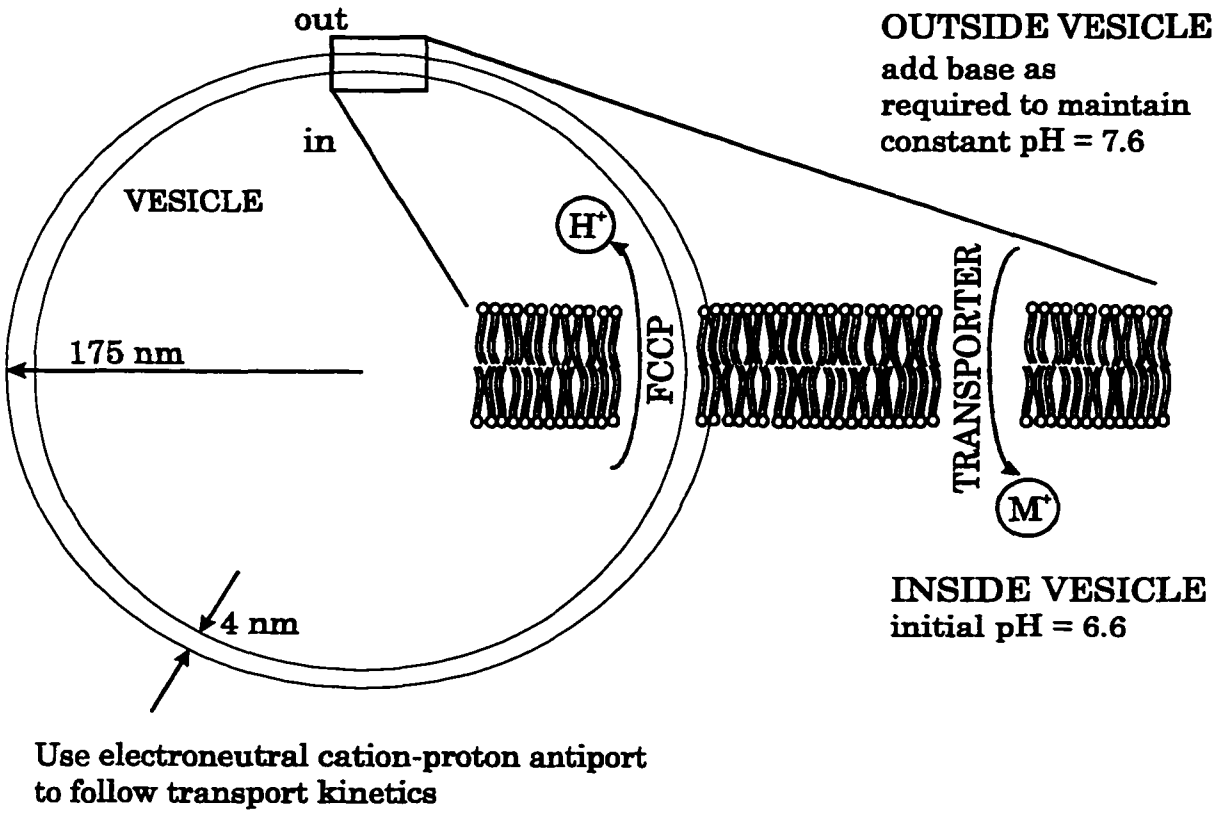

Figure 3.1: Schematic description of pH-stat titration

Figure 3.2 shows a typical titration curve obtained from the pH-stat experiment. After the proton carrier FCCP and alkali metal cation (K^+) were

added, there was only a very slow leakage. However, as soon as the transporter A8TrgPA8TrgA (**13**) was added there was a big pulse of protons released and the titrimeter rapidly added base. At this point in the transport event, the pH-stat lost control of the pH, due to the very rapid proton release in the local volume where transporter was added. Following a period of several minutes of even re-distribution, the titrimeter regained control of the pH. The choline hydroxide base was continuously added and the transport event was followed until it reached a plateau. A detergent, Triton, X-100 then was added to provoke lysis of the remaining vesicles. The total volume of choline hydroxide added was used to indicate 100% of vesicles equilibrated.

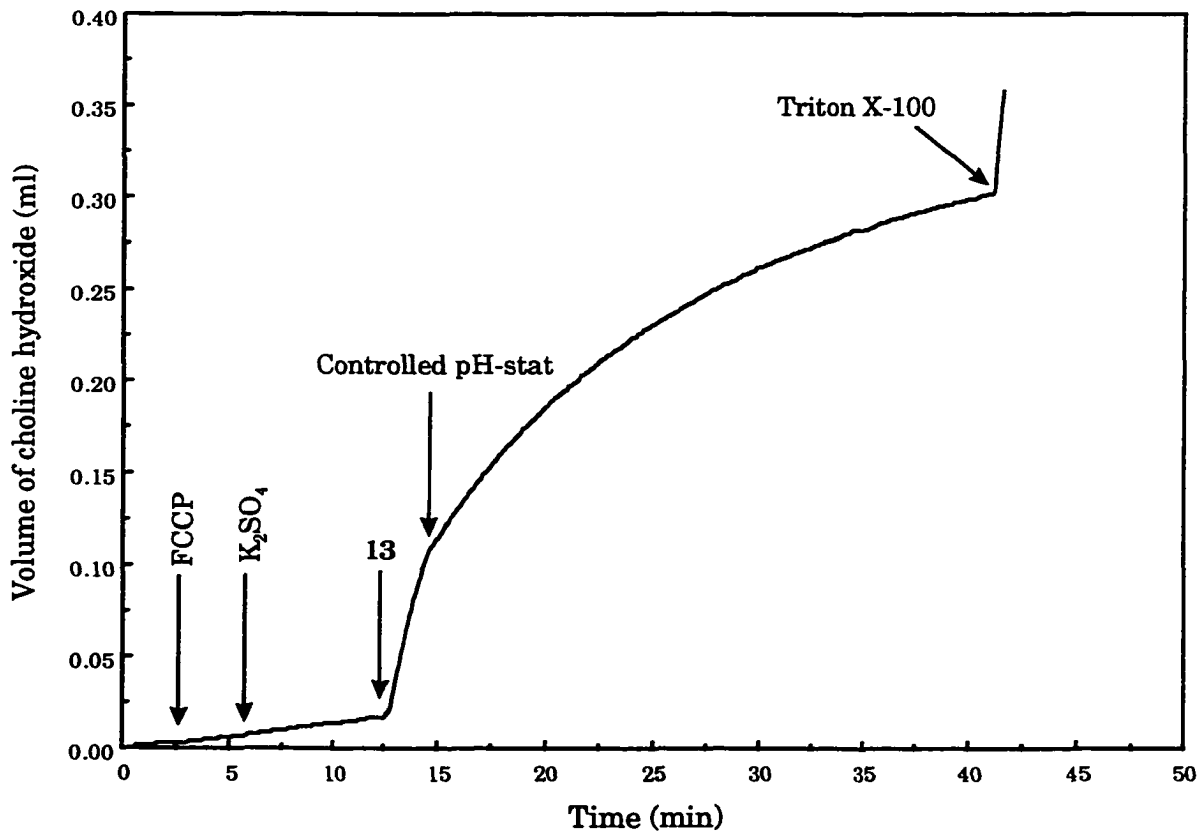

Figure 3.2: A typical pH-stat titration curve of compound **13**

3.3 Analysis of pH-stat results

3.3.1 Data processing and transport rate

For a pseudo first order process, it is expected that the volume of base added as a function of time will follow a conventional rate expression:

$$\ln [(V_{inf} - V_i) / (V_{inf} - V_o)] = k \cdot t$$

Where, V_{inf} is the volume of choline hydroxide added at infinite time.

V_o is the volume of choline hydroxide added at time = 0.

V_i is the volume of choline hydroxide added at time, t.

Although proton release was too rapid for the pH-stat titrimeter to control at the beginning of most of titrations, ln $[(V_{inf} - V_i) / (V_{inf} - V_0)]$ versus time was linear once the titrimeter was able to maintain a constant pH gradient. Figure 3.3 shows the example for compound **13**, using the data from Figure 3.2 for the calculation. From the point of controlled pH-stat to the steady-state plateau, the plot is linear (r^2 = 1.00). Thus the proton efflux is first-order process over the time when the pH titration is controlled. Based on previous studies[30, 32], this first-order process is due to formation of active ion channels, such as gramicidin which exhibit "all or nothing" transport. Ion translocation is so rapid that during a short channel opening, the entire vesicle contents are equilibrated. Under these conditions, the pH-stat experiment shows only the rate at which new channels open in unequilibrated vesicles. All the experimental data for the candidate compounds in this thesis are of this type, suggesting that all are channels.

The reproducibility of transport rate between different vesicle

preparations is estimated to be ±10%, and replicates within a single vesicle preparation can be better than ±5%. Experiments involving a range of concentrations were done in a single vesicle preparation to improve precision.

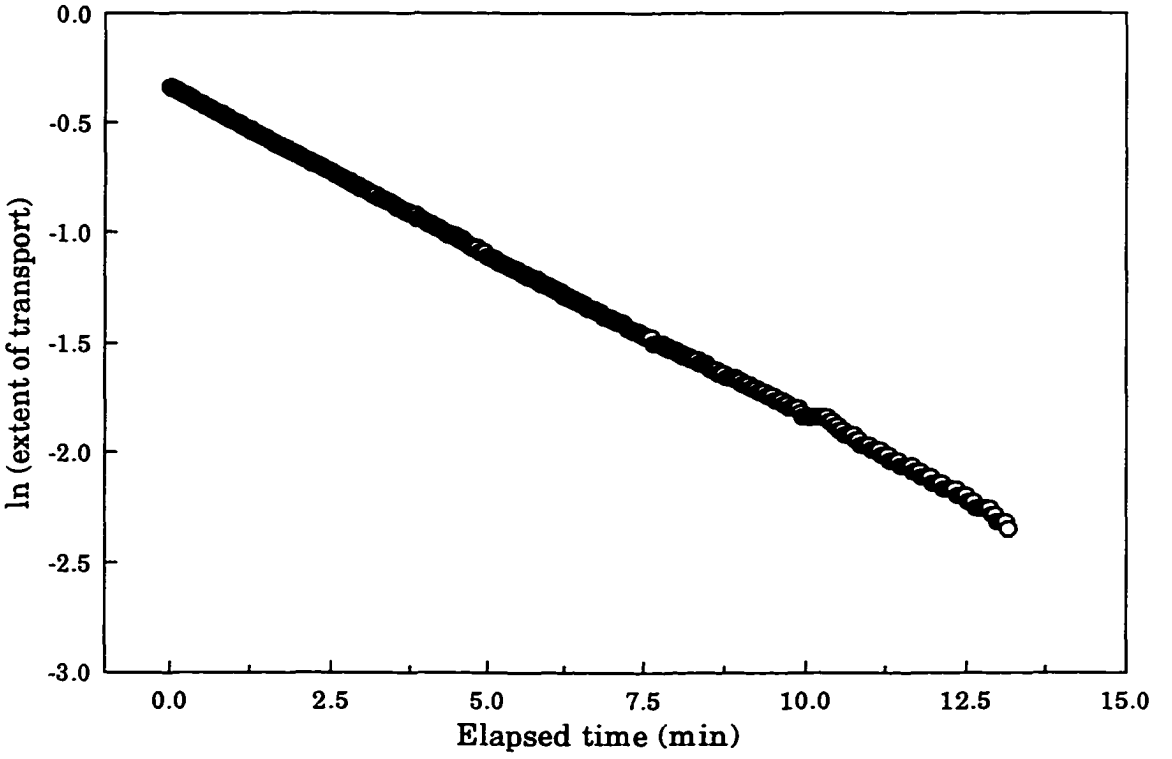

Figure 3.3: First order analysis for compound **13**, data of Figure 3.2. Time started from the point at which pH-stat control was established.

3.3.2 Transporters in the 8Trg series

The data from pH-stat titration experiments for transporter candidates of the 8Trg series are summarized in Table 3.1. Several points emerge from the data. The discussion below begins with the apparent kinetic order of the process, examines an inter-comparison of transporter activity, and concludes with different cation selectivity in the 8Trg series.

Transporter	Kinetic order	[Tr] (μM)	Rate × 10^{10}, mol $H^+ \cdot s^{-1}$ [a]				
			Li^+	Na^+	K^+	Rb^+	Cs^+
G8TrgPA8TrgA (**15**)	2.0	14	8.9	10	9.7	--	8.5
N8TrgPA8TrgA (**14**)	2.3	21	12	13	11	13	13
A8TrgPA8TrgA (**13**)	1.8	20	4.0	4.7	9.5	6.6	4.9
8TrgPA8TrgA (**11**)	2.1	21	4.6	--	6.2	5.7	5.4
S8TrgPA8TrgA (**28**)	>> 2 [b]	21	0.5	1.4	2.0	14	3.4
G8TrgPTaP8TrgG [c]	2.6	60	--	--	8.9	--	--

a. Uncertainty in rate ± 10%

b. Very high, see text

c. Compound G8TrgPTaP8TrgG is an active pore-former made previously[32].

Table 3.1: Transport of alkali metal cation by candidates in the 8Trg series

3.3.2.1 Apparent kinetic order

When different amounts of transporter are added to the titration cell, different transport rates are observed. Figure 3.4 shows a typical example in which the extent of transport for A8TrgPA8TrgA (**13**) increased as its concentration increased in the vesicle solution. The increase of three fold in concentration results in about a six fold increase in rate. This increase in both rate and extent is also the typical behavior for the channel-type transporter such as gramicidin and other synthetic ion channels[48].

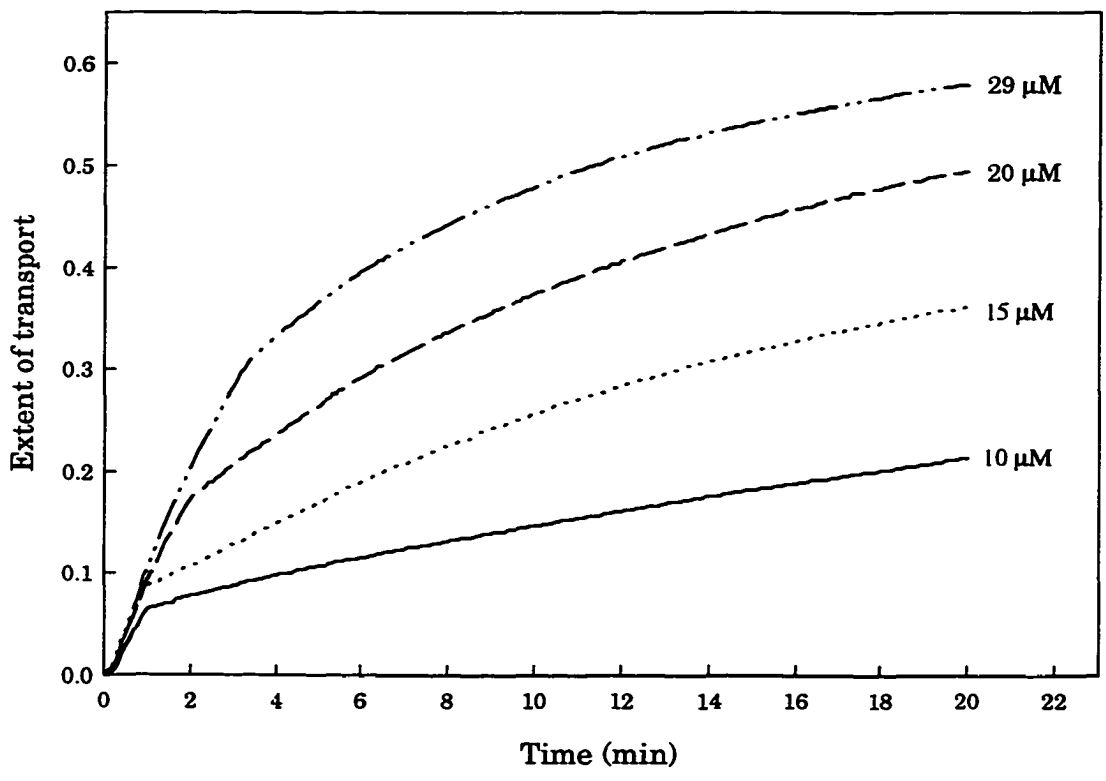

Figure 3.4: The dependence of transport on the concentration of A8TrgPA8TrgA (**13**)

Analysis of the data from experiments of this type can yield an apparent kinetic order. If the process is represented as:

$$\text{rate} = k\,[A]^a\,[B]^b\cdots$$

then at short time, log (initial rate) = logk + a·log[A] + b·log[B]···

In the experiment, if all variables are constant except the concentration of transporter, the plot of log (initial rate) as a function of log (concentration of transporter) will be linear and the slope will be the apparent kinetic order.

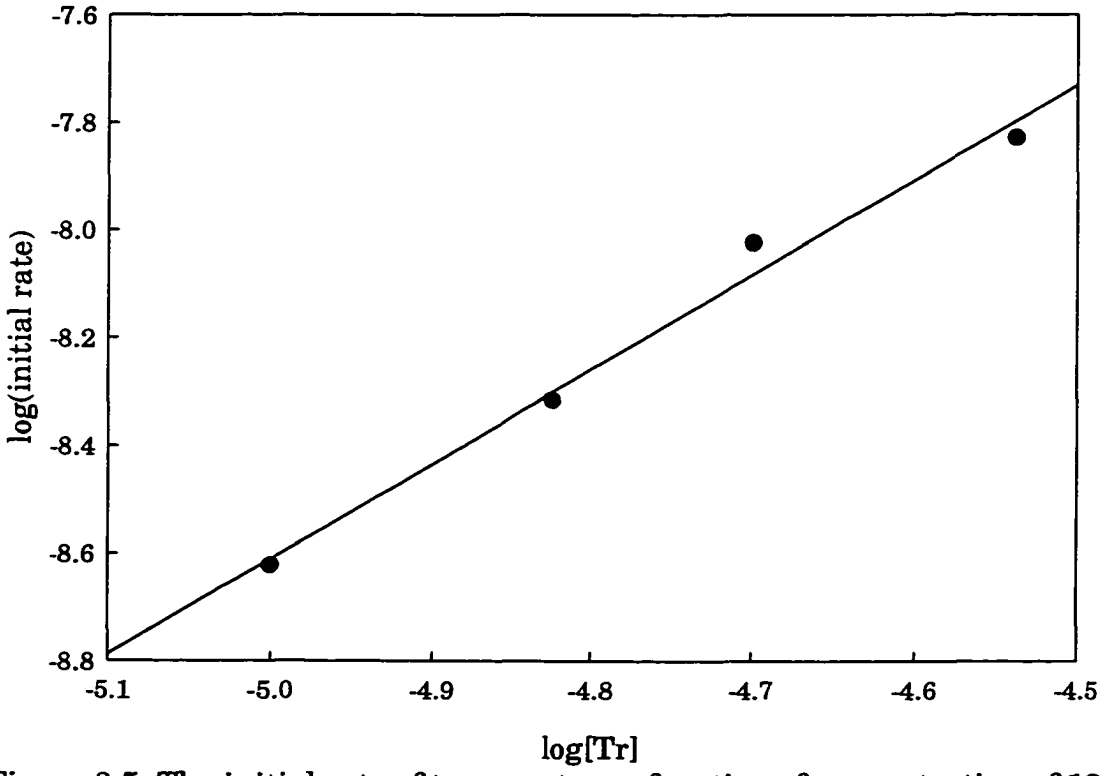

Figure 3.5: The initial rate of transport as a function of concentration of **13**

Figure 3.5 shows an example drawn from data for A8TrgPA8TrgA (**13**) as described in Figure 3.4. From the slope, the kinetic order can be calculated as 1.8 for compound **13** ($r^2 = 0.99$).

Using the same method, the apparent kinetic order for N8TrgPA8TrgA (**14**), G8TrgPA8TrgA (**15**), and the precursor 8TrgPA8TrgA (**11**) were obtained as reported in Table 3.1. All values were about 2 which indicates an aggregation of transporter is required for the initiation of transport. An active dimer would be the simplest model consistent with these results.

In the 8Trg series, S8TrgPA8TrgA (**28**) is an exception. For the same concentration range as Figure 3.4, the rate is significant but invariant (Figure 3.6). However, below 5.3 μM concentration, **28** is inactive, thus saturation is achieved over a very narrow concentration increment (5.3 - 10 μM). This corresponds to about a 16 fold rate increase for double the concentration. The narrow concentration range precludes accurate detection of the kinetic order as in other cases, but it is clear that the apparent kinetic order much greater than 2. This suggests an even larger aggregation is the kinetically active structure for **28** than for the other members of the series.

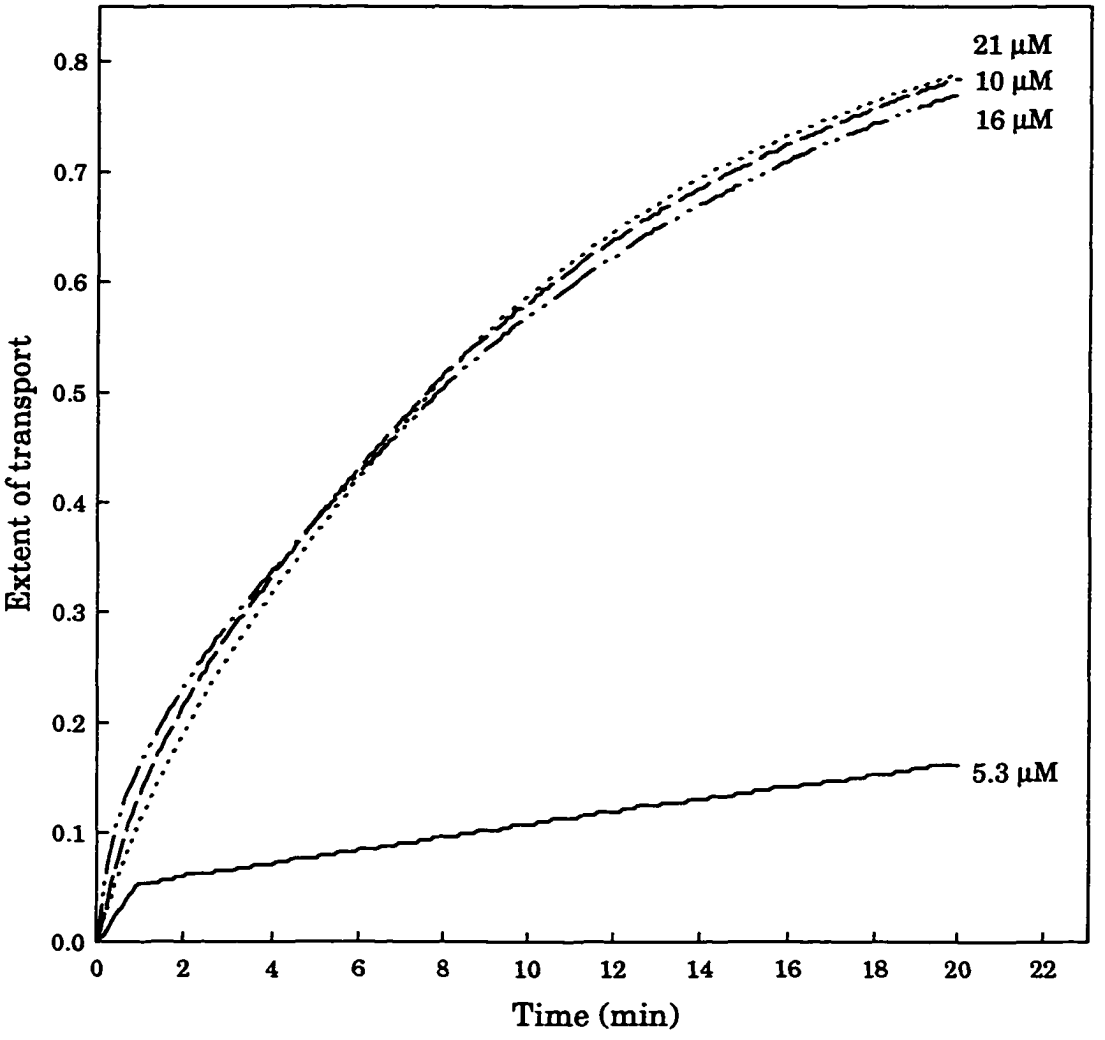

Figure 3.6: The dependence of transport on the concentration of S8TrgPA8TrgA (**28**)

3.3.2.2 Transporter activities

When both the concentration of the transporter and the alkali metal are kept the same, the rate obtained will represent the relative activity of the transporter in bilayers. Experimentally, this is difficult to achieve as each transporter has an optimum concentration for its active transport. Therefore,

the relative activity of transporters can be compared through normalization of the transport rates to the same concentration, normalized concentration. The normalized rate is given by:

$$\text{Normalized rate} = ([Tr]_{\text{normalized}} / [Tr]_i)^{\text{kinetic order}} \times \text{rate}_i$$

Where $[Tr]_i$ is the concentration of transporter which gives an optimum transport rate and $[Tr]_{\text{normalized}}$, normalized concentration, is chosen to fall in the middle of the range where the transporters are active.

Since the kinetic order of compound **28** can not be obtained from experiments and its transport rates were measured at 21 μM concentration, the transport rates for other compounds were normalized to the same concentration, 21 μM. Therefore, Table 3.2 is obtained from the data of Table 3.1 using the additional assumption that the kinetic order determined for K^+ is the same for all other alkali metal cations. The data in Table 3.2 can be used to compare either a cation selectivity for a specific transporter, or a relative activity order for different transporters in presence of a specific cation.

From Table 3.2, the pore-former G8TrgPTaP8TrgG which was an active transporter made previously[32] is compared to the new candidates in the 8Trg series. All the new pore-former candidates are apparently more active. Among them, G8TrgPA8TrgA (**15**) is the most active compound, N8TrgPA8TrgA (**14**) and A8TrgPA8TrgA (**13**) are quite close, but both of them are more active than precursor 8TrgPA8TrgA (**11**), the candidate S8TrgPA8TrgA (**28**) is the least active in the 8Trg series (in K^+ medium).

Transporter	[Tr] (μM)	$Rate_{normalized} \times 10^{10}$, mol H^+ s^{-1} [a]				
		Li^+	Na^+	K^+	Rb^+	Cs^+
G8TrgPA8TrgA (**15**)	21	20	24	22	--	19
N8TrgPA8TrgA (**14**)	21	12	13	11	13	13
A8TrgPA8TrgA (**13**)	21	4.4	5.1	10	7.2	5.3
8TrgPA8TrgA (**11**)	21	4.6	--	6.2	5.7	5.4
S8TrgPA8TrgA (**28**)	21	0.5	1.4	2.0	14	3.4
G8TrgPTaP8TrgG [b]	21	--	--	0.58	--	--

a. $Rate_{normalized}$ is derived from standardized transport rate at 21 μM.

b. Compound G8TrgPTaP8TrgG is an active pore-former made previously[32].

Table 3.2: The normalized transport rates for the 8Trg series

In order to compare the relative activities easily, the data from Table 3.2 can be represented schematically in Figure 3.7. It is found that the relative activity order of transporters in cation Li^+, Na^+, or Cs^+ solution is quite similar to the ones in K^+ solution, **15** > **14** ≥ **13** ≥ **11** > **28**. However, there is one exception which is in Rb^+ solution. The relative activity order is changed to: **28** ≥ **14** > **13** > **11** (The data for **15** was not available.).

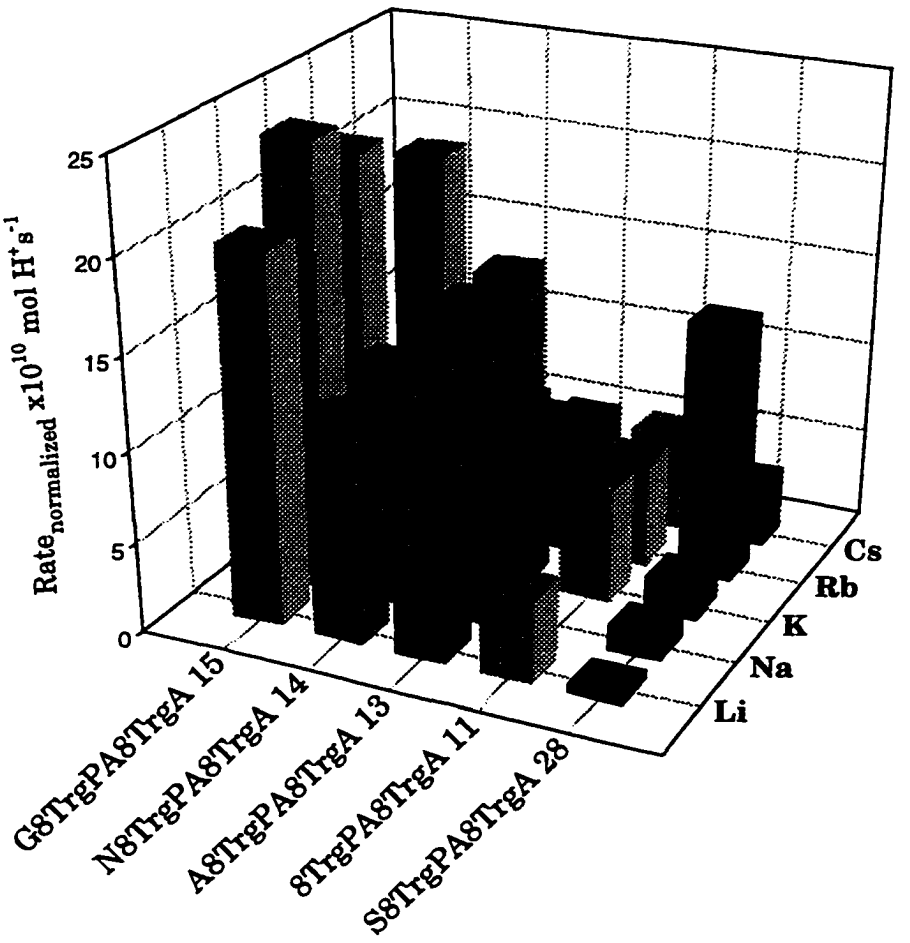

Figure 3.7: The cation selectivity of the 8Trg series

3.3.2.3 Cation dependence

If the concentration of a transporter is kept constant and different alkali metal cations are added, then the cation selectivity for the transporter can be obtained. Figure 3.7 presents the selectivity of alkali metal ion transport for the 8Trg series. While compounds **11, 14,** and **15** have almost no selectivity, **13** has a modest selectivity order as $K^+ > Rb^+ > Cs^+ \sim Na^+ > Li^+$. This is known as

the Eisenman IV selectivity sequence[49,50] and is typical of hard cation interaction with neutral oxygen donors. On the other hand, compound **28** has a more significant selectivity in the order $Rb^+ > Cs^+ > K^+ > Na^+ > Li^+$ (Eisenman II selectivity sequence). This is typical of a "softer" oxygen donor type indicating less cation transporter interaction in the rate-limiting process (channel initiation).

3.3.2.4 Summary for the 8Trg series

The kinetic data show that the five transporters in the 8Trg series form active aggregates in bilayers, either as a dimer or as a higher oligomer. Comparing the relative activity with the pore-former made before, one conclusion can be drawn that the central linkage of the transporter for the 8Trg series plays a significant role in determining overall activity. The head groups are more crucial for controlling cation selectivity.

3.3.3 Transporters in the 8_2 series

In order to compare the hydrophobicity and hydrophicility effects on the wall unit, similar experiments were done for the transporter candidates in the 8_2 series. The data is summarized in Table 3.3.

As found for the transporters in the 8Trg series, compounds **20**, **24**, **26**, and **27** behaved as typical channels in vesicle bilayers, since their titration curves all followed first-order process with increased of extent of transport upon increase in the concentration of transporters .

Transporter	Kinetic order	[Tr] (μM)	Rate × 10^{10}, mol $H^+ \cdot s^{-1}$ [a]				
			Li^+	Na^+	K^+	Rb^+	Cs^+
$A8_2PA8_2A$ (**20**)	0.94	21	2.8	1.6	11	19	5.1
$Pa8_2PPa8_2Pa$ (**24**)	1.0	21	2.4	1.5	5.1	6.5	3.6
$A8_2Su8_2A$ (**26**)	1.1	32	1.1	0.8	2.2	1.6	1.1
$N8_2Su8_2N$ (**27**)	1.0	32	1.7	1.8	2.5	3.1	2.0
$P8_2PTaP8_2P$ [b]	1.6	57	--	--	9.1	--	--

a. Uncertainty in rate ± 10%

b. Compound $P8_2PTaP8_2P$ is an active pore-former made before[32].

Table 3.3: Transport of alkali metal cation by candidates in the 8_2 series

3.3.3.1 Apparent kinetic order

Like the 8Trg series, the extent of transport for the transporters in the 8_2 series also increased as concentration increased in the vesicle solution. Figure 3.8 shows one example for $Pa8_2PPa8_2Pa$ (**24**).

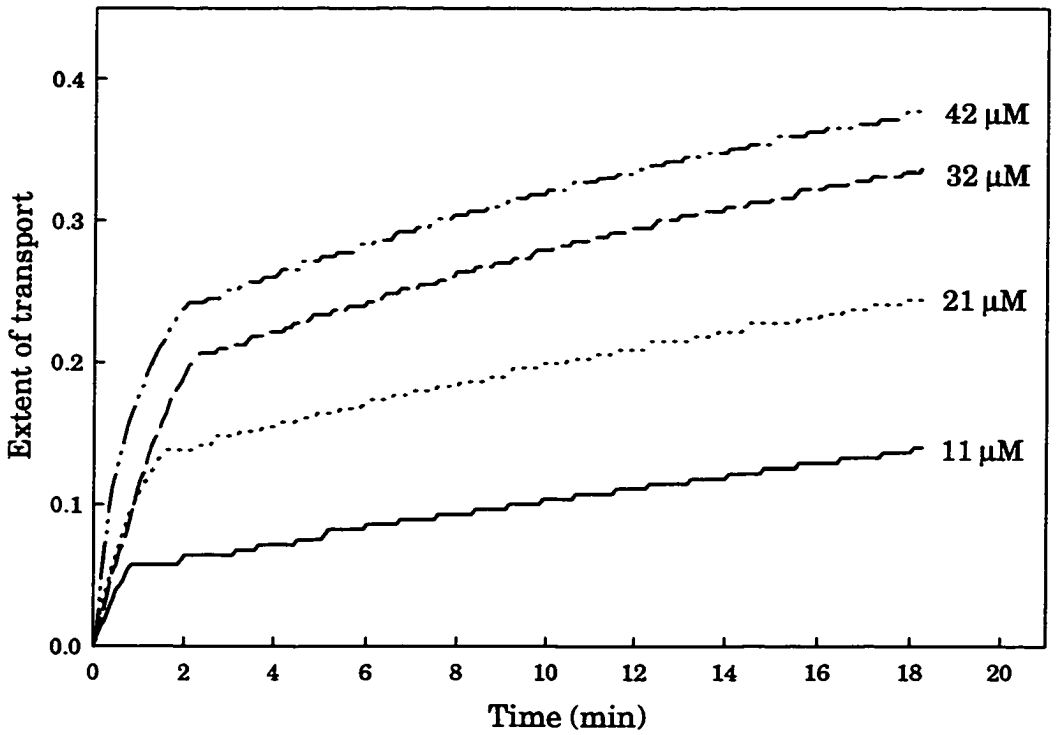

Figure 3.8: The dependence of transport on the concentration of **24**

As above, the apparent kinetic order was determined from a plot of log (initial rate) as a function of log (transporter concentration) for a concentration of transporter between 10 and 40 μM. For compounds **20**, **24**, **26**, and **27** in the 8_2 series the apparent kinetic orders are all around one. This suggests that they do not form aggregates in bilayers to the same extent as the 8Trg series compounds, or that the transport is initiated by a single molecule.

3.3.3.2 Cation selectivity and relative activity

In order to compare the relative transport activity in the 8_2 series, the normalized transport rates were generated following the same data manipulation as in the 8Trg series. The data are given in Table 3.4.

Transporter	[Tr] (μM)	$Rate_{normalized} \times 10^{10}$, mol H^+ s^{-1} [a]				
		Li^+	Na^+	K^+	Rb^+	Cs^+
$A8_2PA8_2A$ (**20**)	21	2.8	1.6	11	19	5.1
$Pa8_2PPa8_2Pa$ (**24**)	21	2.4	1.5	5.1	6.5	3.6
$A8_2Su8_2A$ (**26**)	21	0.71	0.50	1.4	1.0	0.72
$N8_2Su8_2N$ (**27**)	21	1.1	1.2	1.6	2.1	1.3
$P8_2PTaP8_2P$ [b]	21	--	--	1.8	--	--

a. $Rate_{normalized}$ derived from standardized transport rate at 21 μM

b. Compound $P8_2PTaP8_2P$ is an active pore-former made before[32].

Table 3.4: The normalized transport rates of the 8_2 series

Molecular dynamics and mechanics calculations using MM2 force field optimization from the CAChe Scientific program suite suggest that $A8_2Su8_2A$ (**26**) and $N8_2Su8_2N$ (**27**) both adopted a twisted conformation due to the three sulfide bonds on the central linker, and the rest of transporters had quite similar conformation as $A8_2PA8_2A$ (Figure 3.9). The low energy conformers of transporters in the 8Trg series plus **20**, **24** all have a length about 30 Å, but **26** and **27** are both approximate in 19 Å. Even though the central linkers are only one atom shorter than the one of $A8_2PA8_2A$ (**20**), the experimental data indicate

that **26** and **27** are much less active than **20**. This is probably due to the twisted sulfide central linker which shortens the overall length of transporter.

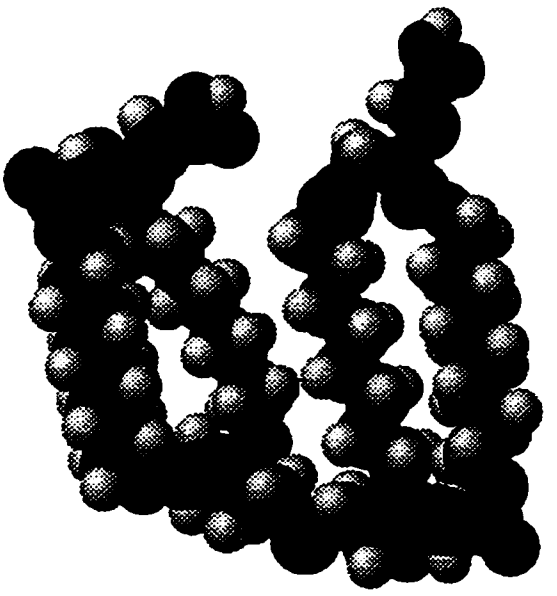

$A8_2Su8_2A$ (**26**)

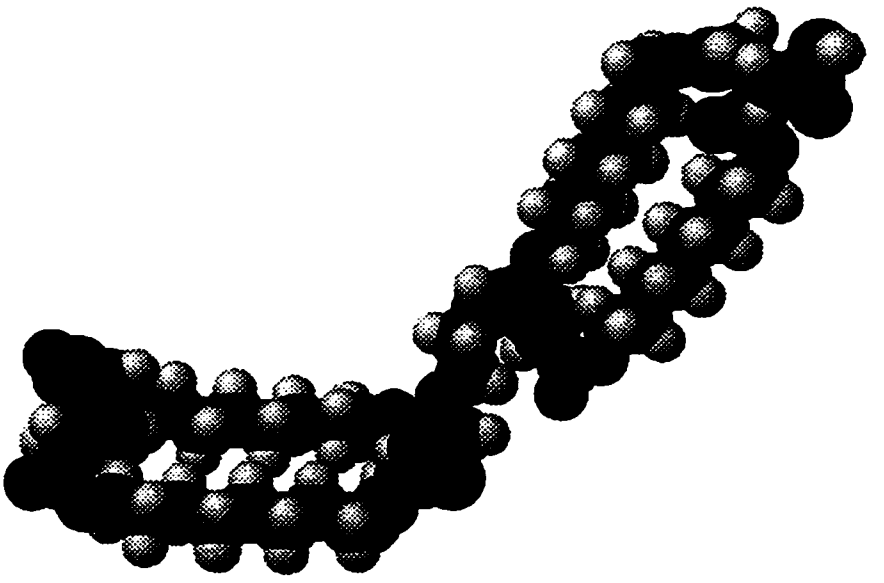

$A8_2PA8_2A$ (**20**)

Figure 3.9: The low energy conformations of $A8_2Su8_2A$ (**26**) and $A8_2PA8_2A$ (**20**)

On the other hand, Pa8$_2$PPa8$_2$Pa (**24**) is one atom longer in the linker, or three atoms longer in the total length than A8$_2$PA8$_2$A (**20**). Its less active transport rate might caused by both linker and head group effects. The relative transport rate of these four compounds in alkali metal cation solution is in the order: A8$_2$PA8$_2$A (**20**) > Pa8$_2$PPa8$_2$Pa (**24**) > N8$_2$Su8$_2$N (**27**) > A8$_2$Su8$_2$A (**26**), see Figure 3.10. These length finding are consistent with James who showed a sharp length dependence in another series of artificial ion channel[31].

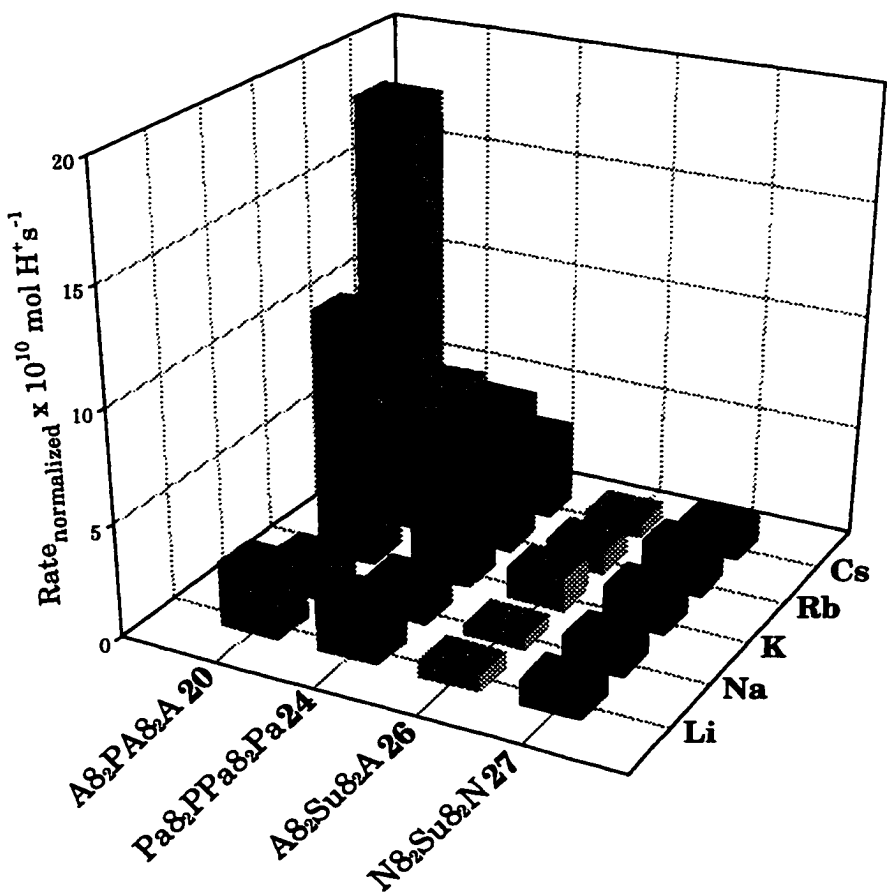

Figure 3.10: Cation selectivity and transport activity in the 8$_2$ series

The data in Table 3.4 can be represented graphically in Figure 3.10 which indicates that the cation selectivity among these four transporters in the 8_2 series was quite different. $A8_2PA8_2A$ (**20**), and $Pa8_2PPa8_2Pa$ (**24**) had a significant cation selectivity in the order $Rb^+ > K^+ > Cs^+ > Li^+ > Na^+$ (Eisenman III sequence). In contrast, $A8_2Su8_2A$ (**26**)and $N8_2Su8_2N$ (**27**) have almost no selectivity. The Eisenman III sequence suggests neutral donors to the cations in a manner intermediate between the extremes in the 8Trg series.

3.3.3.3 Summary for the 8_2 series

From the transport activity comparison in the 8_2 series, a similar conclusion can be drawn to the results in the 8Trg series. In both cases the central linker plays a far more important role than the head groups for controlling the activity of transporters. In the 8_2 series where sulfide was used as a linker, transporters were much less active than ester used as a linker, especially for the larger alkali metal cations K^+, Rb^+, and Cs^+.

3.4 The exploration of voltage-gated ion channel

3.4.1 The significant behavior of S8TrgPA8TrgA in pH-stat titration

There are some interesting perspectives for transporter S8TrgPA8TrgA **28**. First in its structure, one head group has a -2 charge and the other one has -1 charge (pH=7). Therefore, the former head group is more hydrophilic and bulky than the latter one, and these properties will make the -2 charged head group much harder to penetrate the bilayer. Secondly, the results from the

experiment of concentration dependence for **28** are different from other transporters in 8Trg series. From inactive to active, then to saturation, **28** only takes a small concentration increment (5.3 μM to 10 μM) compared to other pore-formers in the 8Trg series (10 μM to > 30 μM). Its apparent kinetic order is obviously much bigger than 2, and this indicates that **28** forms a higher oligomer for its aggregation in the simplest model. The third is its alkali metal ion selectivity (Figure 3.11): for Li^+, Na^+, and K^+, **28** is basically inactive, and it shows only small activity for Cs^+. However, **28** is very active in Rb^+ solution. Finally the behavior of **28** in presence of Rb^+ is remarkable. Not only it is very active at a concentration higher than 5.3 μM, but also it gives the same apparent first-order reaction even when the titrimeter doesn't follow the pH gradient during the early stages of the transport event. This phenomenon implies the channel opening time could be very short, and the transport is well controlled by **28**.

A 350nm diameter vesicle with our buffer system maintains a 1 pH unit gradient which is equivalent to +60 mV of transmembrane potential relative to ground on the outside[36]. A rationale for Figure 3.11 is that there is a threshold for this pore-former S8TrgPA8TrgA (**28**) which depends on the cation. Rb^+ and Cs^+ might reduce the threshold under the present pH condition to a greater extent than K^+, Na^+, or Li^+.

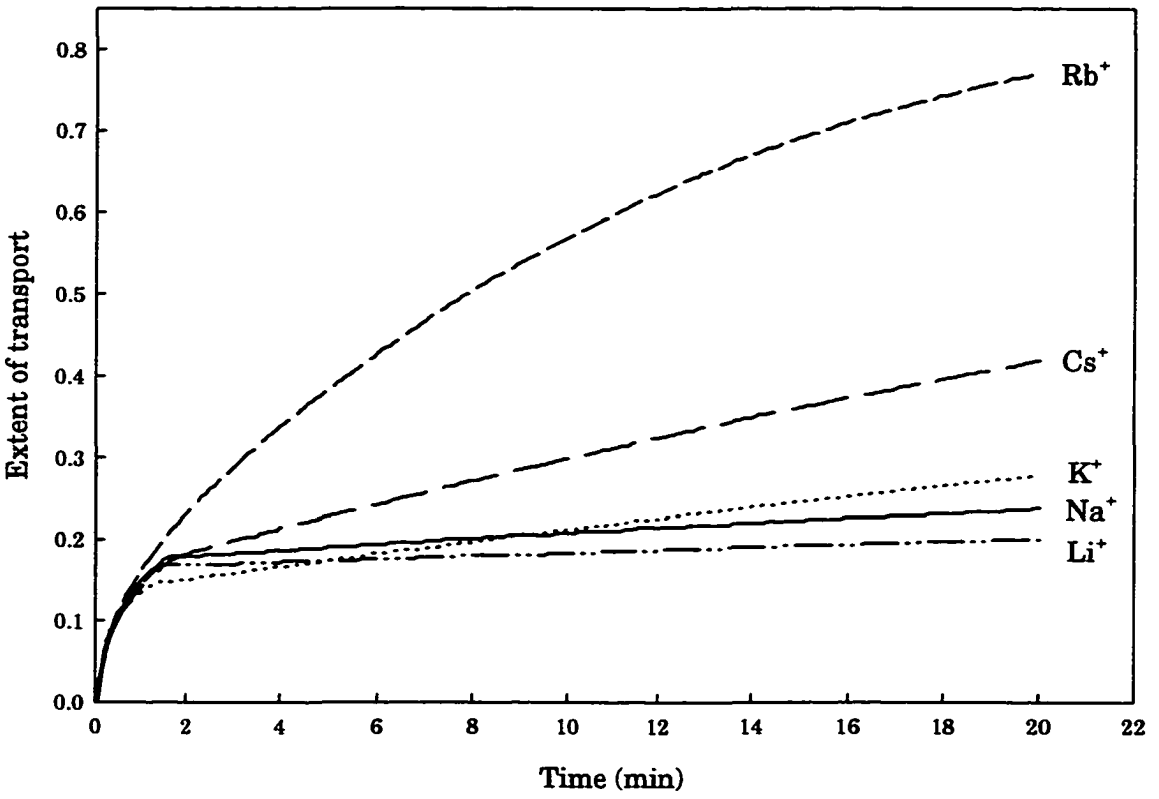

Figure 3.11: The cation effect of S8TrgPA8TrgA (**28**)

In order to test whether or not **28** is a voltage-gated ion channel in vesicle bilayers requires the sign and magnitude of the pH gradient be varied. Basic solution outside of the vesicles relative to the inside corresponds to a positive potential. An acidic external solution would be a negative potential. This latter possibility was explored as follows: The vesicles were made as usual. After mixing with the external solution, the triethylenetetraamine was added in an attempt to neutralize the acidic head group, and sulfuric acid replaced the choline hydroxide titrant to adjust the pH to 5.5. However, after FCCP, cation, and **28** were added, there was no pH gradient collapse.

Numerous attempts established that the pH gradient could not held even before **28** was added. Unfortunately pH-stat titration using this type of vesicles cannot be used to test voltage-gated ion transport events.

3.4.2 Planar bilayer experiment

pH-stat titration does not directly measure the ion translocation process. It simply looks at the initiation rate of a transport event which rapidly saturates each vesicle within the time of a single opening. A more advanced planar bilayer experiment can be used to measure the ion translocation process via bilayer clamp techniques[35, 50]. This experiment measures the time dependence of the current carried across a planar bilayer formed in a small hole in a hydrophobic support barrier. In the presence of an active channel-type transporter, step changes in conductance indicate the "on" and "off" states of the transporter as shown in Figure 3.12. It provides unambiguous demonstration of a channel mechanism and can provide molecular details of the ion translocation process. All of the planar bilayer experiments summarized here were done by D. Loock.

Figure 3.13 shows a typical conductance recording for the pore-former A8TrgPA8TrgA (**13**). From it, the single channel opening and closing, represented by stepwise current changes, can be observed unambiguously. The lifetime of single channel opening could last several seconds. Moreover, the increment for each step was the same magnitude which indicated the pore size was fixed. This is different from the predictions of the "barrel stave" model mentioned in the introduction concerning alamethicin and amphotericin B[4, 5].

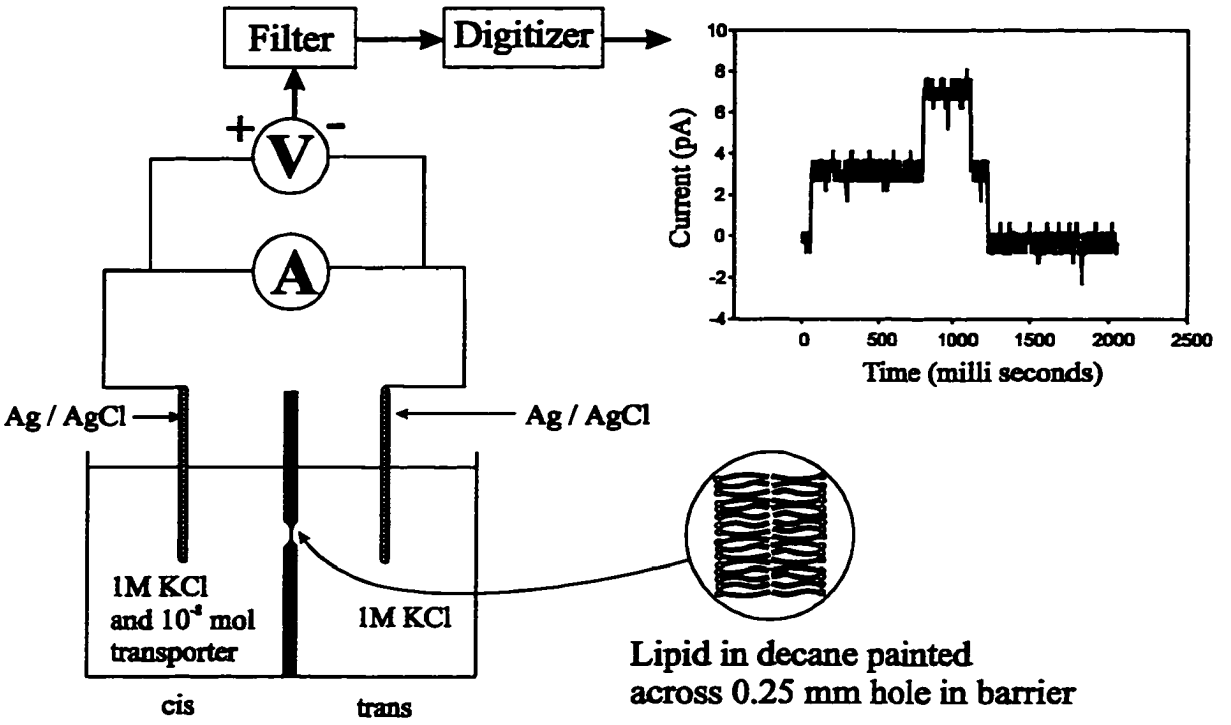

Figure 3.12: Schematic description of planar bilayer experiment

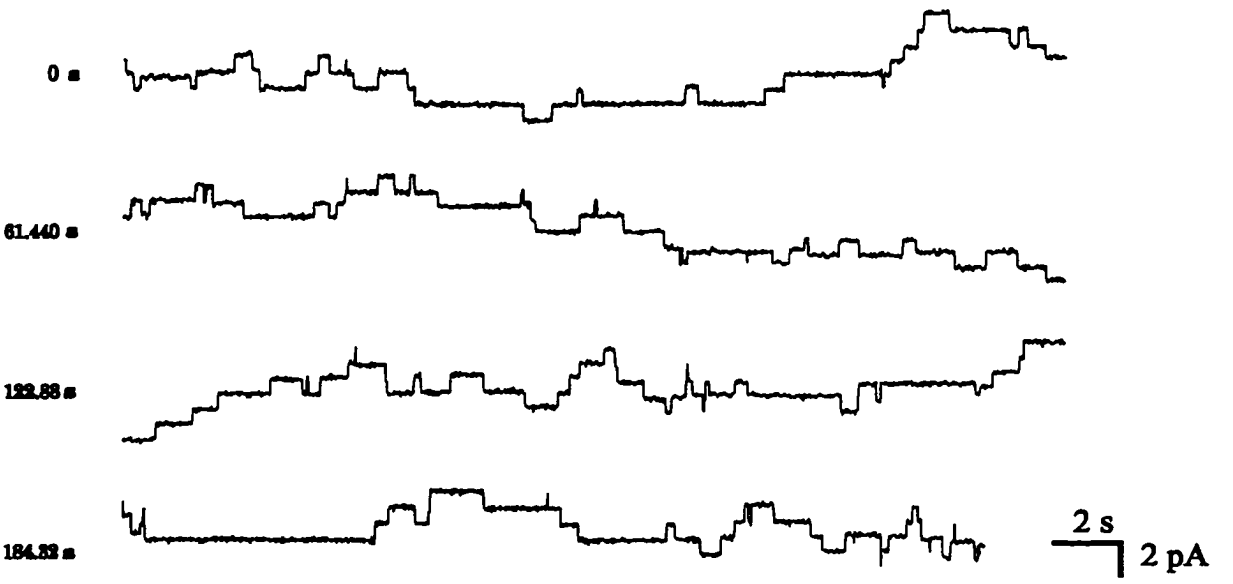

1 M CsCl
+ 50 mV

Figure 3.13: The typical conductance recording of A8TrgPA8TrgA (**13**)

The average of current-time data at different voltages gives a macroscopic current-voltage response for the transport event. It was found that transporters **11**, **13**, **14**, **15** all gave a symmetrical, ohmic current-voltage response (see an example in Figure 3.14) which indicate they are not voltage-gated ion channels.

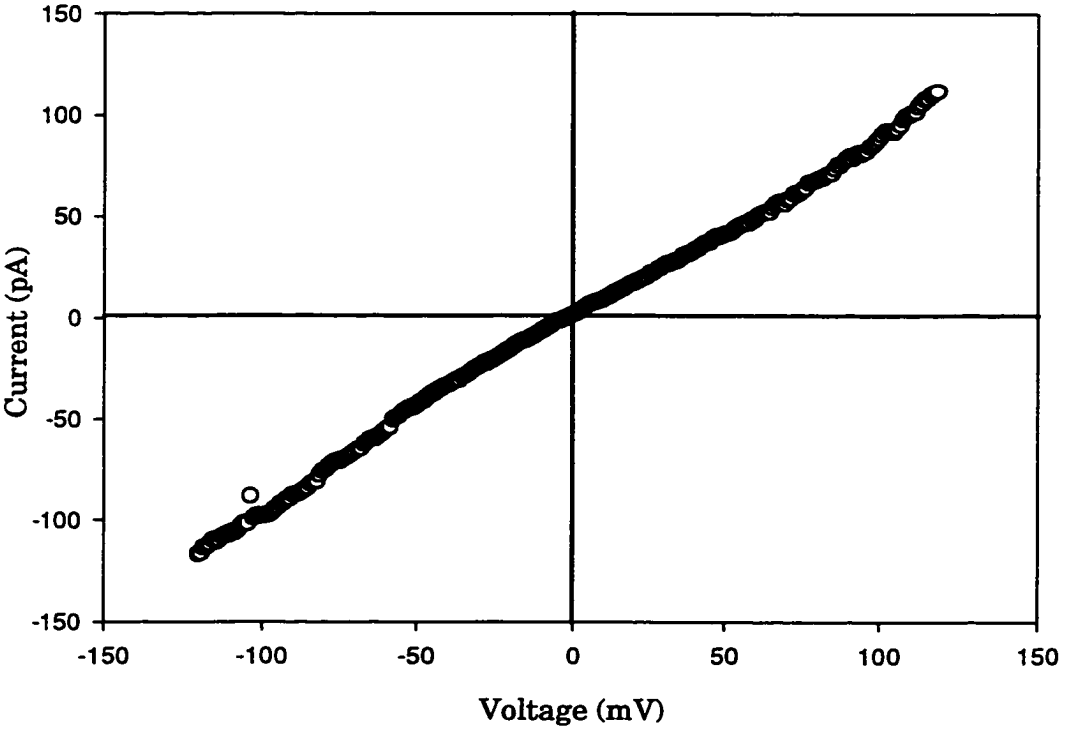

Figure 3.14: The macroscopic current-voltage response of G8TrgPA8TrgA (**15**)

The alkali metal cation selectivity for compounds **13**, **14**, and **15** in the planar bilayers was all found in an order: $Cs^+ > K^+ > Na^+$ [51]. This was different with the cation selectivity in vesicle bilayers. The reason for the different behaviors is the different nature of the kinetic processes being observed in the two experiments. The planar bilayer experiment examines the ion

permeability directly and provides relatively little information about the initiation of transport. Conversely, the vesicle experiments only report the initiation events because channel activity in vesicles is high and a single opening (100 ms) of a 15 pS channel under 1 pH difference would be sufficient to equilibrate a 350 nm vesicle[36]. Therefore, the ion selectivity in vesicles is the cation dependence of initiation of channels, and the ion selectivity in planar bilayers is the ion permeability of the channel for ion translocation.

Under multi-channel conditions, the planar bilayer experiment for **28** gives a very exciting result[52] which indicates **28** indeed is a voltage-gated ion channel. As shown in Figure 3.15(**A**), there were a large amounts of short burst opening of channels at -100 mV (cis side, see Figure 3.12). The channels closed while applied voltage was gradually changed to +100 mV, and they opened again as soon as voltage was switched back to -100 mV. In Figure 3.15(**B**) an asymmetrical current versus voltage diagram macroscopically represents a typical character for the voltage-gated ion channel[5]. In contrast to the natural voltage-gated ion channel, alamethicin, **28** opened the pores at a negative voltage applied to the bilayer membranes, and it closed the pores at a positive voltage. The details of its behavior will be analyzed in D. Loock's thesis.

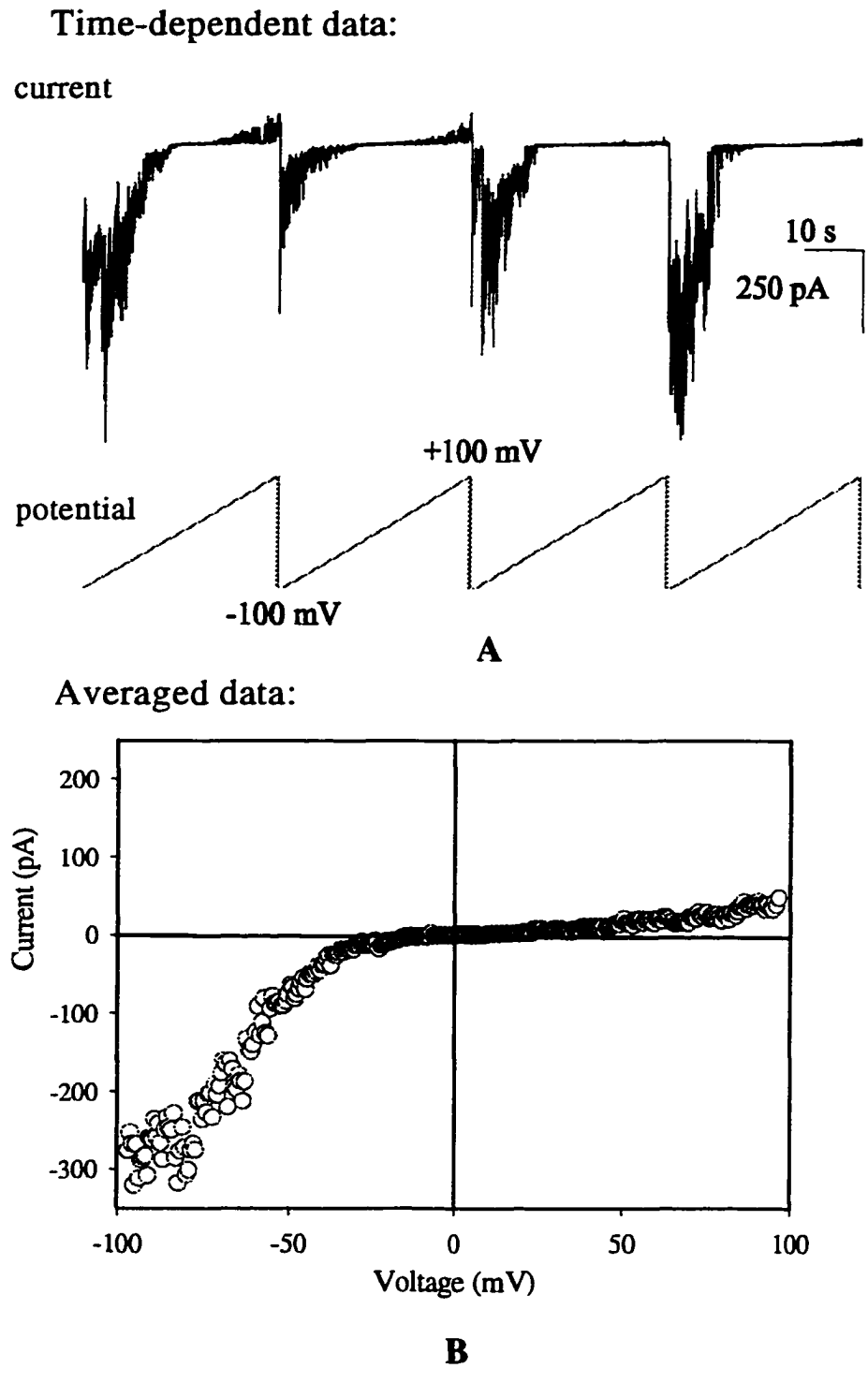

Figure 3.15: The time-dependence recording (**A**) and macroscopic current versus voltage scheme (**B**) for **28**. (Experiment was done by D. Loock.)

3.5 The proposed mechanism of ion transport

Combining information from the pH-stat titration and the planar bilayer experiment, the transport mechanism for the 8Trg series is proposed and schematically represented in Figure 3.16. When a transporter is added into the vesicle solution, the initial state of the channel is a closed state which is supposed to be a combination of two different conformations of the bolaamphiphile in the bilayer. One conformation involves both head groups on the same side of an aqueous phase and the wall units and linker dip into the bilayer membranes (hydrophobic interaction) to form a "U" shaped structure. The other type of conformation envisioned is that one of the head groups has diffused through the bilayer to reach the aqueous phase on the other side to erect a spanning conformation. At the closed stage, these two structures are still surrounded by lipids.

Under the influence of the transmembrane potential either due to applied voltage or a concentration gradient, the electric field and excess cations help monomers aggregate to form an active pore. In the cases of transporter **11**, **13**, **14**, and **15**, transport active pores are composed of dimers since their apparent kinetic orders are all about 2 and conductance steps equally increased or decreased (Figure 3.11). When the polarity of the potential is switched, the small head groups of pore-formers simply flip-flop through the bilayers, reform the dimer structures to adapt to the new electric field and keep the channel active.

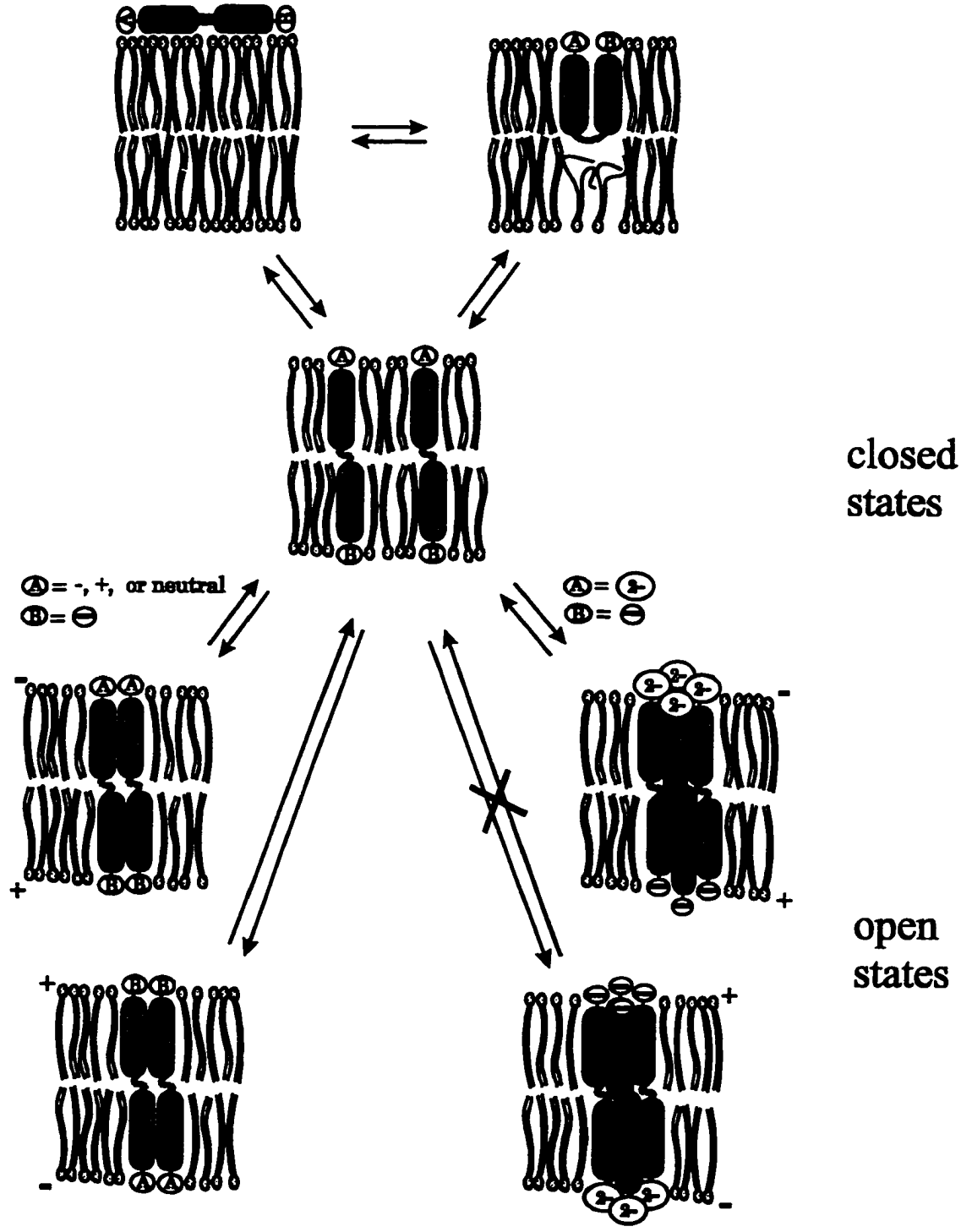

Figure 3.16: The proposed transport mechanisms of the 8Trg series

In the case of the active state of transporter **28**, it is believed that there are loosely structured aggregates in higher oligomer forms due to its higher kinetic order (>> 2) and short burst openings.. However, when the polarity of the potential was switched over, the bulky, -2 charged head group cannot rapidly flip-flop through the bilayer as other compounds in the 8Trg series did. This will force the -2 charged head group to stay at the same aqueous phase interface. The anionic head groups will drive the oligomer apart and close the channel to comply with the electrostatic field. This mechanism explains why the **28** channel opens at negative potentials (cis side, see Figure 3.12) and closes at positive potentials. Since the difficulty in the synthesis prevented further modification of the bulky, negative charged head group, other designed voltage-gated ion channel candidates could not be obtained to provide more evidence to explore the proposed mechanism.

For transporters **20**, **24**, **26**, and **27** in the 8_2 series, no single channel behavior has been observed in planar bilayer experiments so far and their kinetic orders are all about 1. These results suggest the channels in the 8_2 series are formed by monomers, or the transport is initiated by a single molecule. Their "U" shape and/or bilayer spanning conformations may provide transport active structures through disruption in the bilayers in a manner similar to simple detergents.

3.6 Conclusion and prospects

Two series of nine new bola-amphiphiles were successfully synthesized with a convergent synthetic route and maximal use of commercial reagents. Five compounds in the 8Trg series were found to form aggregates via dimers or oligomers in bilayers. They were all more active than the previous pore-formers. They had various alkali metal cation selectivities depending on the head groups. The four compounds in the 8_2 series might be active in a monomer form, or the transport might be initiated by a single molecule.

Although the efforts to make more bulky and hydrophilic head groups failed, the original goal of this project, synthesis and characterization of the voltage-gated ion channel, was well achieved. The investigation of the artificial voltage-gated ion channel will certainly help us to understand the driving force and controlling mechanism of ion transport in our present system, and to design new compounds to obtain better gating properties, ion selectivity and synthetic efficiency.

CHAPTER 4 EXPERIMENTAL

4.1 Synthesis

Proton NMR spectra were recorded with Bruker WM250 (250 MHz), Bruker AC300 (300 MHz), or Bruker AMX360 (360 MHz) spectrometers in $CDCl_3$ or CD_2Cl_2 as solvent referenced to the residual $CHCl_3$ line (7.24 ppm relative to TMS) or the central $CDHCl_2$ line (5.32 ppm relative to TMS). Carbon NMR spectra were recorded with Bruker WM250 (62.89 MHz), Bruker AC300 (75.48 MHz), or Bruker AMX360 (90.57 MHz) spectrometers in $CDCl_3$ or CD_2Cl_2 as solvent referenced to the central solvent line (77.0 ppm or 53.8 ppm relative to TMS respectively). LSIMS spectra were recorded with a Kratos Concept IH mass spectrometer in *meta*-nitrobenzyl alcohol as matrix. Elemental analyses were performed by Canadian Microanalytical Services, New Westminster, B.C. Thin layer chromatography was carried out using Eastman Kodak silica gel on polyester sheets without fluorescent indicator. In addition to the data reported, all samples ran as single sharp peaks on an analytical gel permeation column (Alltech mixed polydivinylbenzene, 10 mm ID × 25 cm) with $CHCl_3$ as eluent. The gel permeation column can resolve products differing by > 50 g/mol. THF was dried by refluxing over then distilling from potassium metal under a dry nitrogen atmosphere. DMF and DMSO were dried by refluxing over then distilling under vacuum from CaH_2 and storing over 4 Å molecular seives.

Compound **2** (8Trg), **7** (8TrgPOH), **8** (8TrgPOMs), **3** (8_2), **16** (8_2POH), and **17** (8_2POMs) were made following the procedures reported before[30, 32].

9. Bis[3- or 4-, 17- or 18-(2-carboxy-1-thiaethyl)]-1,6,9,12,15,20-hexaoxa-2,5,16,19-tetraoxocyclooctacosane A8TrgA

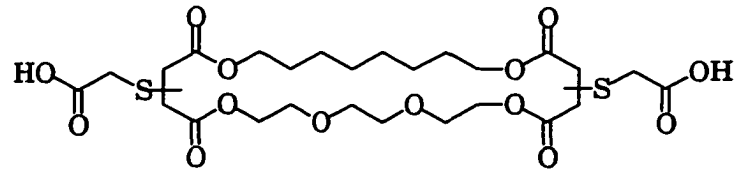

Compound **2** (2.45 g, 5.37 mmol) and 2-mercaptoacetic acid (1.98 g, 21.5 mmol, 4 eq) were added to tetrahydrofuran (300 mL). 2, 2, 6, 6-Tetramethylpiperidine (3.5 mL) was added and the mixture was stirred at 60°C under nitrogen for 72 hours. The tetrahydrofuran was removed under reduced pressure. The pale yellow mixture was dissolved in dichloromethane (330 mL), and washed with 1M hydrochloric acid (5 × 200 mL). The pale yellow oil then was purified on a gel permeation column (LH-20, 3 × 20 cm) using 2-propanol : chloroform (3 : 4) as eluent. The earlier and later fractions contained some unknown impurities. Product **9** was obtained in the middle fractions. The product containing fractions were evaporated to give **9** as a colorless oil (2.34 g, 3.66 mmol, 68%).

^{1}H NMR 300 MHz (δ, $CDCl_3$): 8.75 (br. s, 2H, 2 × CO_2***H***); 4.27 - 4.06 (m, 8H, 4 × CO_2CH_2); 3.89 - 3.82 (m, 2H, 2 × CH_2CHS); 3.69 - 3.64 (m, 8H, 4 × CH_2OCH_2); 3.57 - 3.30 (m, 4H, 2 × SCH_2CO_2H); 3.00 - 2.66 (m, 4H, 2 ×

C***H***$_2$CHS); 1.61 - 1.59 (m, 4H, 2 × CO_2CH_2C***H***$_2$); 1.31 (m, 8H, 4 × CH_2CH_2C***H***$_2$).

^{13}C NMR 75.47 MHz (δ, $CDCl_3$): 173.6, 173.5, 173.4, 173.3 (HO-***C***=O); 171.1, 171.0, 170.2, 170.0 (***C***=O); 70.3, 70.2, 68.9, 68.8 (O***C***H$_2$); 65.6, 65.0, 64.4, 63.9 (CO_2***C***H$_2$); 42.0, 41.9, 41.6 (CH_2***C***HS); 36.1, 35.8 (***C***H$_2$CHS); 33.4, 32.9 (S***C***H$_2$CO$_2$H); 28.5, 25.4, 25.3 (CH_2CH_2***C***H$_2$); 28.3 (CO_2CH_2***C***H$_2$).

MS (-LSIMS, mNBA): 639.1 $(M - H)^-$ 100%.

Exact mass: calculated for $(M - H)^-$, $C_{26}H_{39}O_{14}S_2$, m/e 639.1781; found m/e 639.1832.

10. 3- or 4-(2-carboxy-1-thiaethyl)]-1,6,9,12,15,20-hexaoxa-2,5,16,19-tetraoxocyclooctacos-17-ene 8TrgA

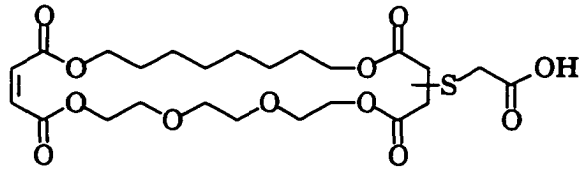

Compound **2** (3.00 g, 6.58 mmol) and 2-mercaptoacetic acid (2.42 g, 26.3 mmol, 4 eq) were dissolved in tetrahydrofuran (250 mL), and 2,2,6,6-tetramethylpiperidine (2 mL) was added into the solution. The mixture was then stirred at 60°C under nitrogen for 6 hours. After the solvent was removed under reduced pressure, the crude oil was dissolved in dichloromethane (200 mL), and washed with 1M hydrochloric acid (4 × 100 mL). The resolved oily mixture was separated by silica column chromatography. The column was made of silica gel (60 g) and a mixed solvent of 30% ethyl acetate / hexanes, and

then it was eluted with a solvent gradient: 30% ethyl acetate / hexanes (150 mL), 40% ethyl acetate / hexanes (150 mL), 50% ethyl acetate / hexanes (200 mL), 75% ethyl acetate / hexanes (150 mL), and 100% ethyl acetate / hexanes (150 mL). Only two spots were identified on TLC and no unreacted 8Trg (**2**) was found. The mono-acid 8TrgA (**10**) came out of the column first, and the later fractions were diacid A8TrgA (**9**). Product-containing fractions were combined to give **10** as a colorless oil (0.44 g, 0.80 mmol, 12%) and by-product **9** as a colorless oil (2.92 g, 4.56 mmol, 69%) for which its spectral data was identical to those reported above.

^{1}H NMR 300 MHz (δ, $CDCl_3$): 8.34 (br. s, 1H, CO_2H); 6.77 (s, 1H, trans C*H*=C*H*); 6.19 (s, 1H, cis C*H*=C*H*); 4.28 - 4.02 (m, 8H, 4 × CO_2CH_2); 3.85 - 3.78 (m, 1H, CH_2CHS); 3.70 - 3.60 (m, 8H, 4 × CH_2OCH_2); 3.52 - 3.26 (m, 2H, SCH_2CO_2H); 2.96 - 2.63 (m, 2H, CH_2CHS); 1.58 (m, 4H, 2 × $CO_2CH_2CH_2$); 1.24 (m, 8H, 4 × $CH_2CH_2CH_2$).

^{13}C NMR 75.47 MHz (δ, $CDCl_3$): 172.9, 172.6 (HO-*C*=O); 170.9, 170.8, 169.9 (*C*=O); 165.3, 165.0 (CH=CH-*C*=O); 133.8, 133.0 (trans *C*H=*C*H); 130.2, 130.1, 129.3, 129.1 (cis *C*H=*C*H); 70.3, 70.2, 70.1, 68.8, 68.6 (CH_2OCH_2); 65.5, 65.2, 64.9, 64.5, 64.1, 63.9 (CO_2CH_2); 41.9, 41.6 (CH_2CHS); 36.1, 35.8 (CH_2CHS); 33.3, 32.9 (SCH_2CO_2H); 29.5, 28.5, 25.4, 25.3 ($CH_2CH_2CH_2$); 28.2, 28.1 ($CO_2CH_2CH_2$).

MS (-LSIMS, mNBA): 547.2 $(M - H)^-$ 100%, $(2M - H)^-$ %.

Exact mass: calculated for $(M - H)^-$, $C_{24}H_{35}O_{12}S_1$, m/e 547.1849; found m/e

547.1881.

11. 3- or 4-[8′-[17″- or 18″-(2‴-Carboxy-1‴-thiaethyl)-1″,6″,9″,12″,15″,20″-hexaoxa-2″,5″,16″,19″-tetraoxocyclooctacos-3″- or 4″-yl]-6′-oxo-5′,1′,8′-oxadithiaoctyl]-1,6,9,12,15,20-hexaoxa-2,5,16,19-tetraoxocyclooctacosa-17-ene 8TrgPA8TrgA

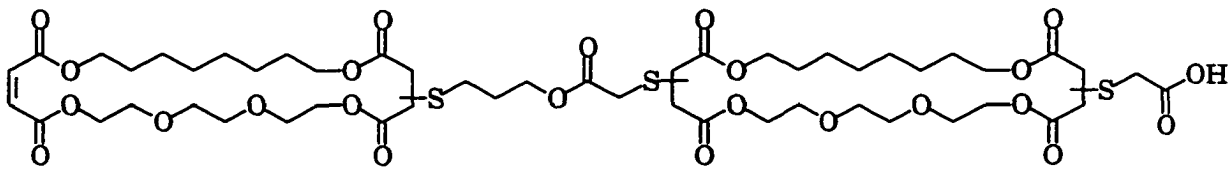

Tetramethylammonium hydroxide pentahydrate (0.29 g, 1.60 mmol) was dissolved in dimethyl sulfoxide (5 mL) at 40°C under nitrogen, and mixed with compound **9** (1.02 g, 1.59 mmol, 1 eq) in dimethyl sulfoxide (7 mL). Compound **8** (1.00 g, 1.60 mmol, 1 eq) in dimethyl sulfoxide (8 mL) was added dropwise and the mixture was held at 40°C under nitrogen for 25 hours. The dimethyl sulfoxide was removed under reduced pressure. The brown mixture was dissolved in chloroform (300 mL), and washed with 1M hydrochloric acid (5 × 150 mL), dried over magnesium sulphate and the solvent was removed. The light brown oil was chromatographed on a gel permeation column (LH-20, 3 × 20 cm) and the product was eluted with 2-propanol : chloroform (3 : 4). A diene product (**12**) of double reaction was obtained in early fractions. The desired **11** was obtained in the middle fractions, and unreacted **8** and **9** were obtained in the last fractions. The product containing fractions were evaporated to give **11**

as a pale yellow oil (0.22 g, 0.19 mmol, 12%):

^{1}H NMR 300 MHz (δ, $CDCl_3$): 7.88 (br. s, 1H, COO***H***); 6.76, 6.17 (s, 2H, C***H***=C***H***); 4.26 - 3.94 (m, 18H, 9 × CO_2CH_2); 3.84 - 3.53 (m, 19H, 8 × CH_2OCH_2, 3 × CH_2CHS); 3.50 - 3.23 (m, 4H, 2 × SCH_2CO_2); 2.95 - 2.55 (m, 8H, 3 × CH_2CHS, SCH_2CH_2); 1.95 - 1.86 (m, 2H, SCH_2CH_2); 1.55 (m, 8H, 4 × $CO_2CH_2CH_2$); 1.24 (m, 16H, 8 × $CH_2CH_2CH_2$).

^{13}C NMR 75.47 MHz (δ, $CDCl_3$): 172.1, 171.9, 171.8 (HO-***C***=O); 171.2, 171.1, 170.9, 170.8, 170.7, 170.6, 170.1, 170.0, 169.9, 169.3 (***C***=O); 165.2, 165.1, 165.0 164.9, 164.6 (CH=CH-***C***=O); 133.8, 132.9, 130.1, 129.9, 129.1, 128.9 (***C***H=***C***H); 70.5, 70.3, 70.2, 70.1, 70.0, 68.8, 68.7, 68.6 (OCH_2); 65.3, 65.2, 65.1, 64.7, 64.4, 64.2, 64.1, 64.0, 63.8, 63.7, 63.6 (CO_2CH_2); 41.9, 41.5, 41.4, 41.2 (CH_2CHS); 36.3, 36.1, 35.9, 35.7 (CH_2CHS); 33.5, 33.0, 32.9 (SCH_2CO_2); 29.4, 28.6, 28.5, 25.5, 25.3, 25.2 ($CH_2CH_2CH_2$); 28.1 ($CO_2CH_2CH_2$); 27.8 (SCH_2CH_2); 27.7, 27.5 (SCH_2CH_2).

MS (-LSIMS, mNBA): 1078.4 (M - head)$^-$ 1.4%; 1169.4 (M - H)$^-$ 20.7%;

Analysis calculated for $C_{51}H_{78}O_{24}S_3$: C 52.29%, H 6.72%, S 8.21%; Found: C 52.17%, H 6.56%, S 8.28%.

Exact mass: calculated for (M - H)$^-$, $C_{51}H_{77}O_{24}S_3$, m/e 1169.3967; found m/e 1169.4041.

13. 3- or 4-[8′-[17″- or 18″-(2‴-Carboxy-1‴-thiaethyl)-1″,6″,9″,12″,15″,20″-hexaoxa-2″,5″,16″,19″-tetraoxocyclooctacos-3″- or 4″-yl]-6′-oxo-5′,1′,8′-

oxadithiaoctyl]-17- or 18-(2-carboxyl-1-thiaethyl)-1,6,9,12,15,20-hexaoxa-2,5,16,19-tetraoxocyclooctacosane A8TrgPA8TrgA

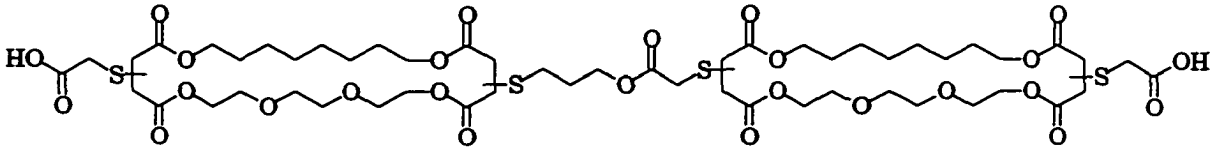

Compound **11** (0.090 g, 0.077 mmol) and 2-mercaptoacetic acid (0.025 g, 0.27 mmol, 3.5 eq) were dissolved in dried tetrahydrofuran (5 mL). 2, 2, 6, 6-Tetramethylpiperidine (0.7 mL) was added and the solution was stirred for 5 hours at 60°C under nitrogen. The tetrahydrofuran was removed under reduced pressure, the light yellow mixture was dissolved in dichloromethane (150 mL), and washed with 1 M hydrochloric acid (5 × 70 mL), dried over magnesium sulphate and the solvent was removed to give a light yellow oil. The crude product was chromatographed on a gel permeation column (LH-20, 3 × 20 cm) eluted with a solvent of 2-propanol : chloroform (3 : 4). The middle fractions containing the expected products were evaporated to give **13** as a light yellow oil (0.040 g, 0.032 mmol, 42%).

^{1}H NMR 360 MHz (δ, $CDCl_3$): 5.14 (br. s, 2H, 2 × CO_2***H***); 4.24 - 4.09 (m, 18H, 9 × CO_2C***H***$_2$); 3.84 - 3.34 (m, 26H, 8 × CH_2OC***H***$_2$, 4 × CH_2C***H***S, 3 × S***C*H**$_2CO_2$); 3.00 - 2.65 (m, 10H, 4 × C***H***$_2$CHS, S***C*H**$_2CH_2$); 1.94 (m, 2H, SCH_2C***H***$_2$); 1.61 (m, 8H, 4 × CO_2CH_2C***H***$_2$); 1.30 (br. s, 16H, 8 × CH_2CH_2C***H***$_2$).

^{13}C NMR 90.57 MHz (δ, $CDCl_3$): 172.1, 171.8, 171.5 (HO-***C***=O); 171.2, 171.1, 170.9, 170.5, 170.3, 170.0, 169.6 (***C***=O); 70.5, 70.3, 70.1 69.3, 69.1, 68.9

(O*C*H_2); 65.6, 65.4, 65.0, 64.7, 64.2, 64.1, 63.9, 63.7 (CO_2*C*H_2); 42.4, 41.7, 41.6,(CH_2*C*HS); 36.4, 35.9 (*C*H_2CHS); 33.9, 33.6, 33.5, 33.2, 32.9 (S*C*H_2CO_2); 29.6, 29.3, 28.6, 25.5, 25.3 (CH_2CH_2*C*H_2); 28.3 (CO_2CH_2*C*H_2); 28.1 (SCH_2*C*H_2); 27.9 (S*C*H_2CH_2).

MS (-LSIMS, mNBA): 1261.4 $(M-H)^-$ 100%; 1303.4 $(M + 43 - H)^-$ 23.5%.

Exact mass: calculated for $(M - H)^-$, $C_{53}H_{81}O_{26}S_4$, m/e 1261.3899; found m/e 1261.3912.

14. 3- or 4-[8′-[17″- or 18″-(2‴-Carboxy-1‴-thiaethyl)-1″,6″,9″,12″,15″,20″-hexaoxa-2″,5″,16″,19″-tetraoxocyclooctacos-3″- or 4″-yl]-6′-oxo-5′,1′,8′-oxadithiaoctyl]-17- or 18-(N,N-dimethyl-4,1-azathiabutyl)-1,6,9,12,15,20-hexaoxa-2,5,16,19-tetraoxocyclooctacosane N8TrgPA8TrgA

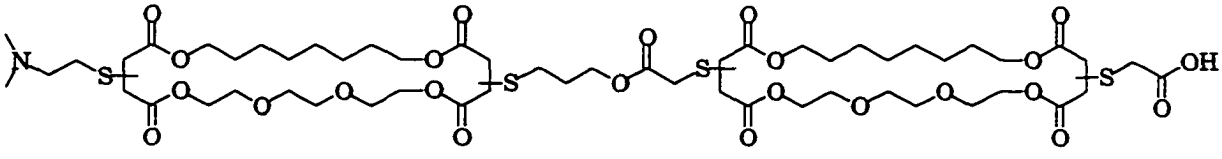

Compound **11** (0.19 g, 0.16 mmol) and 2-(dimethylamino)ethanethiol hydrochloride (0.092 g, 0.65 mmol, 4 eq) were mixed in 2-propanol (15 mL). 2, 2, 6, 6-Tetramethylpiperidine (1 mL) was added and the mixture was heated at reflux for 2 hours under nitrogen. The solvent was evaporated and the crude product was dissolved in chloroform (200 mL), washed with 1M hydrochloric acid (5 × 100 mL), dried with magnesium sulphate, and the solvent was removed to give a pale yellow oil. Gel permeation (LH-20, 3 × 20 cm) of the

product eluted with 2-propanol : chloroform (3 : 4) give the purified material near the void volume. The combined product containing fractions were evaporated to give compound **14** as a pale yellow oil (0.14 g, 0.11 mmol, 68%):

^{1}H NMR 250 MHz (δ, $CDCl_3$): 4.23 - 4.07 (m, 18H, 9 × CO_2CH_2); 3.85 - 3.25 (m, 30H, 8 × CH_2OCH_2, 4 × CH_2CHS, 2 × SCH_2CO_2, 2 × CH_3N); 3.02 - 2.63 (m, 14H, 4 × CH_2CHS, 2 × SCH_2CH_2, NCH_2CH_2S); 1.96 - 1.93 (m, 2H, SCH_2CH_2); 1.61 (m, 8H, 4 × $CO_2CH_2CH_2$); 1.30, 1.26, 1.22 (m, 16H, 8 × $CH_2CH_2CH_2$).

^{13}C NMR 62.89 MHz (δ, $CDCl_3$): 171.2, 170.7, 170.3, 170.1, 169.4 (*C*=O); 70.5, 68.9 (OCH_2); 65.8, 65.5, 65.3, 65.0, 64.9, 64.6, 64.4, 64.1, 63.9 (CO_2CH_2); 56.9 (); 43.0 (CH_3N); 41.9, 41.7 (CH_2CHS); 36.5, 36.4, 36.0 (CH_2CHS); 34.1 (NCH_2); 33.6, 33.2 (SCH_2CO_2); 28.6, 25.6, 25.4, 25.3 ($CH_2CH_2CH_2$); 28.3 ($CO_2CH_2CH_2$); 28.1 (SCH_2CH_2); 27.9, 27.8 (SCH_2CH_2).

MS (-LSIMS, mNBA): 1274.6 $(M - H)^-$.

Exact mass: calculated for $(M - H)^-$, $C_{55}H_{88}O_{24}N_1S_4$, m/e 1274.4579; found m/e 1274.4677.

15. 3- or 4-[8′-[17″- or 18″-(2‴-Carboxy-1‴-thiaethyl)-1″,6″,9″,12″,15″,20″-hexaoxa-2″,5″,16″,19″-tetraoxocyclooctacos-3″- or 4″-yl]-6′-oxo-5′,1′,8′-oxadithiaoctyl]-17- or 18-(β-D-1-thiaglucosyl)-1,6,9,12,15,20-hexaoxa-2,5,16,19-tetraoxocyclooctacosane G8TrgPA8TrgA

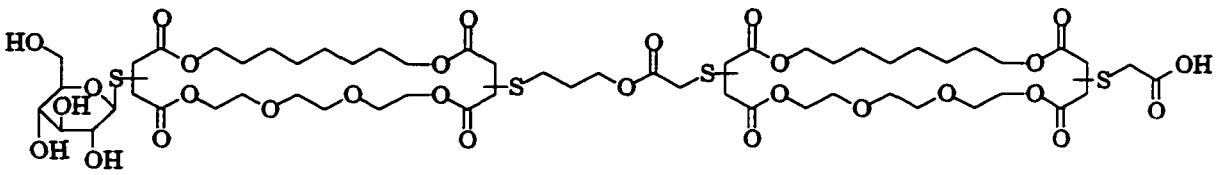

Compound **11** (100 mg, 0.086 mmol) was dissolved into dry THF : 2-propanol (50:50, 10 mL). 1-Thio-β-D-glucose sodium salt dihydrate (43.9 mg, 0.17 mmol, 2 eq) was added, followed by methanesulphonic acid (17.6 mg, 0.18 mmol, 2.1 eq) in 2-propanol (1 mL). The mixture was stirred at 50°C under nitrogen for 1.5 hours, 2, 2, 6, 6-tetramethylpiperidine (0.7 mL) was added, and the reaction was held a further 16 hours at 50°C. After the solvent was removed, the crude product was dissolved into dichloromethane (100 mL), washed with 1 M hydrochloric acid (3 × 50 mL), and dried with sodium sulphate. Dichloromethane was removed, and the yellow oil was chromatographed in three portions on a gel permeation column (LH-20, 3 × 20 cm) eluted with 2-propanol : chloroform (3 : 4). In each portion, the expected product was collected among the middle fractions. The combined products were evaporated to give **15** as a pale yellow oil (0.045 g, 0.033 mmol, 38%).

^{1}H NMR 360 MHz (δ, CD_2Cl_2): 5.33 - 4.65 (m, 4H, 4 × O***H***); 4.24 - 4.10 (m, 18H, 9 × $CO_2C\boldsymbol{H}_2$); 3.94 - 3.60 (m, 22H, 8 × $OC\boldsymbol{H}_2$, 4 × $CH_2C\boldsymbol{H}S$, 2 × O**CH** in the glucose part); 3.57 - 3.37 (m, 9H, 2 × $SC\boldsymbol{H}_2CO_2$, 3 × C**H**OH and $C\mathbf{H}_2OH$ in the glucose part); 3.01 - 2.69 (m, 10H, 4 × $C\boldsymbol{H}_2CHS$, $SC\boldsymbol{H}_2CH_2$); 1.94 (m, 2H, $SCH_2C\boldsymbol{H}_2$); 1.62 (m, 8H, 4 × $CO_2CH_2C\boldsymbol{H}_2$); 1.32, 1.25, 1.23 (m, 16H, 8 × $CH_2CH_2C\boldsymbol{H}_2$).

^{13}C NMR 90.57 MHz (δ, CD_2Cl_2): 172.4, 172.3, 172.0, 171.8 (HO-***C***=O); 171.6, 171.5, 171.3, 171.2, 171.0, 170.8, 170.6, 170.5, 170.4, 169.9 (***C***=O); 85.2, 84.3, 80.1, 78.1, 72.8, 69.9, 62.1 (H**C**–OH and H**C**–O–**C**H in the glucose part); 70.8, 70.7, 70.6, 69.3, 69.2 (O***C***H_2); 66.5, 66.2, 66.0, 65.9, 65.7, 65.5, 65.3, 65.1, 64.9, 64.8, 64.5, 64.4, 64.2 (CO_2***C***H_2); 42.6, 42.2, 42.0, 41.8, 40.7 (CH_2***C***HS); 37.7; 36.9, 36.8, 36.7, 36.5, 36.4, 36.3 (***C***H_2CHS); 33.9, 33.6, 33.5, 33.4 (S***C***H_2CO_2); 30.0, 29.2, 29.1, 25.9, 25.8, 25.7 (CH_2CH_2***C***H_2); 28.7, 28.5, (CO_2CH_2***C***H_2); 28.3 (SCH_2***C***H_2); 28.1 (S***C***H_2CH_2).

MS (-LSIMS, mNBA): 1365.4 $(M-H)^-$ 66.5%.

Exact mass: calculated for $(M - H)^-$, $C_{57}H_{89}O_{29}S_4$, m/e 1365.4372; found m/e 1365.4400.

18. Bis[3- or 4-, 17- or 18-(2-carboxy-1-thiaethyl)]-1,6,15,20-tetraoxa-2,5,16,19-tetraoxocyclooctacosane A8$_2$A

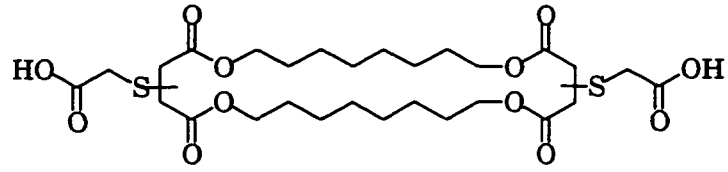

Compound **3** (2.00 g, 4.42 mmol) and 2-mercaptoacetic acid (2.04 g, 22.1 mmol, 5 eq) were dissolved in tetrahydrofuran (150 mL). 2,2,6,6-Tetramethylpiperidine (6 mL) was added and the mixture was stirred at 64°C under nitrogen for 26 hours. The tetrahydrofuran was removed under reduced pressure. The pale yellow mixture was dissolved in dichloromethane (200 mL),

and washed with 1 M hydrochloric acid (4 × 100 mL). After drying with sodium sulphate and removal of dichloromethane, the compound **18** was collected as a pale yellow oil (2.81 g, quantitative).

^{1}H NMR 300 MHz (δ, $CDCl_3$): 9.14 (br. s, 2H, 2 × CO_2***H***); 4.16 - 3.96 (m, 8H, 4 × CO_2C***H***$_2$); 3.79 (d.d., J_1 = 10.7 Hz, J_2 = 3.2 Hz, 2H, 2 × CH_2C***H***S); 3.47 (d.d., J_1 = 56.6 Hz, J_2 = 16.2 Hz, 4H, 2 × S***C***H_2CO_2H); 2.94, 2.70 (d.d., J_1 = 16.9 Hz, J_2 = 11.0 Hz, J_1' = 16.9 Hz, J_2' = 4.4 Hz, 4H, 2 × C***H***$_2$CHS); 1.60 - 1.56 (m, 8H, 4 × CO_2CH_2C***H***$_2$); 1.27 (br. s, 16H, 8 × CH_2CH_2C***H***$_2$).

^{13}C NMR 75.47 MHz (δ, $CDCl_3$): 174.9, 174.8,174.7 (HO-***C***=O); 170.9, 170.1 (***C***=O); 65.7, 65.2 (CO_2***C***H_2); 41.8, 41.7, 41.6 (CH_2***C***HS); 36.1 (***C***H_2CHS); 33.0 (S***C***H_2CO_2H); 29.0, 28.9, 25.6 (CH_2CH_2***C***H_2); 28.4 (CO_2CH_2***C***H_2).

MS (-LSIMS, mNBA): 635.2 $(M - H)^-$ 100%.

Exact mass: calculated for $(M - H)^-$, $C_{28}H_{43}O_{12}S_2$, m/e 635.2196; found m/e 635.2188.

19. 3- or 4-[8′-[17″- or 18″-(2‴-Carboxy-1‴-thiaethyl)-1″,6″,15″,20″-tetraoxa-2″,5″,16″,19″-tetraoxocyclooctacos-3″- or 4″-yl]-6′-oxo-5′,1′,8′-oxadithiaoctyl]-1,6,15,20-tetraoxa-2,5,16,19-tetraoxocyclooctacosa-17-ene 8_2PA8_2A

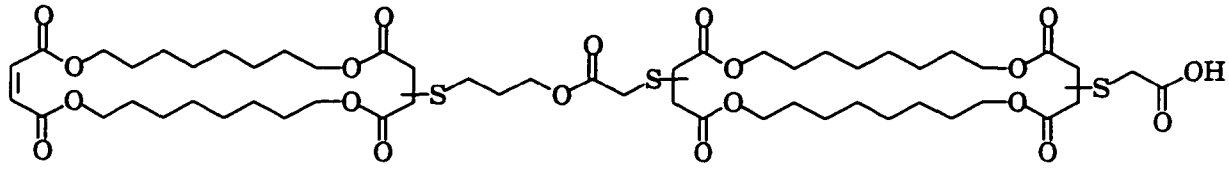

Tetramethylammonium hydroxide pentahydrate (0.29 g, 1.60 mmol) was dissolved in dimethyl sulfoxide (2 mL) at 55°C under nitrogen, and mixed with **18** (1.02 g, 1.60 mmol, 1 eq) in dimethyl sulfoxide (4 mL). Compound **17** (1.00 g, 1.61 mmol, 1 eq) in dimethyl sulfoxide (6 mL) was added dropwise and the solution was stirred at 50°C under nitrogen for 7.5 hours. The dimethyl sulfoxide was removed under reduced pressure. The yellow mixture was dissolved in dichloromethane (200 mL), and washed with 1 M hydrochloric acid (3 × 100 mL). It was dried over magnesium sulphate and the solvent was removed. The yellow oil was chromatographed on a gel permeation column (LH-20, 3 × 60 cm) eluted with a mixed solvent of 2-propanol : chloroform (3 : 4). The desired compound **19** was obtained in the middle fractions, and the product containing fractions were evaporated to give compound **19** as a light yellow oil (0.10 g, 0.086 mmol, 5.4%). The -LSIMS indicated **19** was contaminated by compound **20** due to the retro-Michael addition discussed earlier in the text.

^{1}H NMR 360 MHz (δ, $CDCl_3$): 7.75 (br. s, 1H, COO***H***); 6.79, 6.19 (s, 2H, C***H***=C***H***); 4.19 - 3.95 (m, 18H, 9 × CO_2CH_2); 3.83 - 3.31 (m, 7H, 3 × CH_2CHS, 2 × SCH_2CO_2); 2.97 - 2.59 (m, 8H, $SCH_2CH_2CH_2$, 3 × CH_2CHS); 2.02 - 1.92 (m, 2H, $SCH_2CH_2CH_2$); 1.60 - 1.58 (m, 16H, 8 × $CO_2CH_2CH_2CH_2$); 1.28 (br. s, 32H, 16 ×

$CH_2CH_2C\boldsymbol{H}_2$).

^{13}C NMR 90.57 MHz (δ, $CDCl_3$): 173.5 (HO-***C***=O); 171.1, 170.8, 170.2, 170.1, 170.0, 169.5 (***C***=O); 165.3, 164.9 (CH=CH-***C***=O); 133.5, 129.6, 129.5 (***C***H=***C***H); 65.6, 65.4, 65.3, 65.1, 65.0 ($CO_2\boldsymbol{C}H_2$); 63.9 ($CO_2\boldsymbol{C}H_2CH_2CH_2S$); 41.7, 41.5 ($CH_2\boldsymbol{C}HS$); 36.6, 36.2, 36.1 ($\boldsymbol{C}H_2CHS$); 33.1, 33.0 ($S\boldsymbol{C}H_2CO_2$); 29.1, 29.0, 28.8, 26.0, 25.7, 25.2 ($CH_2CH_2\boldsymbol{C}H_2$); 28.5, 28.4 ($CO_2CH_2\boldsymbol{C}H_2$); 28.0 ($SCH_2\boldsymbol{C}H_2CH_2$); 27.8 ($S\boldsymbol{C}H_2CH_2CH_2$).

MS (-LSIMS, mNBA): 1161.4 $(M - H)^-$ 100%; 1253.3 $(A8_2PA8_2A - H)^-$ 27.8%.

20. 3- or 4-[8′-[17″- or 18″-(2‴-Carboxy-1‴-thiaethyl)-1″,6″,15″,20″-tetraoxa-2″,5″,16″,19″-tetraoxocyclooctacos-3″- or 4″-yl]-6′-oxo-5′,1′,8′-oxadithiaoctyl]-17- or 18-(2-carboxy-1-thiaethyl)-1,6,15,20-tetraoxa-2,5,16,19-tetraoxocyclooctacosane $A8_2PA8_2A$

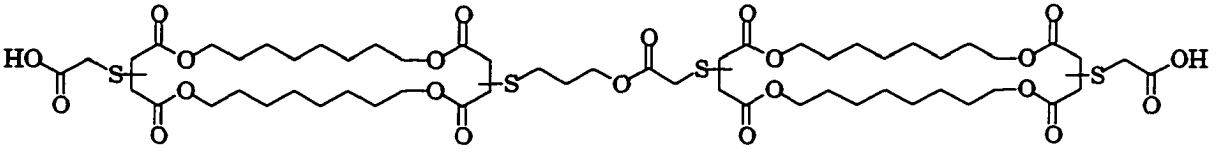

Compound **19** (0.101 g, 0.087mmol) and 2-mercaptoacetic acid (0.079 g, 0.86 mmol, 9.9 eq) were dissolved in tetrahydrofuran (10 mL). 2,2,6,6-Tetramethylpiperidine (1.5 mL) was added and the solution was stirred for 39 hours at 60°C under nitrogen. The tetrahydrofuran was removed under reduced pressure. The light yellow mixture was dissolved in dichloromethane

(150 mL), and washed with 1 M hydrochloric acid (4 × 100 mL), distilled water (3 × 70 mL). It was dried over magnesium sulphate and the solvent was removed to give a light yellow oil. The crude product was chromatographed on a gel permeation column (LH-20, 3 × 20 cm) eluted with a solvent of 2-propanol : chloroform (3 : 4). The middle fractions contained the expected product **20**, and the early and later fractions contained unidentified by-products. The product containing fractions were evaporated to give **20** as a light yellow oil (0.037 g, 0.030 mmol, 34%).

^{1}H NMR 360 MHz (δ, $CDCl_3$): 9.05 (br. s, 2H, 2 × COO***H***); 4.19 - 3.93 (m, 18H, 9 × $CO_2C\boldsymbol{H}_2$); 3.84 - 3.31 (m, 10H, 4 × $CH_2C\boldsymbol{H}S$, 3 × $SC\boldsymbol{H}_2CO_2$); 2.98 - 2.59 (m, 10H, $SC\boldsymbol{H}_2CH_2CH_2$, 4 × $C\boldsymbol{H}_2CHS$); 1.94 - 1.87 (m, 2H, $SCH_2C\boldsymbol{H}_2CH_2$); 1.59 - 1.56 (m, 16H, 8 × $CO_2CH_2C\boldsymbol{H}_2$); 1.27 (br. s, 32H, 16 × $CH_2CH_2C\boldsymbol{H}_2$).

^{13}C NMR 90.57 MHz (δ, $CDCl_3$): 174.3 (HO-***C***=O); 171.3, 170.8, 170.4, 170.1, 170.0, 169.5 (***C***=O); 65.6, 65.5, 65.1 ($CO_2\boldsymbol{C}H_2$); 63.9 ($CO_2\boldsymbol{C}H_2CH_2CH_2S$); 41.7, 41.5 ($CH_2\boldsymbol{C}HS$); 36.5, 36.2, 36.1 ($\boldsymbol{C}H_2CHS$); 33.1, 33.0 ($S\boldsymbol{C}H_2CO_2$); 29.1, 29.0, 25.7, 25.6 ($CH_2CH_2\boldsymbol{C}H_2$); 28.4 ($CO_2CH_2\boldsymbol{C}H_2$); 28.0 ($SCH_2\boldsymbol{C}H_2CH_2$); 27.8 ($S\boldsymbol{C}H_2CH_2CH_2$).

MS (-LSIMS, mNBA): 1253.5 $(M - H)^-$ 100%; 1275.5 $(M + Na - 2H)^-$ 4.0%.

Exact mass: calculated for $(M - H)^-$, $C_{57}H_{89}O_{22}S_4$, m/e 1253.4728; found m/e 1253.4706.

21. Bis[3- or 4-, 17- or 18-(3-carboxy-1-thiapropyl)]-1,6,15,20-tetraoxa-2,5,16,19-tetraoxocyclooctacosane Pa8$_2$Pa

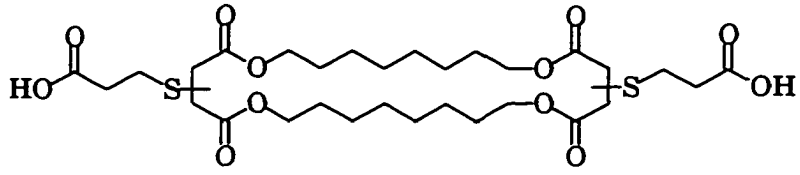

Compound **3** (1.00 g, 2.21 mmol) and 3-mercaptopropionic acid (1.17 g, 11.0 mmol, 5 eq) were dissolved in tetrahydrofuran (40 mL). 2,2,6,6-Tetramethylpiperidine (3 mL) then was added to the solution, and it was kept to reflux for 47 h under nitrogen. The tetrahydrofuran was removed under reduced pressure, and the residual oil was dissolved in dichloromethane (200 mL) and washed with 1M hydrochloric acid (6 × 100 mL). The solution was dried over magnesium sulphate, and solvent was removed to give a acidic mixture. It was chromatographed with a silica column (50 g silica) and eluted by the following solvent gradient: 30% ethyl acetate : hexanes (300 mL), 50% ethyl acetate : hexanes (200 mL), and 100% ethyl acetate (200 mL). The early fractions were unreacted **3**, the middle fractions were the desired mono-adduct **22**, and the later fractions were double-adduct **21**. Product-containing fractions were combined to give **21** as a oily solid (0.44 g, 0.66 mmol, 30 %), **22** as a oily solid (0.20 g, 0.36 mmol, 16%), and recovered **3** as a white solid (0.28 g, 0.62 mmol, 28%).

^{1}H NMR 300 MHz (δ, $CDCl_3$): 9.91 (br. s, 2H, 2 × COO***H***); 4.14 - 3.94 (m, 8H, 4 × $CO_2C\boldsymbol{H}_2$); 3.40 (d. d., J_1 = 11.0 Hz, J_2 = 4.4 Hz, 2H, 2 × $CH_2C\boldsymbol{H}$S); 2.98 -

2.60 (m, 12H, 2 × C***H***$_2$CHS, 2 × SC***H***$_2$CH$_2$, 2 × SCH$_2$C***H***$_2$); 1.60 - 1.57 (m, 8H, 4 × CO_2CH_2C***H***$_2$); 1.28 (br. s, 16H, 8 × CH_2CH_2C***H***$_2$).

^{13}C NMR 75.47 MHz (δ, $CDCl_3$): 177.3 (HO-***C***=O); 171.3, 171.2, 170.2 (***C***=O); 65.5, 65.0 (CO_2***C***H$_2$); 41.7 (CH$_2$***C***HS); 36.5 (***C***H$_2$CHS); 34.1 (SCH$_2$***C***H$_2$); 29.1, 29.0, 25.7, 25.6 (CH_2CH_2***C***H$_2$); 28.4 (CO_2CH_2***C***H$_2$); 26.1 (S***C***H$_2$CH$_2$).

MS (-LSIMS, mNBA): 485.2 (M - Pa - $CH_2CH_2CO_2H$)$^-$ 9.3%; 663.2 (M - H)$^-$ 100%.

Exact Mass: calculated for (M - H)$^-$, $C_{30}H_{47}O_{12}S_2$, m/e 663.2509; found m/e 663.2522.

22. 3- or 4-(3-Carboxy-1-thiapropyl)]-1,6,15,20-tetraoxa-2,5,16,19-tetraoxocyclooctacos-17-ene 8$_2$Pa

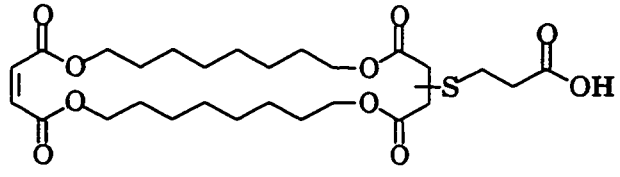

The experimental procedures are described as above (compound **21**), and product **22** was purified and obtained as a oily solid (0.20 g, 0.36 mmol, 16%).

^{1}H NMR 300 MHz (δ, $CDCl_3$): 10.16 (br. s, 1H, COO***H***); 6.75, 6.16 (s, 2H, C***H***=C***H***); 4.17 - 3.90 (m, 8H, 4 × CO_2C***H***$_2$); 3.60 (d. d., J_1 = 11.0 Hz, J_2 = 4.4 Hz, 1H, CH$_2$C***H***S); 2.94 - 2.55 (m, 6H, C***H***$_2$CHS, SC***H***$_2$CH$_2$, SCH$_2$C***H***$_2$); 1.61 - 1.53 (m, 8H, 4 × CO_2CH_2C***H***$_2$); 1.25 (br. s, 16H, 8 × CH_2CH_2C***H***$_2$).

^{13}C NMR 75.47 MHz (δ, $CDCl_3$): 176.6 (HO-***C***=O); 171.1, 170.0 (***C***=O);

165.2 (CH=CH-*C*=O); 133.4 (trans *C*H=*C*H); 129.5, 129.4 (cis *C*H=*C*H); 65.4, 65.2 (CO_2CH_2); 41.6 (CH_2CHS); 36.4 (CH_2CHS); 34.0 (SCH_2CH_2); 29.0, 25.6 ($CH_2CH_2CH_2$); 28.3, 28.2 ($CO_2CH_2CH_2$); 26.0 (SCH_2CH_2).

MS (-LSIMS, mNBA): 485.2 (M - $CH_2CH_2CO_2H$)$^-$ 9.4%; 557.2 (M - H)$^-$ 100%; 1115.2 (2M - H)$^-$ 24%.

Exact Mass: calculated for (M - H)$^-$, $C_{27}H_{41}O_{10}S_1$, m/e 557.2420; found m/e 557.2440.

23 3- or 4-[9′-[17″- or 18″-(3‴-Carboxy-1‴-thiapropyl)-1″,6″,15″,20″-tetraoxa-2″,5″,16″,19″-tetraoxocyclooctacos-3″- or 4″-yl]-6′-oxo-5′,1′,9′-oxadithianonyl]-1,6,15,20-tetraoxa-2,5,16,19-tetraoxocyclooctacosa-17-ene 8_2PPa8_2Pa

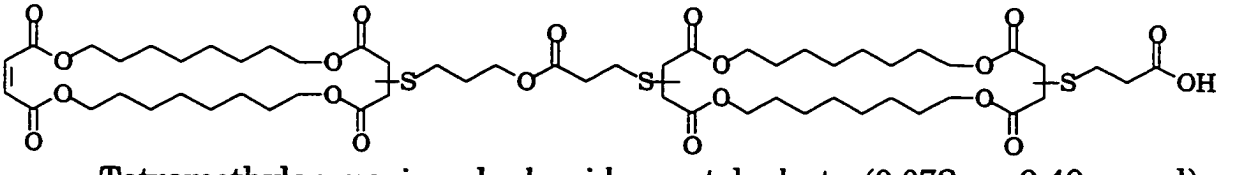

Tetramethylammonium hydroxide pentahydrate (0.072 g, 0.40 mmol) was dissolved in dimethylsulfoxide (2 mL) at 60 °C under nitrogen, and mixed with compound **21** (0.24 g, 0.39 mmol, 1 eq) in dimethylsulfoxide (4 mL). Compound **17** (0.26 g, 0.39 mmol, 1 eq) in dimethylsulfoxide (6 mL) was added dropwise and the solution was stirred for 22 hours at 62 - 65°C under nitrogen protection. After dimethylsulfoxide was removed under reduced pressure, the yellowish mixture was dissolved in dichloromethane (200 mL) and washed with 1 M hydrochloric acid (4 × 100 mL). The organic layer was dried over sodium

sulphate and the dichloromethane was removed. The crude oil was chromatographed on a gel permeation column (LH-20, 3 × 60 cm) and eluted with a mixed solvent of 2-propanol : chloroform (3 : 4). The desired compound **23** was obtained in the middle fractions, and the product containing fractions were evaporated to give the compound **23** as a pale yellow oil (0.14 g, 0.12 mmol, 31%). The negative LSIMS indicated **23** was contaminated by compound **24** due to the retro-Michael addition discussed earlier in the text.

^{1}H NMR 300MHz (δ, $CDCl_3$): 8.70 (br. s, 1H, COO***H***); 6.79, 6.77, 6.18 (s, 2H, C***H***=C***H***); 4.19 - 3.97 (m, 18H, 9 × CO_2CH_2); 3.63 - 3.56 (m, 3H, 3 × CH_2CHS); 2.96 - 2.59 (m, 16H, 3 × CH_2CHS, S$CH_2CH_2CH_2$, 2 × S$CH_2CH_2CO_2$, 2 × S$CH_2CH_2CO_2$); 1.87 (m, 2H, S$CH_2CH_2CH_2$); 1.58 - 1.56 (m, 16H, 8 × $CO_2CH_2CH_2$); 1.26 (br. s, 32H, 16 × $CH_2CH_2CH_2$).

^{13}C NMR 75.47 MHz (δ, $CDCl_3$): 175.9 (HO-***C***=O); 171.4, 171.3, 171.1, 170.5, 170.2, 170.1 (***C***=O); 165.2, 164.9 (CH=CH-***C***=O); 133.4, 129.6, 129.4 (***C***H=***C***H); 65.4, 65.3, 65.2, 65.0, 64.8 63.0, 62.7 (CO_2CH_2); 41.6, 41.5, 41.4 (CH_2CHS); 36.5, 36.4 (CH_2CHS); 34.2, 33.9 (S$CH_2CH_2CO_2$); 29.0, 28.8, 28.7, 25.7, 25.6, 25.2 ($CH_2CH_2CH_2$); 28.4, 28.3, ($CO_2CH_2CH_2$); 28.1 (S$CH_2CH_2CH_2$); 27.8 (S$CH_2CH_2CH_2$); 26.4, 26.1 (S$CH_2CH_2CO_2$).

MS (-LSIMS, mNBA): 1189.5 $(M - H)^-$ 80.7%; 1295.6 [Pa(8$_2$)PPa(8$_2$)Pa - H]$^-$ 11.8%.

24. 3- or 4-[9′-[17″- or 18″-(3‴-Carboxy-1‴-thiapropyl)-1″,6″,15″,20″-

tetraoxa-2″,5″,16″,19″-tetraoxocyclooctacos-3″- or 4″-yl]-6′-oxo-5′,1′,9′-oxadithianonyl]-17- or 18-(3-carboxy-1-thiapropyl)-1,6,15,20-tetraoxa-2,5,16,19-tetraoxocyclooctacosane Pa8_2PPa8_2Pa

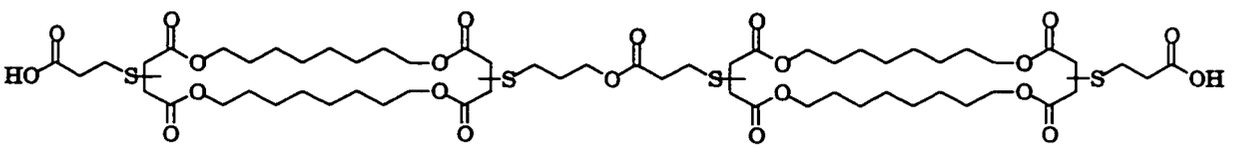

Compound **23** (0.12 g, 0.10 mmol) and 3-mercaptopropionic acid were dissolved in tetrahydrofuran (10 mL). 2,2,6,6-Tetramethylpiperidine (0.7 mL) was added to the solution, and it was refluxed for 18 hours under nitrogen protection. After tetrahydrofuran was removed under reduced pressure, the yellowish solution was dissolved in dichloromethane (150 mL), and washed with 1 M hydrochloric acid (3 × 100 mL). The organic layer was dried over sodium sulphate and dichloromethane was removed. The crude oil was chromatographed on a gel permeation column (LH-20, 3 × 60 cm) and eluted with a mixed solvent, 2-propanol : chloroform (3 : 4). The desired compound **24** was in the middle fractions, and the product containing fractions were evaporated to give the compound **24** as a pale yellow oil (0.080 g, 0.062 mmol, 62%).

^{1}H NMR 300 MHz (δ, $CDCl_3$): 8.38 (br. s, 2H, 2 × COO***H***); 4.14 - 3.97 (m, 18H, 9 × $CO_2C\boldsymbol{H}_2$); 3.66 - 3.57 (m, 4H, $CH_2C\boldsymbol{H}S$); 2.98 - 2.60 (m, 22H, 4 × $C\boldsymbol{H}_2CHS$, $SC\boldsymbol{H}_2CH_2CH_2$, 3 × $SC\boldsymbol{H}_2CH_2CO_2$, 3 × $SCH_2C\boldsymbol{H}_2CO_2$); 1.89 (m, 2H, $SCH_2C\boldsymbol{H}_2CH_2$); 1.58 - 1.56 (m, 16H, 8 × $CO_2CH_2C\boldsymbol{H}_2$); 1.27 (br. s, 32H, 16 ×

$CH_2CH_2C\boldsymbol{H}_2$).

^{13}C NMR 75.47 MHz (δ, $CDCl_3$): 176.6 (HO-***C***=O); 171.4, 171.2, 170.3, 170.2, 170.1 (***C***=O); 65.5, 65.0, 63.1 ($CO_2\boldsymbol{C}H_2$); 41.7, 41.5 ($CH_2\boldsymbol{C}HS$); 36.5 ($\boldsymbol{C}H_2CHS$); 34.2, 34.0 ($SCH_2\boldsymbol{C}H_2CO_2$); 29.6, 29.0, 25.7 ($CH_2CH_2\boldsymbol{C}H_2$); 28.4 ($CO_2CH_2\boldsymbol{C}H_2$); 28.1 ($SCH_2\boldsymbol{C}H_2CH_2$); 27.9 ($S\boldsymbol{C}H_2CH_2CO_2$); 26.4, 26.1 ($S\boldsymbol{C}H_2CH_2CO_2$).

MS (-LSIMS, mNBA): 1295.4 $(M - H)^-$ 100%; 1334.7 $(M + K - H)^-$ 4.3%.

Exact mass: calculated for $(M - H)^-$, $C_{60}H_{95}O_{22}S_4$, m/e 1295.5198; found m/e 1295.5187.

25. 3- or 4-[7′-(1″,6″,15″,20″-tetraoxa-2″,5″,16″,19″-tetraoxocyclooctacos-17-enyl-3″- or 4″-yl)]-1′,4′,7′-trithiahepta]-1,6,15,20-tetraoxa-2,5,16,19-tetraoxocyclooctacosa-17-ene 8_2Su8_2

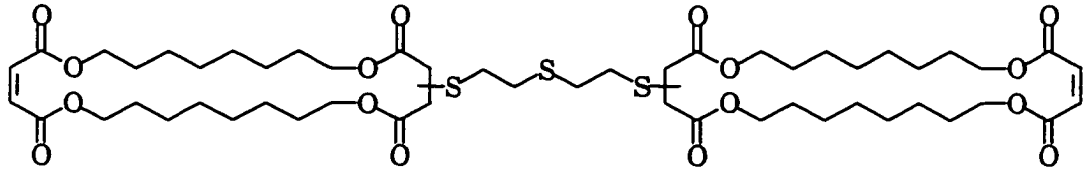

Compound **3** (3.53 g, 7.8 mmol) and 2,2,6,6-tetramethylpiperidine (8 drops) were dissolved in tetrahydrofuran (15 mL). 2-Mercaptoethyl sulfide (0.30 g, 1.95 mmol, 0.25 eq) in tetrahydrofuran (7 mL) was added dropwise for 1 hour and 45 minutes at 63 - 68°C under nitrogen. The solution was then kept at reflux for 23 hours. After removal of tetrahydrofuran under reduced pressure, the crude product was added to a column of silica gel (50 g) prepared

in 20% ethyl acetate/hexanes as a slurry. A solvent gradient was used to elute the column: 20% ethyl acetate/hexanes (400 mL), 35% ethyl acetate/hexanes (250 mL), 50% ethyl acetate/hexanes (400 mL), 100% ethyl acetate/hexanes (200 mL). Two cycles of separation were applied following the same procedures, and the unreacted **3** was eventually separated from the mixture . The rest of the mixture was put on a Lipophilic Sephadex gel permeation column (LH-20, 3 × 60 cm), and eluted with 2-propanol : chloroform (3 : 4). After two cycles of purification, the expected compound **25** came out in the middle fractions. The analytical gel permeation column indicated it was a single sharp peak. The combined product containing fractions were evaporated to give compound **25** as colorless oil (0.50 g, 0.47 mmol, 24%):

^{1}H NMR 300 MHz (δ, $CDCl_3$): 6.76, 6.17 (s, 4H, C***H***=C***H***); 4.16 - 3.90 (m, 16H, 8 × $CO_2C\boldsymbol{H}_2$); 3.65 - 3.60 (m, 2H, 2 × $CH_2C\boldsymbol{H}S$); 2.95 - 2.58 (m, 12H, 2 × $C\boldsymbol{H}_2CHS$, 2 × $SC\boldsymbol{H}_2C\boldsymbol{H}_2S$); 1.60 - 1.56 (m, 16H, 8 × $CO_2CH_2C\boldsymbol{H}_2$); 1.27 (br. s, 32H, 16 × $CH_2CH_2C\boldsymbol{H}_2$).

^{13}C NMR 75.47 MHz (δ, $CDCl_3$): 171.0, 170.0 (***C***=O); 165.2, 165.1 (CH=CH-***C***=O); 133.4, 129.6, 129.4 (***C***H=***C***H); 65.4, 65.2, 64.9 ($CO_2\boldsymbol{C}H_2$); 41.5 ($CH_2\boldsymbol{C}HS$); 36.5 ($\boldsymbol{C}H_2CHS$); 31.5 ($S\boldsymbol{C}H_2\boldsymbol{C}H_2S$); 29.1, 29.0, 28.8, 25.7, 25.6 ($CH_2CH_2\boldsymbol{C}H_2$); 28.4, 28.3 ($CO_2CH_2\boldsymbol{C}H_2$).

MS (-LSIMS, mNBA): 1058.4 $(M - H)^-$ 70.0%.

Exact mass: calculated for $(M - H)^-$, $C_{52}H_{81}O_{16}S_3$, m/e 1057.4687; found m/e 1057.4737.

26. 3- or 4-[7′-[17″- or 18″-(2‴-Carboxy-1‴-thiaethyl)-1″,6″,15″,20″-tetraoxa-2″,5″,16″,19″-tetraoxocyclooctacos-3″- or 4″-yl]-1′,4′,7′-trithiahepta]-17- or 18-(2-carboxy-1-thiaethyl)-1,6,15,20-tetraoxa-2,5,16,19-tetraoxocyclooctacosane $A8_2Su8_2A$

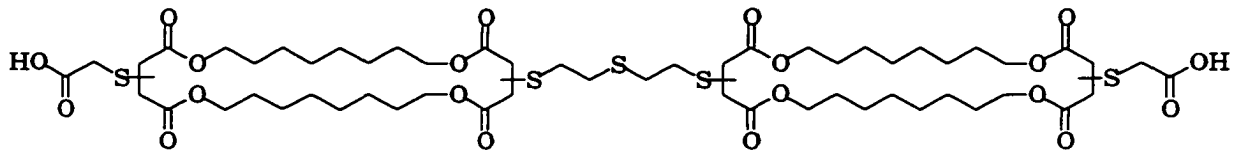

Compound **25** (0.20 g, 0.19mmol) and 2-mercaptoacetic acid were dissolved in tetrahydrofuran (15 mL), and 2,2,6,6-tetramethylpiperidine (0.5 mL) was added into the solution. The mixture was refluxed for 36 hours under nitrogen. After evaporation of tetrahydrofuran under reduced pressure, the crude product was dissolved in dichloromethane (150 mL) and washed with 1 M hydrochloric acid (5 × 100 mL). Drying with magnesium sulphate and evaporation gave a colorless oil. Gel permeation (LH-20, 3 × 60 cm) of the product eluted with 2-propanol : chloroform (3 : 4) gave the desired product **26** in the middle fractions. The combined product containing fractions were evaporated to give compound **26** as a colorless oil (0.15 g, 0.12 mmol, 63%).

^{1}H NMR 300 MHz (δ, $CDCl_3$): 7.61 (br. s, 2H, COO***H***); 4.12 - 3.93 (m, 16H, 8 × CO_2CH_2); 3.81, 3.65 (d.d., $J_1=J_1'=4.4$ Hz, $J_2=J_2'=11.1$ Hz, 4H, 4 × CH_2CHS); 3.46 (d.d., $J_1=16.2$ Hz, $J_2=56.6$ Hz, 4H, 2 × SCH_2COOH); 2.97 - 2.60 (m, 16H, 4 × CH_2CHS, 2 × SCH_2CH_2S); 1.57 (br. s, 16H, 8 × $CO_2CH_2CH_2$); 1.27 (br. s, 32H, 16 × $CH_2CH_2CH_2$).

^{13}C NMR 75.47 MHz (δ, $CDCl_3$): 174.1 (*C*OOH); 171.2, 170.8, 170.3, 170.0 (*C*=O); 65.6, 65.5, 65.1 (CO_2*C*H_2); 41.7, 41.5 (CH_2*C*HS); 36.5, 36.1 (*C*H_2CHS); 33.0 (S*C*H_2COOH); 31.6, 31.5 (S*C*H_2*C*H_2S); 29.1, 29.0, 25.7, 25.6 (CH_2CH_2*C*H_2); 28.4 (CO_2CH_2*C*H_2).

MS (-LSIMS, mNBA): 1241.4 $(M - H)^-$ 100%.

Exact mass: calculated for $(M - H)^-$, $C_{56}H_{89}O_{20}S_5$, m/e 1241.4551; found m/e 1241.4549.

27. 3- or 4-[7′-[17″- or 18″-(N,N-dimethyl-3‴,1‴-azathiapropyl)-1″,6″,15″,20″-tetraoxa-2″,5″,16″,19″-tetraoxocyclooctacos-3″- or 4″-yl]-1′,4′,7′-trithiahepta]-17- or 18-(N,N-dimethyl-3,1-azathiapropyl)-1,6,15,20-tetraoxa-2,5,16,19-tetraoxocyclooctacosane $N8_2Su8_2N$

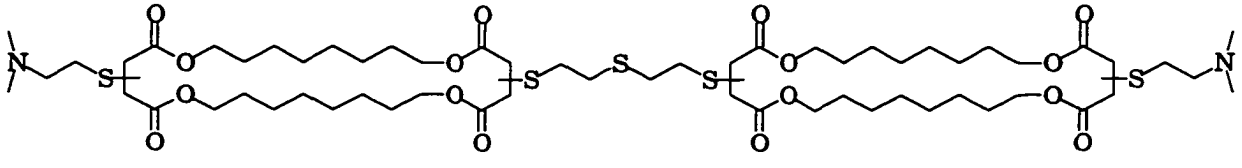

Compound **25** (0.20 g, 0.19 mmol) and 2-dimethylaminoethanethiol (0.11 g, 0.78 mmol, 4.1 eq) were dissolved in 2-propanol (15 mL), and 2,2,6,6-tetramethylpiperidine (0.5 mL) was added. The solution was refluxed for 4 hours under nitrogen. After solvent evaporation, the crude product was dissolved in chloroform (150 mL), washed with 1 M hydrochloric acid (5 × 100 mL), and dried over magnesium sulphate. Following evaporation of chloroform, the crude product was chromatographed by a gel permeation

column (LH-20, 3 ×60 cm) eluted with 2-propanol : chloroform (3 : 4). The desired compound **27** was in the middle fractions. The combined product containing fractions were evaporated to give compound **27** as a colorless oil (0.18 g, 0.14 mmol, 74%).

^{1}H NMR 300 MHz (δ, $CDCl_3$): 4.01 - 3.83 (m, 16H, 8 × CO_2CH_2); 3.61 - 3.53 (4H, 4 × CH_2CHS); 2.91 - 2.52 (m, 36H, 4 × CH_2CHS, 2 × SCH_2CH_2S, 4 × NCH_3, 2 × NCH_2CH_2S); 1.48 (br. s, 16H, 8 × $CO_2CH_2CH_2$); 1.18 (br. s, 32H, 16 × $CH_2CH_2CH_2$).

^{13}C NMR 75.47 MHz (δ, $CDCl_3$): 170.8, 170.7, 169.8 (*C*=O); 65.4, 65.2, 64.8, 64.7 (CO_2CH_2); 57.1 (NCH_2CH_2S); 43.4 (NCH_3); 41.5, 41.3 (CH_2CHS); 36.3, 36.1 (CH_2CHS); 31.4, 31.3 (SCH_2CH_2S); 28.9, 28.8, 28.7, 25.5, 25.4 ($CH_2CH_2CH_2$); 28.2 ($CO_2CH_2CH_2$); 26.6 (NCH_2CH_2S).

MS (+LSIMS, mNBA): 1269.4 $(M + H)^+$ 100%.

Exact mass: calculated for $(M - H)^-$, $C_{60}H_{103}O_{16}N_2S_4$, m/e 1267.5911; found m/e 1267.6014.

28. 3- or 4-[8′-[17″- or 18″-(2‴-Carboxy-1‴-thiaethyl)-1″,6″,9″,12″,15″,20″-hexaoxa-2″,5″,16″,19″-tetraoxocyclooctacos-3″- or 4″-yl]-6′-oxo-5′,1′,8′-oxadithiaoctyl]-17- or 18-[2,3-dicarboxy-1-thiapropyl]-1,6,9,12,15,20-hexaoxa-2,5,16,19-tetraoxocyclooctacosane S8TrgPA8TrgA

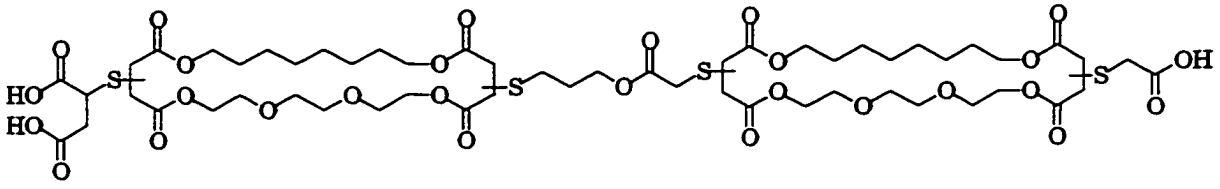

Compound **11** (100 mg, 0.086 mmol) and 2-mercaptosuccinic acid (51mg, 0.34 mmol, 4 eq) were dissolved in tetrahydrofuran (15 mL), and followed by adding 2,2,6,6-tetramethylpiperidine (1.5 mL). The solution was refluxed for 6 hours under the nitrogen. After evaporation of the 2-propanol, the crude oil was dissolved in dichloromethane (200 mL), washed with 1M hydrochloric acid (4 × 100 mL), and dried over sodium sulphate. Following evaporation of solvent, the yellowish mixture was chromatographed by a gel permeation column (LH-20, 3 × 60 cm) eluted with a solvent of 2-propanol : chloroform (3 : 4). The middle fractions were the expected compound based on results of the analytical GPC (Alltec, ID 10 × 100 mm) which gave a single sharp peak.. The combined products were evaporated to give compound **28** as a pale yellow oil (100 mg, 0.076 mmol, 88%).

^{1}H NMR 360 MHz (δ, $CDCl_3$): 7.37 (br. s, 3H, COO***H***); 4.20 - 4.06 (m, 18H, 9 × $CO_2C\boldsymbol{H}_2$); 3.90 - 3.61 (m, 21H, 8 × $CH_2OC\boldsymbol{H}_2$, 5 × $CH_2C\boldsymbol{H}S$); 3.53 - 3.27 (m, 4H, 2 × $SC\boldsymbol{H}_2CO_2$); 3.01 - 2.66 (m, 12H, 5 × $C\boldsymbol{H}_2CHS$, $SC\boldsymbol{H}_2CH_2$); 2.12 - 1.90 (m, 2H, $SCH_2C\boldsymbol{H}_2$); 1.59 (br. s, 8H, 4 × $CO_2CH_2C\boldsymbol{H}_2$); 1.28, 1.19 (br. s, 16H, 8 × $CH_2CH_2C\boldsymbol{H}_2$).

^{13}C NMR 90.57 MHz (δ, $CDCl_3$): 173.4, 172.5 (***C***OOH); 171.1, 171.0, 170.2, 70.0, 169.6 (***C***=O); 70.4, 70.2, 68.9, 68.8 ($OC\boldsymbol{H}_2$); 66.4, 65.8, 65.5, 65.0,

64.6, 64.3, 64..0, 63.9, 63.8 ($CO_2\mathbf{C}H_2$); 42.4, 41.7 ($CH_2\mathbf{C}HS$); 36.7, 36.2, 35.9 ($\mathbf{C}H_2CHS$); 33.5, 33.1, 33.0 ($S\mathbf{C}H_2CO_2$); 29.6, 28.5, 28.2, 25.4, 25.2 ($CH_2CH_2\mathbf{C}H_2$); 28.0 ($CO_2CH_2\mathbf{C}H_2$); 27.9 ($SCH_2\mathbf{C}H_2CH_2$).

MS (-LSIMS, mNBA): 1227.5 (M - $HSCH_2CO_2H$ - H)$^-$ 5.0%; 1319.5 (M - H)$^-$ 100%.

Exact mass: calculated for (M - H)$^-$, $C_{55}H_{83}O_{28}S_4$, m/e 1319.3954; found m/e 1319.3916.

4.2 Molecular modeling

The low energy conformations of transporter candidates were generated by molecular dynamics and mechanics calculation using CAChe Scientific program suite. The standard MM2 force field was used as the potential field which included bond stretching, angle bending, stretch-bend, torsion, hydrogen bonding, and Van der Waals terms. The calculation started from a local minimum which derived from a mechanics optimisation, each molecule was thermally excited to 373 K then allowed to reach a thermal equilibrium over 500 time steps. The actual trajectory was a total of 10,000 time steps, with a sampling every 20 time steps. Those conformations with significantly low energy were then optimized to the corresponding local minimum using the molecular mechanics calculation again.

APPENDIX 1 VESICLE PREPARATION AND PH-STAT TITRATION

The experimental procedures of vesicle preparation and pH-stat titration followed the Master thesis of K. C. Kaye with minor changes.

The titration system consisted of a Metrohm 655 Dosimat burette, a 614 automatic titrimeter, a 632 pH-meter and a titration cell. The burette was linked to an IBM PC, and the automatic titration and data acquisition was programmed as a Windows based software by David Robertson. A W385 Ultrasonic sonicator in Biochemistry and Microbiology Department, University of Victoria was used for sonication in the vesicle preparation. A Nicomp model 370 Submicron Particle Sizer was used for size distribution analysis.

Egg phosphatidyl choline (PC) and egg phosphatidic acid (PA) were obtained from Avanti Polar Lipids (Alabaster, AL). Cholesterol, choline hydroxide (48 - 50% in water), D-mannitol, Bis-Tris (2,2-bis(hydroxymethyl)-2,2',2"-nitrilotriethanol) were obtained from Sigma. PD-10 Sephadex G-25 columns were obtained from Pharmacia. D^3 (deionized, double distilled) water was used to make all of aqueous solution.

Gramicidin D, alamethicin, valinomicin, melittin, FCCP (carbonyl cyanide 4-(trifluoromethoxy)phenlhydrazone), Triton X-100, and the sulphates of lithium, potassium, sodium, rubidium, and cesium, were obtained from Sigma/Aldrich.

Stock solutions

Lipid stock solution: A phospholipid mixture was composed of egg PC, egg PA and cholesterol in 8:1:1 molar ratio. It was dissolved in chloroform at a concentration of 50 mg PC per 3 mL and stored under argon in a refrigerator (0 - 5°C).

Choline sulfate: Choline hydroxide (200 mL of 48 - 50% in water) was titrated to pH 6.5 with concentrated sulphuric acid. Activated charcoal was added, and the solution was stirred for 10 minutes. The charcoal was then removed by filtration through Celite, and the solution was concentrated by rotary evaporation. 100% Ethanol (300 mL) was added to dissolve the tarry residue, followed by adding anhydrous ether (250 ml), and the solution started to precipitate. The solution was cooled in a freezer overnight and precipitate was collected through filtration. The mother liquor was returned to the freezer overnight for another crop of precipitate. The combined batches of choline sulfate precipitate were dried for 24 hours under vacuum.

Internal buffer solution: 0.2 M bis-tris, and 0.054 M D-mannitol; the pH was adjusted to 6.6 by sulphuric acid. Internal buffer solution was made in 500 mL batches.

External solution: 0.11 M choline sulfate, and 0.093 M D-mannitol; made in 500 mL batches. It was filtrated through Millipore GS 0.22 μM to extend its life. It was then portioned into 150 mL brown glass bottles and kept in a refrigerator.

Choline hydroxide titrant: one liter of 5.27 mM choline hydroxide, and 0.35 M D-mannitol, was quickly dissolved in D^3 water to make a basic titrant. Its concentration was calibrated by standard potassium acid phthalate.

Lipid vesicle preparation

3 mL Lipid/chloroform solution was transferred into a round-bottom flask and evaporated to dryness. The trace of chloroform was removed under vacuum overnight at room temperature and it gave a dried lipid film. 6 mL Anhydrous diethyl ether was added to dissolve the dry lipid and 2 mL internal solution was gently added to form a two-phase mixture. It was then sonicated to give a transparent, homogeneous solution. The ether was slowly removed by evaporation at a controlled pressure. The bubbles were formed and the solution was turned to thicker gradually. After the bubbling stopped for 5 minutes, 3 mL external solution was added and rotary evaporation was continued for another 20 minutes. The solution was injected into a sizer to be forced through a 1.0 μm Nucleopore filter, then a 0.4 μm filter under nitrogen pressure. The filtration flow rate was controlled to usually less than 1 drop per second. A Sephadex G-25 disposable column was equilibrated with 10 mL external solution, and the vesicle solution was then purified via gel filtration to give medium unilamellar vesicles which was in the middle fractions. The first 12 drops of vesicle band (multi-lamellar vesicles) and latter fraction (small lipid aggregates and excess internal solution) were discarded, and the desired

unilamellar vesicle was collected for 3 mL. The vesicle size distribution was monitored by dynamic light scattering. Although the vesicle solutions were stable as prepared for 72 hour, they were used typically in 36 hour.

pH-stat titration

Gramicidin D, alamethicin, valinomicin, melittin, FCCP, and transporter candidates were dissolved in methanol. Triton X-100 was diluted by D^3 water in a factor of 20.

0.2 mL Vesicle solution was mixed with 4 mL external solution in a titration cell, and pH value of the solution was adjusted to 7.6 via adding choline hydroxide titrant. A PC connected to the titrimeter started to collect data. Typically, FCCP, alkali metal cation salt, and transporter were added in the titration cell following the order, and choline hydroxide from a pH-stat controlled automatic burette was continuously added to maintain the pH value at 7.6. After the transporter was saturated by cation and titration curve reached a plateau, the Triton X-100 solution (0.2 mL) was added in cell to provoke lysis of the remaining vesicles.

All of the data process including the first-order fitting were done with Microsoft Excel, and the graphs were generated by Sigmaplot.

APPENDIX 2 SUPPLEMENTARY ^{1}H AND ^{13}C NMR SPECTRA

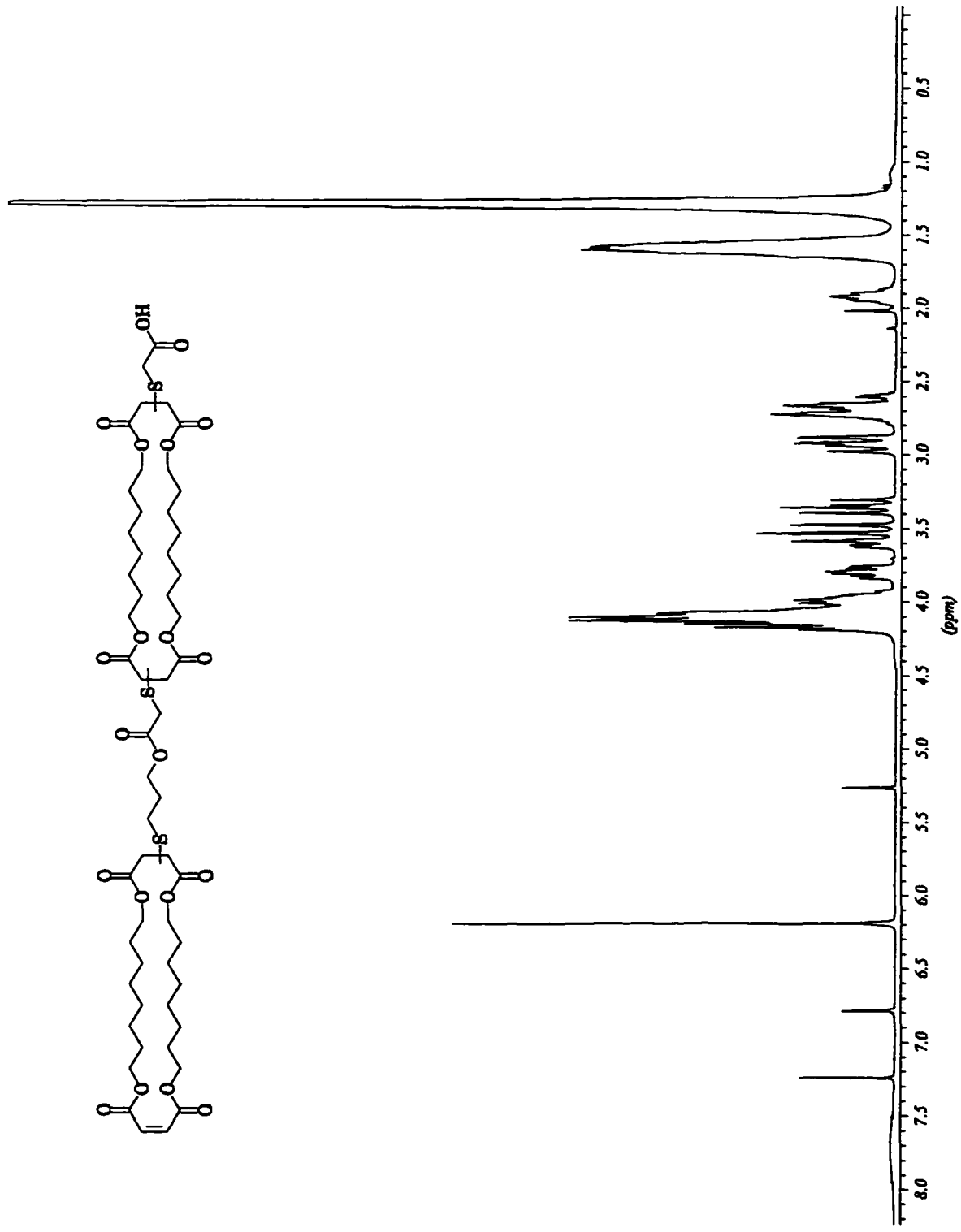

Figure A.1: ^{1}H NMR spectrum of 8_2PA8_2A (**19**)

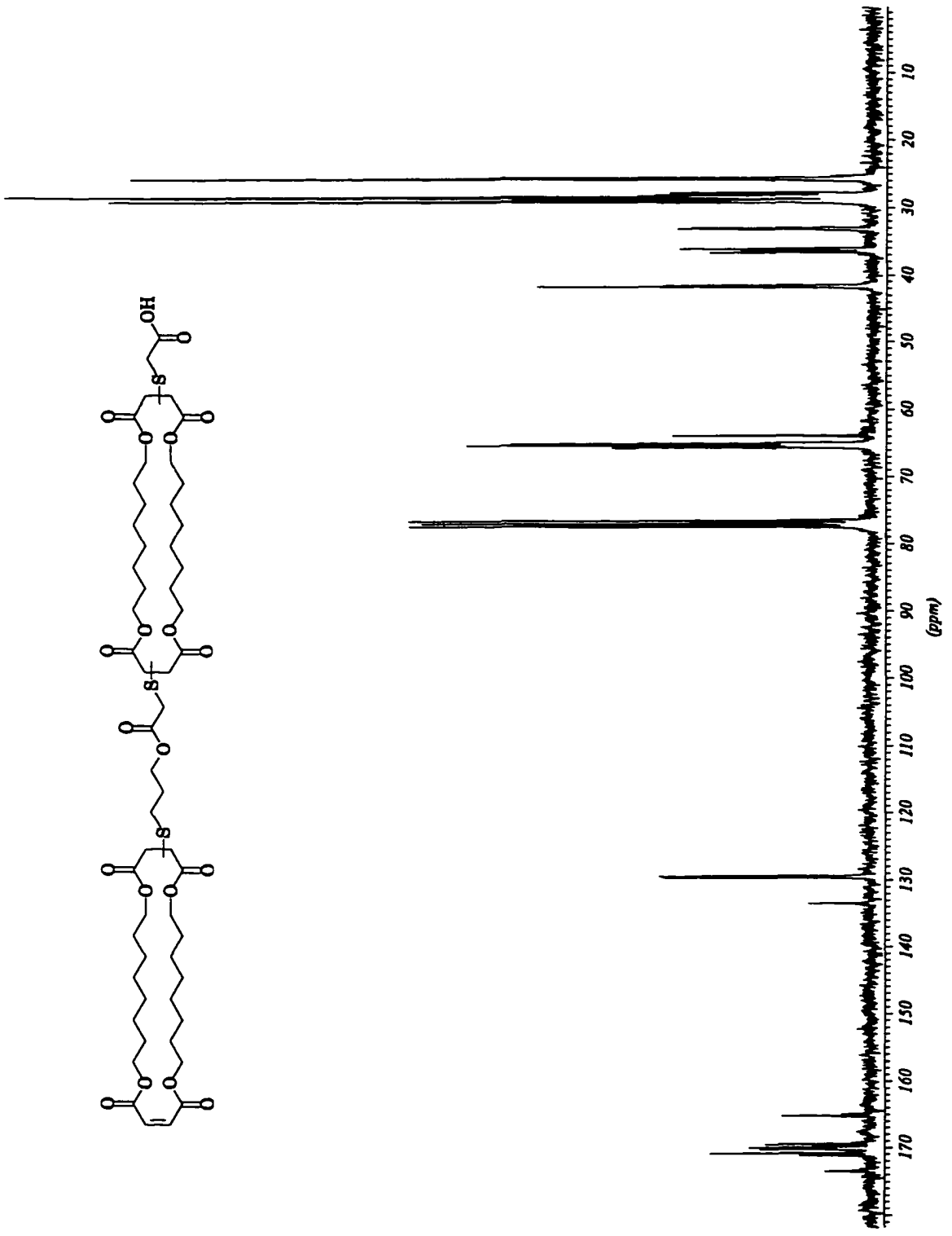

Figure A.2: ^{13}C NMR spectrum of 8_2PA8_2A (**19**)

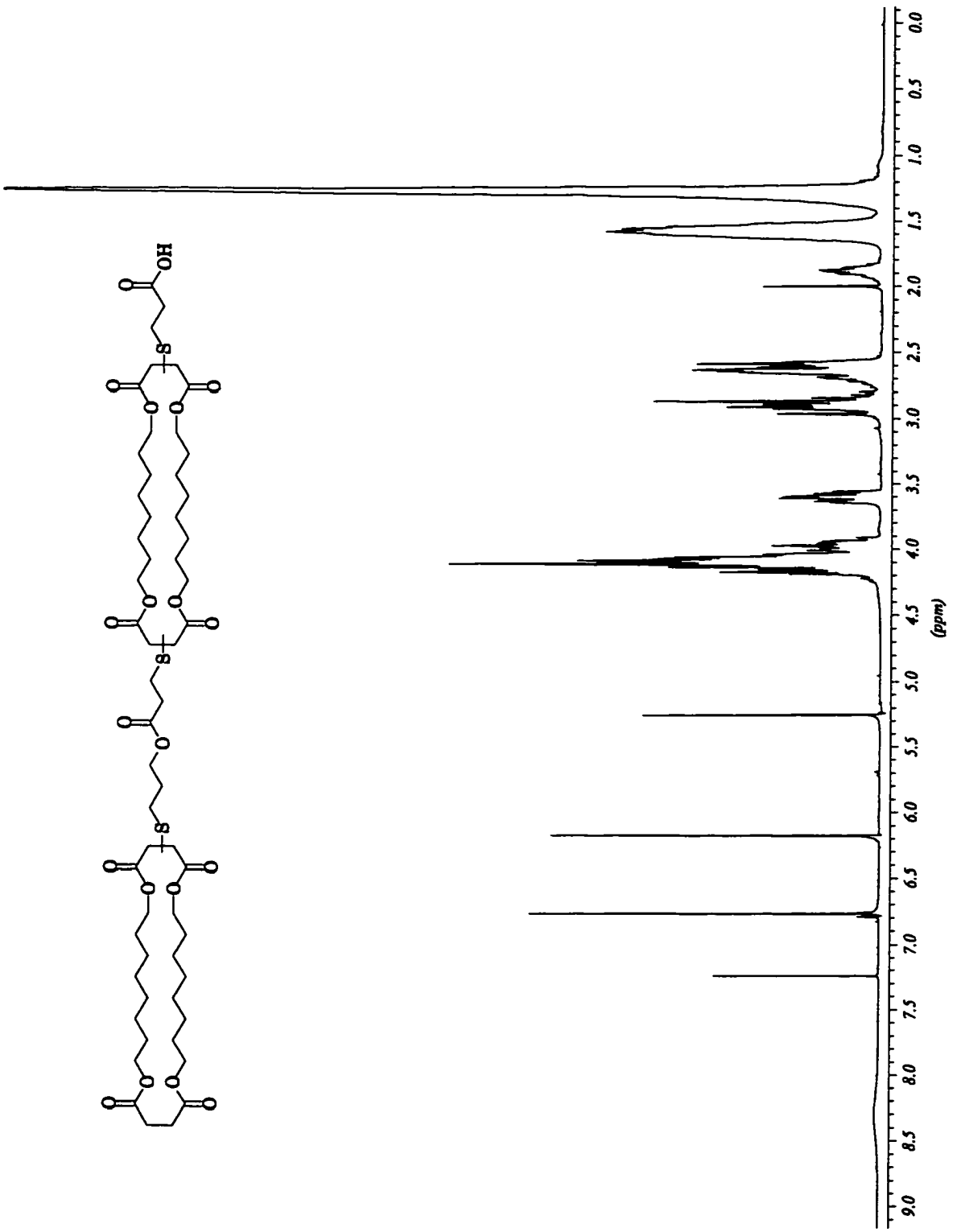

Figure A.3: ^{1}H NMR spectrum of 8_2PPa8_2Pa (**20**)

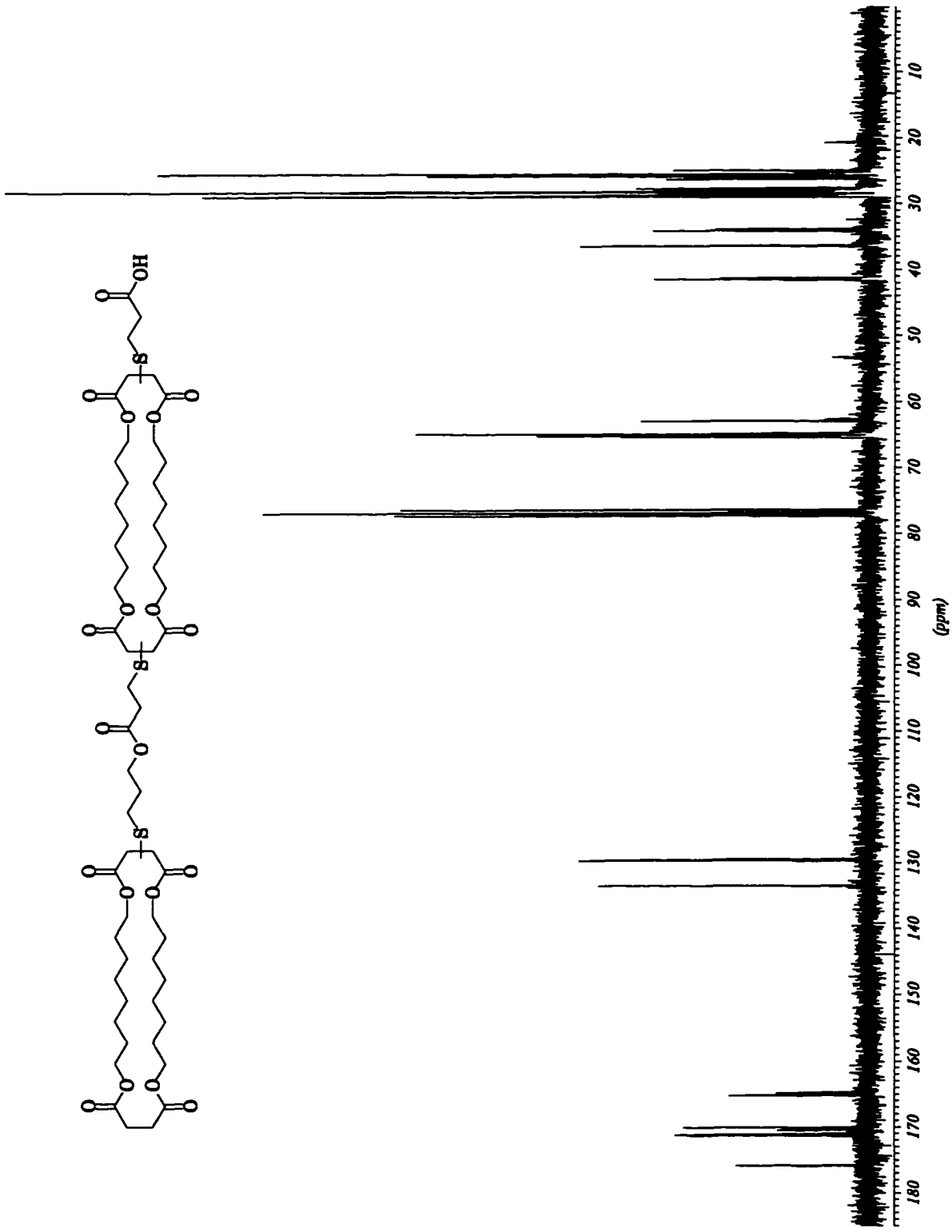

Figure A.4: ^{13}C NMR spectrum of 8_2PPa8_2Pa (**20**)

REFERENCES

1 Stryer, L., Ed. *Biochemistry*, 3rd ed.; W. H. Freeman and Company: New York, 1988; p. 949.

2 Luecke, H.; Chang, B., T; Mailliard, W., S; Schlaepfer, D., D; Halgler, H., T. *Nature* **1995**, *378*, 512-515.

3 Unwin, N. *Nature* **1995**, *373*, 37-43.

4 Sansom, M., S.P. *Prog. Biophys. Molec. Biol.* **1991**, *55*, 139.

5 Woolley, G., A; Wallace, B., A. *J. Membrane Biol.* **1992**, *129*, 109-136.

6 Sarges, R.; Witkop, B. *J. Am. Chem. Soc.* **1965**, *87*, 2011-2020.

7 Veatch, W., R; Fossel, E., T; Blout, E., R. *Biochemistry* **1974**, *13*, 5249-5256.

8 Wallace, B., A; Ravikumar, K. *Science* **1988**, *241*, 182-187.

9 Myers, V., B; Haydon, D., A. *Biochim. Biophys. Acta* **1972**, *274*, 313-322.

10 Bamberg, E.; Lauger, P. *J. Membrane Biol.* **1977**, *35*, 351-375.

11 Hartsel, S., C; Hatch, C.; Ayenew, W. *J. of Liposome Res.* **1993**, *3*, 377-408.

12 Holz, R., W. *Ann. N.Y. Acad. Sci.* **1974**, *235*, 469.

13 Andreoli, T., E. *Ann. N.Y. Acad. Sci.* **1974**, *234*, 448.

14 Gordon, L., G. M.; Haydon, D., A. *Biochim. Biophys. Acta* **1976**, *436*, 541-556.

15 Measurement was done by D. Loock.

16 Dempsey, C., E. *Biochim. Biophys. Acta* **1990**, *1031*, 143-161.

17 Gokel, G., W; Murillo, O. *Acc. Chem. Res.* **1996**, *29*, 425.

18 Grove, A.; Mutter, M.; Rivier, J., E; Montal, M. *J. Am. Chem. Soc.* **1993**, *115*, 5919-5924.

19 Akerfeldt, K., S; Lear, J., D; Wasserman, Z., R; Chung, L., A; DeGrado, W., F. *Acc. Chem. Res.* **1993**, *26*, 191-197.

20 Tabushi, I.; Kuroda, Y.; Yokota, K. *Tetrahedron Lett.* **1982**, *23*, 4601-4604.

21 Jullien, L.; Lehn, Jean-M. *Tetrahedron Lett.* **1988**, *29*, 3803-3806.

22 (a) Pregel, M.; Jullien, L.; Lehn, J-M. *Angew. Chem. Int. Ed. Engl., 12* **1992**, *31*, 1637-1640. (b) Pregel, M., J; Jullien, L.; Canceill, J.; Lacombe, L.; Lehn, Jean-M. *J. Chem. Soc. Perkin Trans. 2* **1995**, 417-426.

23 Voyer, N.; Robitaille, M. *J. Am. Chem. Soc.* **1995**, *117*, 6599.

24 (a) Ghadiri, M., R; Granja, J., R; Buehler, L. *Nature* **1994**, *369*, 301-304. (b) Engels, M.; Bashford, D.; Ghadiri, M., R. *J. Am. Chem. Soc.* **1995**, *117*, 9151-9158.

25 Murillo, O.; Watanabe, S.; Nakano, A.; Gokel, G., W. *J. Am. Chem. Soc.* **1995**, *117*, 7665-7679.

26 (a) Fuhrhop, J-H.; Liman, U. *J. Am. Chem. Soc.* **1984**, *106*, 4643-4644. (b) Fuhrhop, J-H.; Liman, U.; David, H., Hermann. *Angew. Chem. Int. Ed. Engl., 4* **1985**, *24*, 339. (c) Fuhrhop, J-H.; David, H-H.; Mathieu, J.; Liman, U.; Winter, H-J; Boekema, E. *J. Am. Chem. Soc.* **1986**, *108*, 1785-1791.

27 (a) Kobuke, Y.; Ueda, K.; Sokabe, M. *J. Am. Chem. Soc.* **1992**, *114*, 7618-7622. (b) Kobuke, Y.; Ueda, K.; Sokabe, M. *Chemistry Letters* **1995**, 435.

28 (a) Jayasuriya, N.; Bosak, S.; Regen, S., L. *J. Am. Chem. Soc.* **1990**, *112*, 5844-5850. (b) Nagawa, Y.; Regen, S., L. *J. Am. Chem. Soc.* **1991**, *113*, 7237-7240.

29 (a) Stadler, E.; Dedek, P.; Yamashita, K.; Regen, S., L. *J. Am. Chem. Soc.* **1994**, *116*, 6677-6682. (b) Deng, G.; Merritt, M.; Yamashita, K.; Janout, V.; Sadownik, A.; Regen, S., L. *J. Am. Chem. Soc.* **1996**, *118*, 3307.

30 Fyles, T., M; James, T., D; Pryhitka, A.; Zojaji, M. *J. Org. Chem.* **1993**, *58*, 7456.

31 Fyles, T., M; James, T., D; Kaye, K., C. *J. Am. Chem. Soc.* **1993**, *115*, 12315.

32 Fyles, T., M; Kaye, K., C; Pryhitka, A.; Tweddell, J.; Zojaji, M. *Supramol. Chem.* **1994**, *3*, 197-209.

33 Cross, G., G; Fyles, T., M; Montoya-Pelaez, P., J; van Straaten-Nijenhuis, W., F; Zhou, X. *Interfacial design and chemical sensing*; ACS symposium series 561; American Chemical Society: Washington, DC, 1994; p. 38.

34 Fyles, T., M. In *Bioorganic chemistry frontiers*; Springer-Verlag: Heidelberg, Berlin, 1990; Vol. 1, pp. 72-113.

35 Sakmann, B.; Neher, E., Eds. *Single-channel recording*; Plenum Press: New York and London, 1983.

36 Fyles, T., M; Loock, D.; van Straaten-Nijenhuis, W., F; Zhou, X. *J. Org. Chem.* **1996**, *61*, 8866-8874.

37 (a) Duuddeck, H., Dietrich, W. *Structure Elucidation by Modern NMR*, Steinkopff Verlag Darmstadt, Springer-Verlag, New York, **1989**. (b) Derome, A.,E. *Modern NMR Techniques for Chemistry Research*, Pengamon Press, Oxford, **1987**.

38 (a) Hiskey, R., G; Adams, J., B. Jr. *J. Org. Chem.* **1965**, *30*, 1340. (b) Hiskey, R., G; Mizoguchi, T.; Igeta, H. *J. Org. Chem.* **1966**, *31*, 1188-1192.

39 Newkome, G., R; Baker, G. R.; Arai, S.; Saunders, M., J; Russo, P., S; Theriot, K., J; Moorefield, C., N; Rogers, L., Edward.; Miller, J., E; Lieux, T., Richard.; Murray, M., E; Phillips, B.; Pascal, L. *J. Am. Chem. Soc.* **1990**, *112*, 8458-8465.

40 Photaki, I.; Taylor-Papadimitriou, J.; Sakarellos, C.; Mazarakis, P.; Zervas, L. *J. Chem. Soc.* **1970**, 2683-2687.

41 1,2-18C6-dicarboxylic acid was made by a summer student, S. Buckler.

42 Behr, Jean-P.; Girodeau, J-M.; Hayward, R., C; Lehn, J-M.; Sauvage, Jean-P. *Helvetica Chimica Acta* **1980**, *63*, 2096-2111.

43 The peptide Cys-Asp-Asp was made by D. Hardie in Department of Biochemistry and Microbiology, University of Victoria.

44 Cameron, L. Ph.D. Thesis, 1997

45 Kaye, K. C. Master Thesis, 1991.

46 (a) Szoka, F. J.; Papahadjopoulos, D. *Proc. Natl. Acad. Sci. USA* **1978**, *75*, 4194-4198. (b) New, R. R. C. et al. *Liposomes*, 1st ed.; Oxford University

Press: New York, 1990; p. 71.

47 New, R. R. C. et al. *Liposomes*, 1st ed.; Oxford University Press: New York, 1990; p. 154.

48 Fyles, T., M; James, T., D; Kaye, K., C. *Can. J. Chem.* **1990**, *68*, 976-978.

49 Eisenman, G.; Horm, R. *J. Membrane Biol.* **1983**, *76*, 197-225.

50 Hille, B. *Ionic channels of excitable membrane*, 2rd ed.; Sinauer Associates: Sunderland, MA, 1992; p. 178.

51 Fyles, T. M.; Heberle, D.; van Straaten-Nijenhuis, W. F.; Zhou, X. *Supramol. Chem.* **1995**, *6*, 71-77.

52 D.Loock's unpublished result